

Neotectonic faults of the Paralana Escarpment and their influence on uranium-bearing fluid flow

Jonathan David Donauer Berthiaume

**This thesis is submitted in fulfilment of the requirements for the
degree of Master of Philosophy in the Faculty of Science, University of Adelaide**

February 2018



Contents	<i>i</i>
List of Figures	<i>iii</i>
List of Tables	<i>vii</i>
Abstract	<i>viii</i>
Thesis Declaration	<i>ix</i>
Acknowledgements	<i>x</i>
Chapter 1: Introduction and Background	1
1.1 Geological Setting of the Study Area	2
1.2 Geological History	4
1.2.1. Pre-Paleogene	4
1.2.2. Paleogene	6
1.2.3. Neogene-Recent	6
1.3 Neotectonism	7
1.3.1. Brittle Structures at Surface	7
1.3.2 Relationship Between Faulting, Seismicity and Heat Flow	9
Chapter 2: Structural Evolution of the Northern Flinders Ranges	12
2.1. Methods	13
2.1.1. Field Observations and Remote Sensing	13
2.2. Observations	18
2.2.1. Lady Buxton Fault Locality	18
2.2.2. Teasdale Fault Locality	20
2.2.3. Cadna-Owie Fault Locality	21
2.2.4. Faults in the Mount Painter Inlier	22
2.2.5. Conjugate Sets of Faults	24
2.3. Discussion	25
2.3.1. Relative Dating of the Faults	25
2.3.2. Neotectonic Landscape Evolution	29
2.3.3. Fault Displacement Estimation	32
2.3.4. Influence of Neotectonic Faulting on the Uranium Systems	35
Chapter 3: Microstructures and Fluid Flow events	38
3.1. Fault Rock Classification	38
3.2. Cementation	40
3.3. Mineralized Fracture	41
Chapter 4: Hydrogeology of Escarpment-proximal springs	48
4.1. Geologic Setting	49
4.1.1. Hydrostratigraphy of the Paralana Trough	49
4.2. Site Descriptions	51
4.2.1. Paralana Hot Spring	51
4.2.2. Black Spring	53
4.2.3. Old Paralana Homestead Spring	55
4.2.4. Arkaroola Spring	56
4.2.5. Nepouie Spring	57
4.3. Sample Methods and Results	59
4.3.1. Water Sampling Methodology	59
4.2.2. Temperature of the range-proximal springs	59
4.2.3. Elemental Geochemistry	60
4.3. Discussion	63
4.3.1. Faults as fluid conduits and sources	63
4.3.2. Dissolved uranium within the spring waters	64

Conclusions	67
Recommendations for future work	67
References	68

Figure Captions

Figure 1.1	Geological map of the Mount Lofty Ranges and Flinders Ranges showing the extent of the Curnamona Craton with historical and active mines	3
Figure 1.2	Time-temperature landscape evolution model for the Mount Painter Inlier. Box A shows thermochronology, thermal history, uplift, isotopic dating and paleomagnetic dating modified from Wülser (2009). Box B shows the relative uplift and erosion events deduced by apatite fission-track thermochronology, zircon provenance and cosmogenic isotope dating. Figure includes data from Kleeman (1946), Lottermoser & Plimer (1987), Lottermoser (1988), Idnurm & Heinrich (1993), Foster et al. (1994), McLaren et al. (2002), Mitchell et al. (2002), Elburg et al. (2003), McElhinny et al. (2003), Brugger et al. (2005), Bakker & Elburg (2006), Foden et al. (2006), Quigley et al. (2007), Davey (2009), Wülser (2009), and Cross et al. (2010)	5
Figure 1.3	Stratigraphic column of the Frome Embayment from the Cretaceous to Recent (From Skirrow et al., 2009)	8
Figure 1.4	Simplified geological cross-section of the Mount Painter Region (Modified from Hore, 2015)	9
Figure 1.5	Distribution, magnitude (proportional to the size of the circles, $M_l > 4.5$), and relative depth range (blue <20 km shallow to red >100km) of global seismicity (from 1960 to 2018) dominates at plate boundaries. Note the relatively quiet continental regions of Australia, North America and Central Asia. (data source USGS, presented through GeoMapApp)	10
Figure 1.6	Historical earthquakes magnitude > 4.0 (1960 to 2018), interpolated heat flow based on database held by the International Heat Flow Commission, University of North Dakota	11
Figure 2.1	Map of the research area with observation locations coloured relative to the minimum age of the lithologies juxtaposed by the faulting	15
Figure 2.2	Landsat 7 hyperspectral image (Bands 7,5,1 corresponding to the R,G,B colours respectively). Grey lines represent faults identified by historical maps, AEM interpretation and field mapping. (Note: the horizontal striping and the line of anomalous colour on the left are relics of the compilation process)	17
Figure 2.3	Lady Buxton Fault locality; Fault attitude:211/40NW	19
Figure 2.4	Teasdale Fault Locality; Fault attitude:203/29NW	21

Figure 2.5	Cadna-Owie Fault. Fault attitude: 026/31 SE	22
Figure 2.6	Fault locality 26; Fault attitude: 202/64 NW	23
Figure 2.7	Fault Locality 8; Fault attitude: 203/29NW	23
Figure 2.8	Contoured equal area lower hemisphere stereonet plots: a) All 55 observed reverse faults, b) Conjugate Set 1 – Striking NE-SW, c) Conjugate Set 2 – Striking E-W, d) Conjugate Set 3 – Striking NW-SE, e) Unassigned Faults	25
Figure 2.9	Compilation of paleostress models through time from Muller et al., (2012). A) Modelled contemporary (6–0 Ma) maximum horizontal stress. B) Modelled maximum horizontal stress for the Late Miocene (11–6 Ma). C) Modelled maximum horizontal stress for the Early to Middle Miocene (23–11 Ma). D) Modelled maximum horizontal stress for the Eocene (ca 55 Ma). E) Modelled maximum horizontal stress for the Cretaceous (ca 100 Ma).	28
Figure 2.10	Shaded Relief Map of Eastern Range Front with overlain extent of the Paralana High Plains (Orange), Sandiford (2008) interpreted faults (White), AEM-interpreted faults (Black) (Roach et al., 2014), Locations of the Paralana and Poontana troughs), and locations of uranium deposits.	30
Figure 2.11	Map showing the coalescing drainage pattern representative of the Wooltana Fault and Poontana Fault, which define the eastern and western edges of the Poontana Inlier, respectively. Faults shown were identified by AEM in Roach et al., (2014).	31
Figure 2.12	Displacement vs. length diagram for select faults using the fault-scaling properties described by Torabi and Berg (2011)	33
Figure 2.13	Range Front Elevation vs. Length profile as a proxy for displacement-length; imagery from Google Earth, 2018	34
Figure 2.14	Conceptual hydrogeological model for the Four Mile region. From Brugger et al., (2005)	36
Figure 3.1	Fault rock classification scheme proposed by Woodcock and Mort (2008) and adopted for the classification of samples for this study	39
Figure 3.2	Crackle Breccia. Left: fractures and grain boundaries highlighted to facilitate textural analysis. Right: unaltered optical scan of the sample. (sample JB16-015)	39

Figure 3.3	Mosaic Breccia. Left: fractures and grain boundaries highlighted to facilitate textural analysis. Right: unaltered optical scan of the sample. (sample JB16-007)	40
Figure 3.4	Chaotic Breccia. Left: fractures and grain boundaries highlighted to facilitate textural analysis. Right: unaltered optical scan of the sample. (sample JB16-022)	40
Figure 3.5	Sample JB16-024A. (A) imaged in plane-polarized light, (B) Reflected Light, (C) SEM, (D) Mineral Liberation Analysis (MLA), (E) MLA over reflected light to visualize textures	42
Figure 3.6	SEM images of Hematite filled fracture showing composite syntaxial and crack seal infill textures leading to a pseudo wood-grain texture (Sample JB16-024A)	43
Figure 3.7	SEM Images of Maghemite crystals exhibiting boxwork weathering (Sample JB16-024A)	44
Figure 3.8	Mineral Liberation Analysis of sample JB16-024A. Note the hematite vein on the left side of the image and stark change in mineralogy in the centre-right with abundant aluminum-silicate ± Iron clay (Orange).	46
Figure 4.1	Simplified Stratigraphic column of the Callabonna Sub-Basin area with stratigraphic positioning of major aquifers	50
Figure 4.2	Spring locations of the Northern Flinders Ranges. Sampled springs are in green. Base map from Google Earth, 2018	51
Figure 4.3	Paralana Hot Springs through time. Left: 1897 (approximately) by Robert Mitchell (Mitchell, 1897) Right: 2016 – As part of this study	52
Figure 4.4	Paralana Hot Spring (54J 349934E 6660782N) looking upstream (NE) towards the Flinders Ranges	53
Figure 4.5	Aerial photo of the Black Spring Locality. (Google Earth, 2018)	54
Figure 4.6	Black Spring obscured by a thick wall of vegetation (54J 350366E 6657590N)	54
Figure 4.7	Aerial photo of the Paralana Homestead Spring and Black Spring Localities. (Google Earth, 2018)	55
Figure 4.8	Old Paralana homestead's very small spring-fed pond (54J 351369E 6657693N)	56

Figure 4.9	Aerial photo of the Arkaroola Spring Locality. (Google Earth, 2018)	57
Figure 4.10	Arkaroola Spring (54J 349831E 6644483N)	57
Figure 4.11	Aerial photo of the Nepouie Spring Locality. (Google Earth, 2018)	58
Figure 4.12	Nepouie Spring (54J 342433E 6627939N)	58
Figure 4.13	Uranium radiometric map of the Mount Painter Inlier with superimposed historical ground water concentrations of uranium (modified from Michaelsen et al., 2016)	66

Table Captions

Table 2.1	Table of fault observations	14
Table 2.2	Calculated Offset using Length vs. Displacement calculation	34
Table 3.1	Fault rock samples and the classification of their textures using the proposed methods of Woodcock and Mort (2008).	41
Table 4.1	Temperature, pH and Major Cation analyses from natural spring along the range front.	61
Table 4.2	Major element and stable isotope analyses from natural springs along the range front. Elements quoted in ppm were measured by ICP-AES and those in ppb by ICP-MS. All concentrations from Grant (1938) and Heathgate Resources (1998) were quoted in ppm and are converted to ppb by Brugger et al., (2005).	62

Abstract

The Paralana Fault Zone is situated on the eastern flank of the northern Flinders Ranges and separates the Mesoproterozoic Mount Painter Domain to the west and the Mesozoic-Cenozoic Lake Frome Embayment to the east. West-over-east neotectonic faults within the fault zone have been identified previously; the main ones having been described in literature but to date there have been no regional structural studies focusing on the geometry and kinematics of the Paralana Fault Zone. The fault zone juxtaposes uraniferous granites of the Mount Painter Inlier and the sandstone-hosted uranium deposits of the Lake Frome Embayment. Due to their proximity to such prospective zones of economic mineralization, understanding the interplay between these faults and the groundwater of the area is of crucial importance for future mineral exploration strategies.

We have identified three individual thrust fault sets from a total of 56 catalogued faults, within an area of 150km². Fault Set 1 strikes approximately NW-SE with moderate dip in both directions and a NE-SW principal stress direction (σ_1). Fault Set 2 strikes N-S and has a shallow dip and E-W σ_1 . Fault Set 3 has an overall NE-SW strike, moderate dip, and is representative of the current stress regime with a σ_1 of NW-SE. Fault Set 3 features spectacular examples of neotectonic faulting, with Mesoproterozoic marbles and granites of the Mount Painter Inlier overlying Quaternary sandstones and conglomerates of the Frome Embayment. Observed fault displacements since the end of the Miocene range from 10 cm up to an estimated maximum of 800 m. We have sampled fault rocks from 34 measured faults and characterized micro textures ranging from unconsolidated fault gouge and breccia to heavily silicified fault gouge, indicating a range of fluid-flow conditions. To understand the possible fluids to have flowed through the faults, a hydrogeochemical study was conducted with water samples taken from range-proximal natural springs.

After careful consideration of the fault orientation and attitudes, fault rock textures and chemical composition of spring waters, I conclude that there is no evidence for direct interaction between surficial neotectonic faults and uranium-bearing fluids.

Thesis Declaration

I certify that this work contains no material which has been accepted for the award of any other degree or diploma in my name, in any university or other tertiary institution and, to the best of my knowledge and belief, contains no material previously published or written by another person, except where due reference has been made in the text. In addition, I certify that no part of this work will, in the future, be used in a submission in my name, for any other degree or diploma in any university or other tertiary institution without the prior approval of the University of Adelaide and where applicable, any partner institution responsible for the joint-award of this degree.

I give permission for the digital version of my thesis to be made available on the web, via the University's digital research repository, the Library Search and also through web search engines, unless permission has been granted by the University to restrict access for a period of time.

I acknowledge the support I have received for my research through the provision of an Australian Government Research Training Program Scholarship.

Signature:



Date: 19 February 2018

Acknowledgements

This project has been generously supported by the Government of South Australia and the University of Adelaide. I would not have been able to pursue my studies in Australia without their continued financial support.

I would like to first thank my supervisors: Associate Professor Rosalind King, Dr. Simon Holford, and Dr. Mark Bunch. Their support, even when I lacked motivation, has helped me to complete this milestone. Thanks to Dr. Steven Hill and Stephen Hore of the Geological Survey of South Australia for always being enthusiastic about my work and for introducing me to the Arkaroola area. A special thanks to the Saskatchewan Geological Survey and especially Dr. Gary Delaney for first putting together the collaborative project between the SGS and the GSSA which made my studies possible, and secondly for putting me in contact with those who would become my supervisors.

I would like to extend warm gratitude to Doug, Margaret and Mark Sprigg. Thank you for sharing with me the unique beauty of the Arkaroola Wilderness Sanctuary. The Sprigg family, descendants of the eminent geologist Dr. Reg Sprigg, remain avid supporters of active scientific research throughout the area and have broad scientific interests. Your stalwart dedication to environmental protection of your spectacular sanctuary is greatly appreciated. I would also like to thank all the Arkaroola Staff I've met on my many trips through the Village; you took me in and made me feel at home every time I was there.

The post-graduate earth science group at the University of Adelaide took this long, tedious, taxing experience and made it into an enjoyable one. Thank you to all my new friends.

I must acknowledge my wonderful partner, Hilary for her unconditional love and support. Being so far from home has been incredibly difficult at times, but the challenges were made easier by being here together on this great Australian adventure. I appreciate you always being there to help me through. Here's to many more adventures together.

A special thanks to my mom, dad and sister. You've always been my emotional rocks throughout these past two years. Thank you for all your help and support.

Chapter 1 – Introduction and Background

The Northern Flinders Ranges, South Australia represent one of the most spectacular examples of neotectonic landscape evolution in Australia. The area is a zone of active intraplate deformation manifested by ongoing reverse faulting within an otherwise low to the moderately seismically active continental plate (Sandiford, 1998; Celerier et al., 2005; Holford et al., 2014). The Paralana Fault Zone's exposed reverse faults allow researchers a unique opportunity to study these fresh tectonic structures without relying on geophysical methods such as seismic surveying or ground-penetrating radar (ex. Jayawardena, 2013). Much of the area, and especially the ranges' flanks, are obscured by a veneer of Quaternary to recent overburden, making delineating individual fault structures difficult (Drexel and Preiss, 1995; Skirrow, 2009). Numerous phases of deformation along the long-lived NE-SW trending Paralana Fault Zone complicates the differentiation of individual faulting events. Despite the challenges presented, the area has been actively investigated since the late 1800s for its rich mineral potential, including deposits and showings of copper, gold, lead, radium, uranium and other minor elements (Coats and Blissett, 1971). One of the major drivers of continued geological research into the Northern Flinders Ranges remains the numerous uranium deposits situated both within the Mesoproterozoic Mount Painter Inlier and mineralized in the onlapping Cenozoic sediments of the Frome Embayment (Skirrow, 2009, 2011). There are approximately 55 uranium prospects throughout the Mount Painter Inlier (SARIG, n.d.), including numerous deposits around Radium Ridge, Armchair, Hodgkinson, East Painter, and Mount Gee the latter of which the area's highest uranium concentrations (Skirrow, 2011). Exploration programs conducted by Marathon Resources delineated an indicated and inferred resource of 51 Mt at 615 ppm U_3O_8 at the Mount Gee deposit (Skirrow, 2011). Within the Cretaceous to recent sedimentary rocks of the Eromanga Basin there are six distinct uranium deposits, including active mines at the Beverley, Four Mile East, and Four Mile West deposits (Wulser, 2009; Skirrow 2009). The Arkaroola area, which includes all of the Mount Painter Inlier, was designated a Wilderness Sanctuary, and thus off-limits to mineral exploration and mining in 2012 (Government of South Australia, 2011; 2012). Exploration for and extraction of uranium in Eromanga Basin east of the Mount Painter Inlier is ongoing.

One of the main aims of this project is the production of a model of meso-scale neotectonic faulting along the Paralana Escarpment. The Paralana Fault Zone is zone of active tectonism with ongoing brittle deformation. The reverse faults which bound the range front are directly in between the uranium-rich granitoid rocks of the Mount Painter Inlier and mineralized sandstone units of the Frome Embayment. Understanding the orientation, growth history, and

segmentation these faults has direct implications for the flow of mineralizing fluids between the two uranium-enriched environments. As such, understanding which faults may have influenced uranium-bearing fluid flow directly impacts our understanding of ore-mineral transportation processes. Along the Paralana fault zone are several naturally-occurring springs; based on the positioning of some of these springs directly between the crystalline uranium deposits of the Mount Painter Inlier and the sediment-hosted deposits of the Eromanga Basin, the chemistry of expelled water may contain information as to the origin and pathways of uranium-bearing, mineralizing fluids.

In this thesis, I will expand upon previous works to ascertain the relationship between neotectonic faulting of the northern Flinders Ranges and uranium-enriched fluid flows with the goal of identifying conduits for fluid flows. Using field mapping of fault exposures, microstructural analysis of fault rocks and hydrogeochemical analysis of spring waters the complex interplay of structural evolution and fluid-rock interactions will be explored.

1.1 Geological Setting of the Study Area

The Flinders Ranges and Mount Lofty Ranges of South Australia form an extensive upland system from Kangaroo Island in south-eastern South Australia northward toward Arkaroola and branching out toward Olary and Marree, (Fig. 1.1). The Ranges are widely considered among the most geomorphologically active zones of Australia and are relatively seismically active compared to much of the Australian continent (Sprigg, 1945; Sandiford, 2003; Holford, 2012). While most of the ranges average approximately 500 m elevation above sea level, some of the peaks in the Flinders Ranges reach ~1000 m elevation (Sarig, 2017). To the east of the Flinders Ranges, and north of Olary lies Lake Frome, a salt lake overlying the Frome Embayment. The Lake Frome Region hosts three major basins: the Arrowie Basin (Cambrian); the Eromanga Basin (Lower Jurassic to Upper Cretaceous); and the Callabonna Sub-Basin (Cenozoic). (Fig.1.1; Coats and Blissett, 1971). The ranges are typified by Neoproterozoic sediments of the Adelaidean Rift Complex.

At the far north-eastern extent of the Flinders Ranges lies a pair of tectonic windows through overlying Neoproterozoic to Recent sequences into the underlying Curnamona Craton. These windows are known as the Mount Painter Inlier to the south-east and Mount Baggage Inlier to the north. Collectively these two inliers are known as the Mount Painter Domain (Coats and Blissett, 1971). The two inliers are separated by the Terrapina Corridor, a Neoproterozoic shear zone overlain by Neoproterozoic sediments of the Adelaidean Rift Complex (Preiss et al., 1995). The Mount Painter Inlier and overlapping Frome Embayment are the focus of this study.

The geology of the Mount Painter Domain has been thoroughly described in many research and review papers, including Coats and Blissett (1971), Preiss (1995) Skirrow (2009), Wülser et al., (2011), Roach et al., (2014). Despite these numerous studies, there has been relatively little research into the complex interplay between active intraplate tectonism and uranium-mineralizing fluid flow.

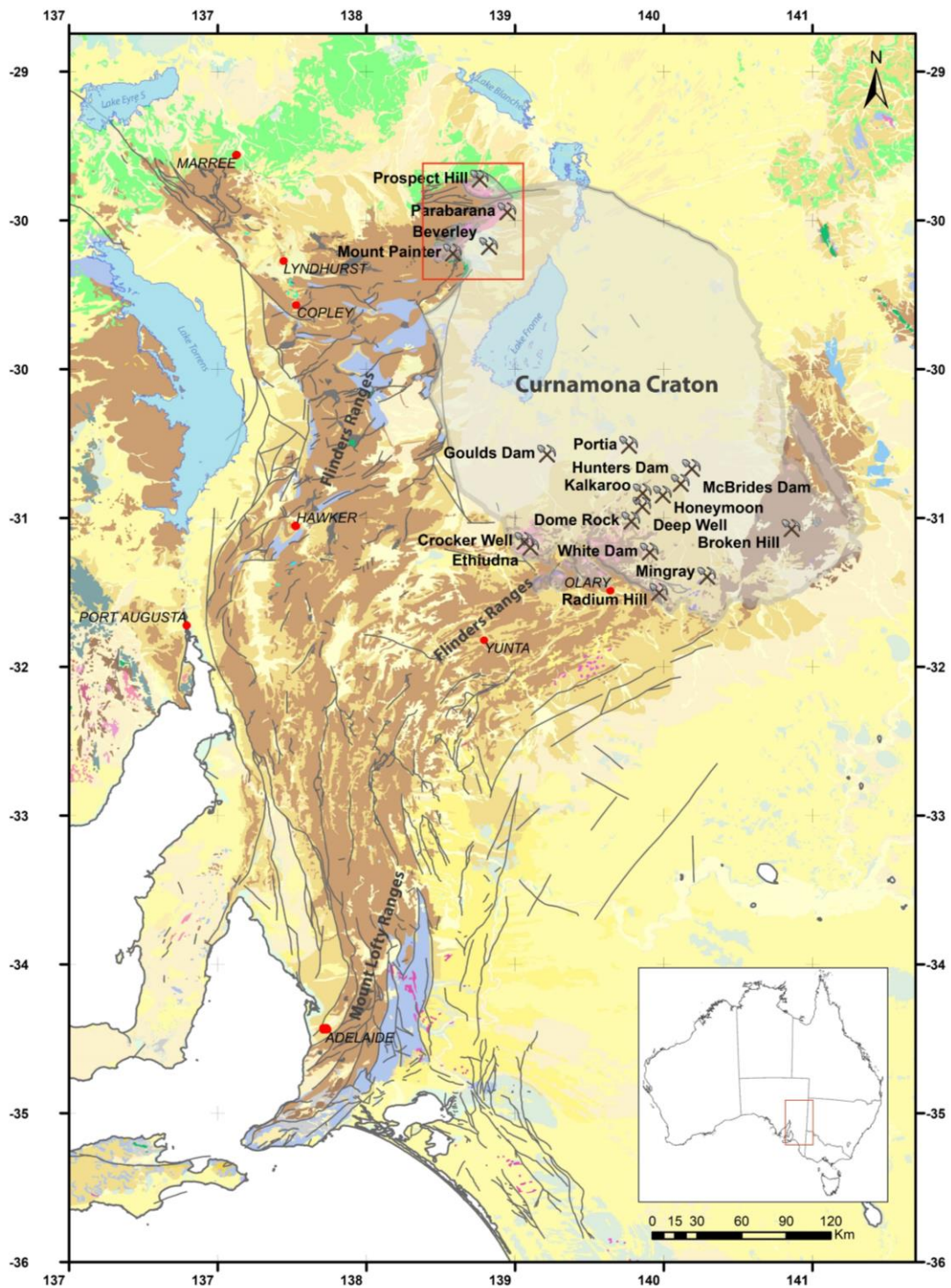


Fig.1.1: Geological map of the Mount Lofty Ranges and Flinders Ranges showing the extent of the Curnamona Craton with historical and active mines.

1.2 Geological History

1.2.1. Pre-Paleogene

Mesoproterozoic lithologies are predominantly metasedimentary rocks of the Radium Creek Group and type-A granitoids which are subdivided into $\pm 1,575$ Ma Coulthard suite and $\pm 1,555$ Ma Moolawatana suite (Coats and Blissett, 1971; Elburg et al., 2001; Cowley et al., 2012; Elburg et al., 2012; Weisheit et al., 2013). Surrounding and unconformably overlying the Mount Painter Domain are Neoproterozoic (800-500 Ma) metasedimentary and basaltic rocks of the Adelaidean Sequence (Preiss 1987, 2000; Weisheit et al., 2013).

By the mid-Cryogenian Period, approximately 800 Ma, the Mesoproterozoic crystalline basements of the Curnamona Craton (Fig. 1.1) were exposed (Preiss, 1987). The onset of Adelaidean rift sedimentation from 830 Ma to 550 Ma (Preiss, 1987; Sandiford et al., 1998; Preiss, 2000) was facilitated by the activation of a series of major normal faults, predominantly the Paralana Fault Zone and Norwest Fault which remained active from approximately 1400 Ma to 500 Ma (Preiss, 1987; Teale, 1993) leading to approximately 7 to 12 km of Adelaidean rift-related sedimentation (Preiss, 1987; 2000).

These faults were then reactivated and inverted during the Delamerian Orogeny between 515 Ma and 490 Ma which coincides with a cessation of sedimentation into the Adelaidean rift zone (Harrison and Macdougall, 1981; Sandiford et al., 1998; Dutch et al., 2005; Foden et al., 2006). This inversion and subsequent movement along the fault accommodated ~10-20% shortening during orogenic deformation (Flöttmann et al., 1994; Flöttmann and James, 1997; Paul et al., 1999). The Delamerian orogeny continued through 490 ± 3 Ma with rapid uplift and cooling (Foden et al., 2006). A regional thermal event at 440 Ma resulted in emplacement the British-Empire S-Type granitic (McLaren et al., 2006) and mafic intrusions (Elburg et al., 2003). Renewed movement along the Paralana Fault occurred during the mid-Paleozoic with 3 to 4 km of Flinders Ranges uplift between 430 and 395 Ma and a further 3 km of uplift between 330 and 325 Ma (McLaren et al., 2002).

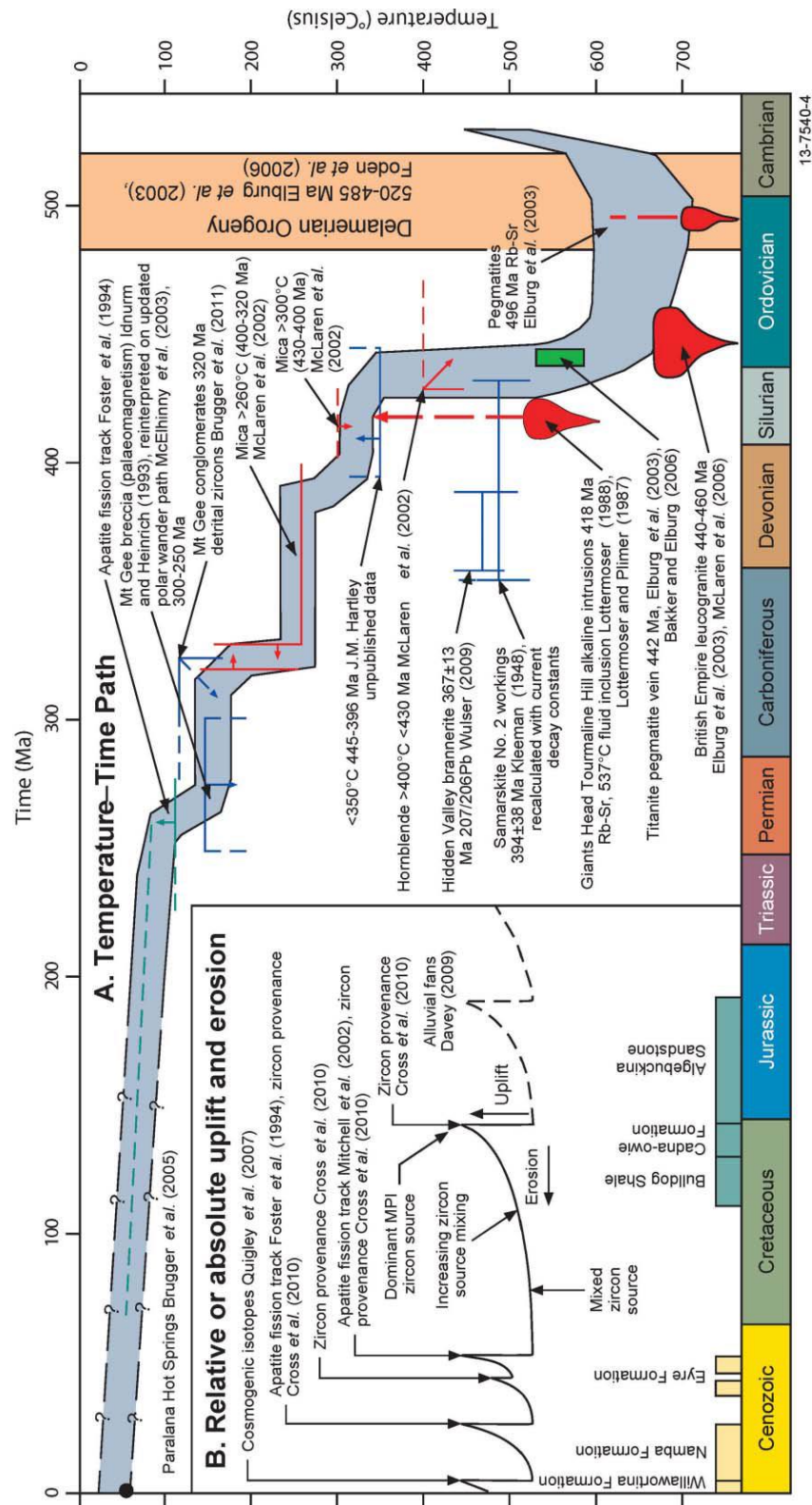


Fig. 1.2: Time-temperature landscape evolution model for the Mount Painter Inlier. Box A shows thermochronology, thermal history, uplift, isotopic dating and paleomagnetic dating modified from Wülser (2009). Box B shows the relative uplift and erosion events deduced by apatite fission-track thermochronology, zircon provenance and cosmogenic isotope dating.

Figure includes data from Kleeman (1946), Lottermoser & Plimer (1987), Lottermoser (1988), Idnurm & Heinrich (1993), Foster et al. (1994), McLaren et al. (2002), Mitchell et al. (2002), Elburg et al. (2003), McElhinny et al. (2003), Brugger et al. (2005), Bakker & Elburg (2006), Foden et al. (2006), Quigley et al. (2007), Davey (2009), Wülser (2009), and Cross et al. (2010).

Glacially-derived sediments of the Lower Cretaceous Cadna-Owie Formation are present throughout the Lake Frome Basin, onlapping the Mount Painter Domain and unconformably overlying the Adelaidean Rift Sediments (Krieg et al., 1995). By 125 Ma (Aptian), the main depositional environment had changed to marine-dominated sedimentation throughout the Frome Basin, represented by the spatially-extensive Bulldog Shale (Drexel et al., 1995). Late Cretaceous sedimentation was dominated by deposition of non-marine siliciclastic units, including shales, siltstones, sandstones and occasional minor coal beds (Krieg et al., 1995). The depositional environment was likely marshes and wetlands, supported by the presence of large quantities of organic matter, and the low energy of this environment allowed the deposition of shales and siltstones. Uplift in the latest Cretaceous resulted in a shallowing of the basin and increased drainage toward the south-west (Senior and Mabbutt, 1979).

1.2.2. Paleogene

Following the Late Cretaceous uplift of the northern Flinders Ranges, Paleocene tectonic subsidence of the Lake Eyre Basin led to fluvial and lacustrine sedimentation (Callen et al., 1995). This sedimentation continues to the present day. The basal unit of the Lake Eyre basin is the Eyre formation, a mature sandstone with minor siltstone and cobbles, interpreted to be a braided stream deposit (Alley and Benbow, 1995). Following deposition of the Eyre formation, there was a hiatus which lasted until the Late Oligocene when local folding and uplift reactivated the Birdsville Track Ridge to the north (Skirrow, 2009).

1.2.3. Neogene-Recent

The new sediments mobilized by the Late Oligocene uplift were partially deposited in the Frome Embayment as the Namba Formation, which disconformably overlies the Eyre Formation. The Namba Formation includes units of poorly-consolidated green-grey clays, fine-grained sandstone with minor conglomeratic lenses (Alley and Benbow, 1995). The basal member of the Namba Formation is the Alpha Mudstone which contains minor woody plant fragments. The upper surface of the Alpha mudstone is incised by a sand-filled north-trending paleochannel system which hosts part of the Beverley deposit mineralization (McConachy et al., 2006). The Beverley Sands form the middle member and consist of grey silt with minor sandy lenses and host the main mineralization for the Beverley Uranium Mine (Curtis et al., 1990). The Namba Formation is capped by the Beverley Clay which acts as a prominent aquitard, separating the Beverley Sands from the overlying Quaternary sediments. The presence of the impermeable Alpha Mudstone below the mineralization and Beverley Clays

above, allows the in-situ leaching process used at the Beverley Uranium Mine to be viable (Skirrow, 2009).

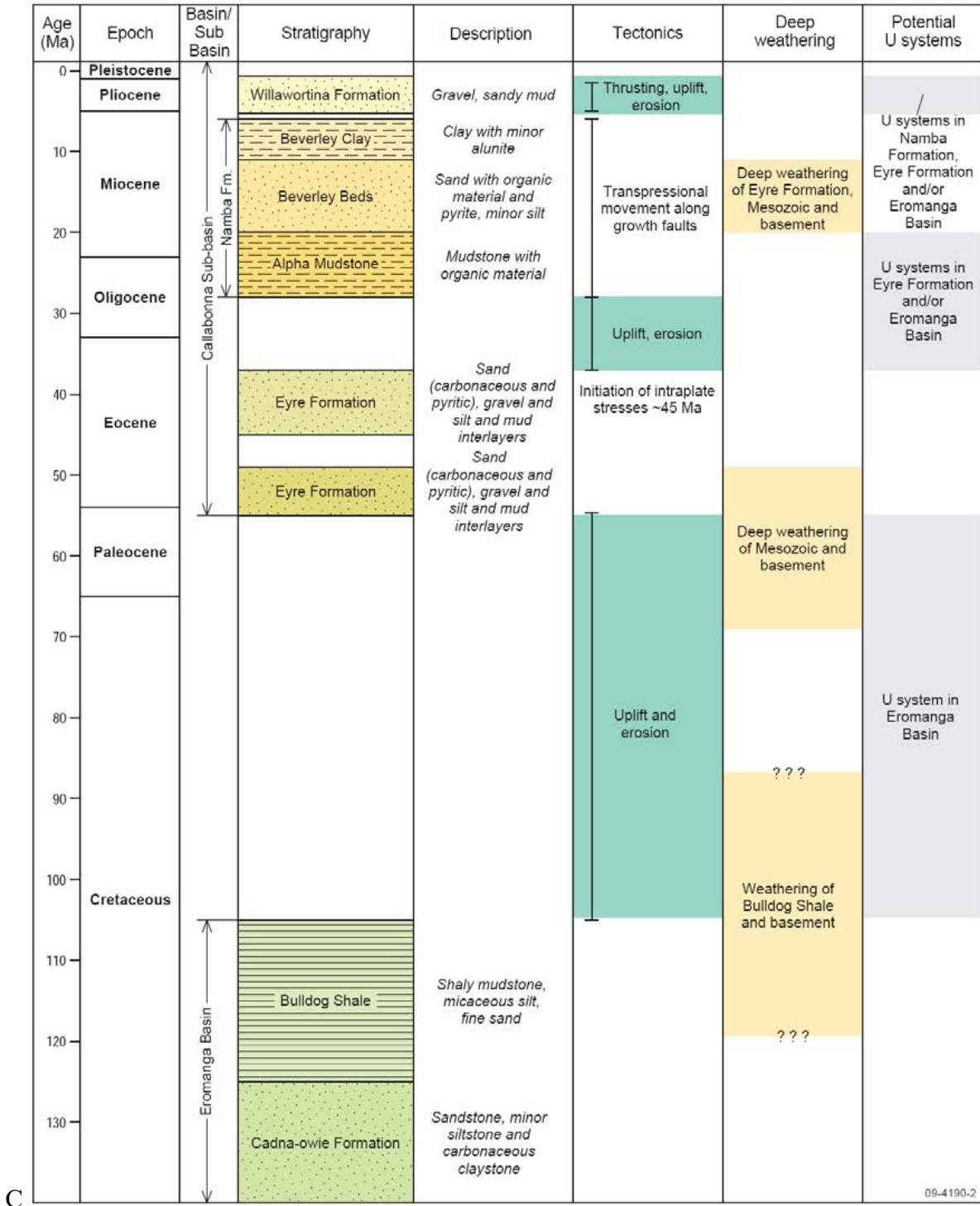
Quaternary deposition into the Callabonna Sub-basin has been predominantly alluvial fans and ephemeral stream sediments shed from the Northern Flinders ranges (Skirrow, 2009). The Willawortina Formation represents late Tertiary to late Plio-Pleistocene deposition of a fine to coarse facies, with the coarser facies dominant in the Beverley Area (Callen et al., 1995). Late Pliocene to Recent deposition is mainly in the form of paleochannel deposits formed in the upper surface of the Willawortina Formation (Callen and Benbow, 1995)

The last major phase of uplift began approximately 6-10 Ma (Skirrow, 2009) and is still ongoing (Quigley et al., 2007b). Skirrow (2009) suggest that this uplift has provided the hydrostatic head necessary to drive fluids through the Namba Formation as well as potential energy to mobilize uranium-rich detritus from the Mount Painter Inlier into the mineralized Frome Embayment.

1.3. Neotectonism

1.3.1. Brittle Structures at Surface

The Paralana Fault Zone has been previously studied for its examples of neotectonic faulting (Sandiford 2003; 2008 – see Heathgate Resources (2009); C  lerier et al., 2005; Quigley et al., 2006a; 2007b; 2010). Airborne electromagnetic surveys flown in 2010, further defined a series of imbricate thrust faults within the Frome Embayment that offset the embayment itself and produce both the Poontana Trough and the Poontana Inlier. The Poontana Trough is an approximately 150 m deep, range-parallel basin; the Poontana Inlier is an upthrust area of the Mount Painter Inlier (Fig. 1.4) (Roach et al., 2014). The Wooltana Range Front Fault is a westward-dipping thrust fault outcropping along the Wooltana Range (Sandiford, 2008 – in Heathgate Resources, 2009) and continuing under cover to the north, where it is truncated by the Poontana-Parabarana Fault System (Skirrow, 2009; Roach et al., 2014). The Poontana-Parabarana Fault (Vidnee Yarta Fault in Roach et al., 2014) has been identified through airborne electromagnetic surveying (Roach et al., 2014) and through drilling (Skirrow, 2009).



C

09-4190-2

Fig. 1.3: Stratigraphic column of the Frome Embayment from the Cretaceous to Recent (From Skirrow et al., 2009)

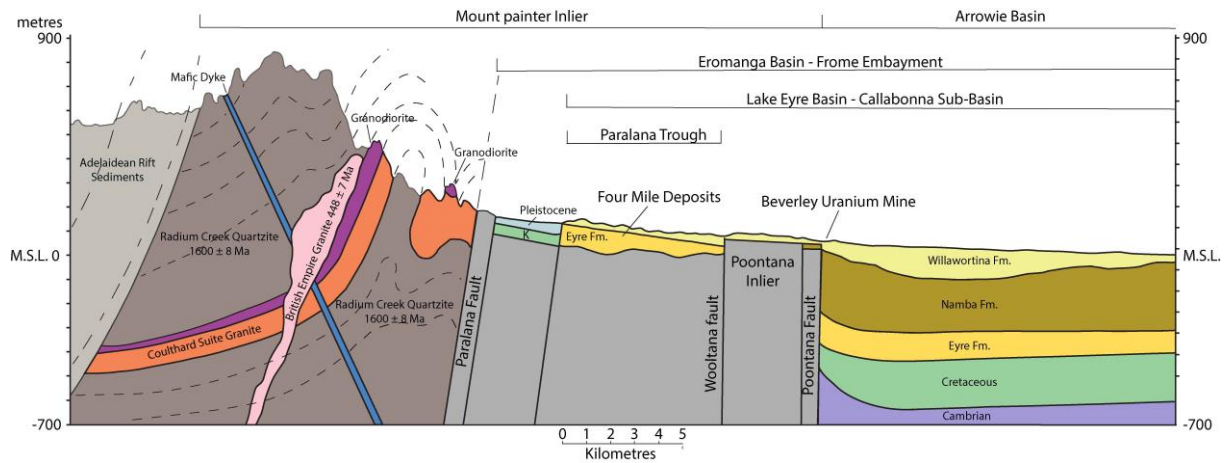


Figure 1.4: Simplified geological cross-section of the Mount Painter Region (Modified from Hore, 2015)

As previously mentioned in section 1.3.1, the Parolana Fault is interpreted to be one of the major faults defining the extent of Adelaidean Rif Complex sedimentation. The reactivation and inversion of this fault has produced the shallow westward-dipping thrust fault we see today (Preiss et al., 1987). Previous studies into the nature of the Parolana Fault Zone have differentiated a series of individual faults. Sandiford (2003) identified seven range-bounding faults responsible for much of the uplift of the Mount Painter Inlier: Wooltana-Range Front Fault, Poontana Fault, Lady Buxton Fault, Parolana Fault, Four Mile Fault, Adams Fault, and the Parolana Fault, all of which are westward-dipping thrust faults. Some of the observed examples of neotectonic faulting are exposed along the Adams and Lady Buxton faults where Meso- and Neoproterozoic rocks are juxtaposed against the low-lying Cretaceous to Recent pediplains of the Lake Frome Embayment (see Chapter 2)

1.3.2. Relationship between Faulting, Seismicity, and Heat Flow

In general, earthquakes are much less in intraplate settings relative to plate boundaries (Figure 1.5), but large intracontinental earthquakes have been observed (Hancock, 1988). Australia, while categorized as a relatively stable continental region, shows active seismicity in zones across the continent (Crone *et al.*, 1997; Leonard, 2008; Holford et al., 2014) with active intraplate deformation in distinct seismic zones (Figure 1.6). The South Australian Flinders Seismic Zone (FSZ) displays an abundant record seismicity with more than 75% of South Australian earthquakes (Glanville, 2010) (Figure 1.6). The seismicity is relatively low-level with only five earthquakes with magnitude >5.0 within the past century (Greenhalgh et al., 1994). Greater than 80% of recorded earthquakes have occurred within the upper crust at depths less than 20 km (Belperio, 1995; Tokarev, 2005). Sandiford (2008) conducted an in-depth study of the earthquake ground movement parameters of the Northern Flinders Ranges as part of the Four Mile West Mining Proposal. While there have been many earthquakes in the immediate

area, the most intense of them has been only an ML 4.0. As such, Sandiford (2008) concludes that ongoing earthquakes in the Northern Flinders region are responsible for estimated slip rates up to 0.065mm/year on the major faults of the Poontana Inlier.

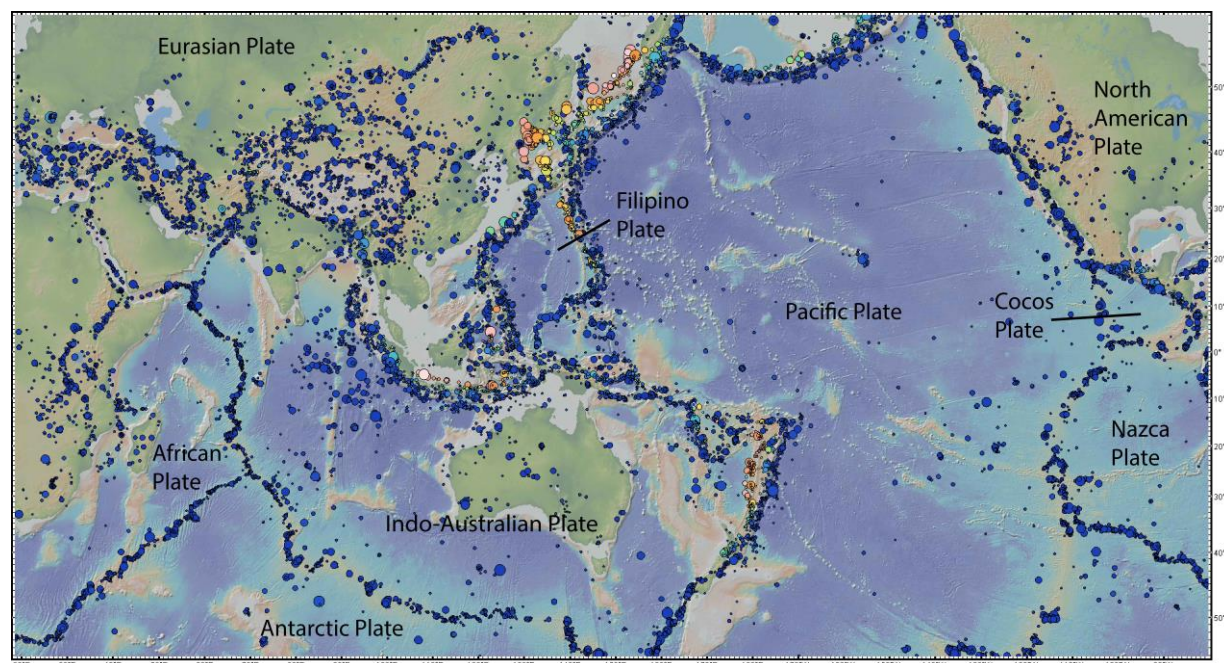


Figure 1.5: Distribution, magnitude (proportional to the size of the circles, $M_l > 4.5$), and relative depth range (blue < 20 km shallow to red > 100 km) of global seismicity (from 1960 to 2018) dominates at plate boundaries. Note the relatively quiet continental regions of Australia, North America and Central Asia. (data source USGS, presented through GeoMapApp).

The South Australian Heat Flow Anomaly is a broad zone of extreme heat flow that extends from the eastern Gawler Craton to the Mount Painter Inlier. Heat flow measurements from the Mount Painter area have recorded readings up to 125 mWm^{-2} (Neumann et al., 2000; Hillis et al., 2004; Holford et al., 2012). The high heat flow of the area has been attributed to an abundance of U, Th & K in the Mesoproterozoic rocks of the Mount Painter Inlier, where U concentrations regularly exceed 100 ppm (Paul 1998; Wülser, 2009). The radiogenic heat contribution of these elements to the overall heat flow depends greatly upon the age of the crust, rheology, elemental distribution, lithospheric thickness and geodynamic settings (Cull et al., 1982; Paul 1998; Sandiford et al., 1998). The average surface heat flow of continents has been measured at $\sim 65 \text{ mW/m}^2$ (McLennan & Taylor 1996). The Mount Painter Inlier, meanwhile, has a measured heat flow of over 125 mW/m^2 (Paul, 1998; Neumann et al., 2000; Holford et al., 2012). The enrichment of heat-producing elements within the Mount Painter Inlier implies a thermal weakening of the lithosphere (Sandiford et al., 1998b; Neumann et al., 2000; Celerier et al., 2005; Hillis et al., 2008). This thermal weakening of the crust and upper mantle has resulted in active intraplate deformation of the Flinders Ranges as demonstrated by directly

measured seismicity of the neotectonic record (see Figure 1.6; Hillis et al., 2008; Holford et al., 2012).

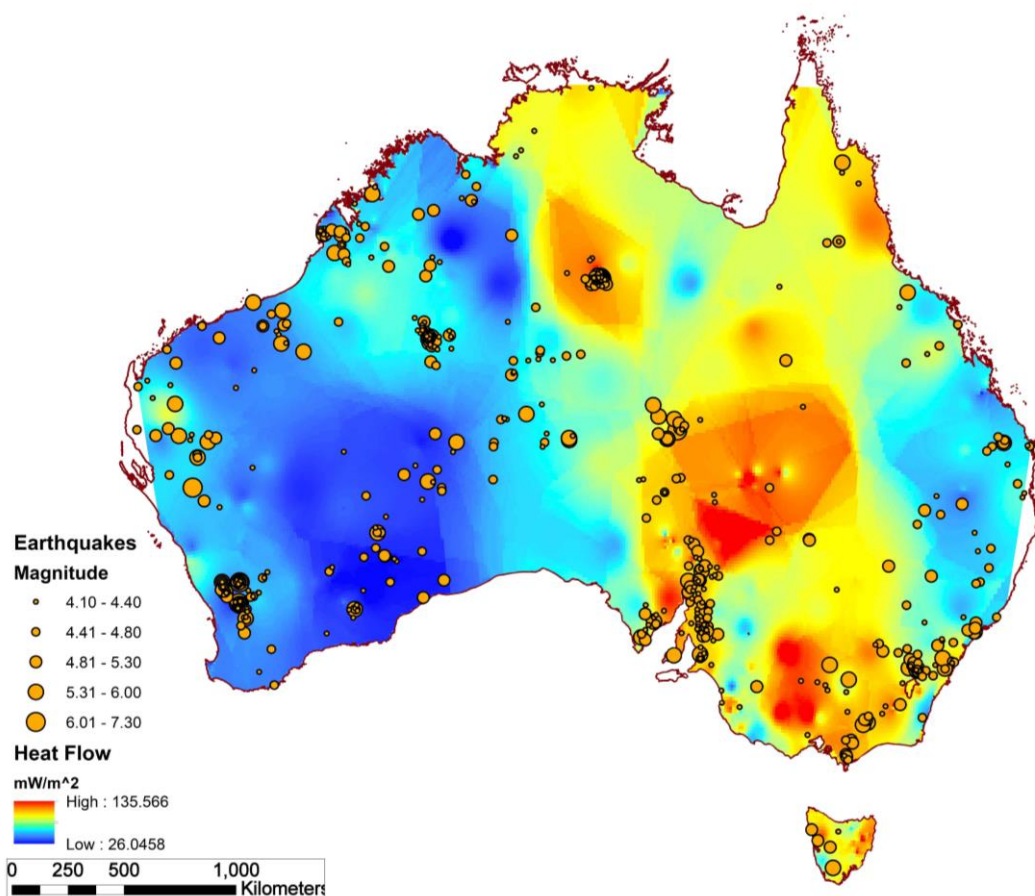


Figure 1.6: Historical earthquakes magnitude > 4.0 (1960 to 2018), interpolated heat flow based on database held by the International Heat Flow Commission, University of North Dakota

Chapter 2 – Structural Evolution of the Northern Flinders Ranges

The Mount Lofty and Flinders Ranges are an extensive zone of elevated topographic relief which corresponds with a region of active seismicity, referred to as the Flinders Seismic Zone, and the southern section of the Australian heat anomaly (Greenhalgh *et al.*, 1994; Belperio, 1995; Tokarev, 2005; Holford *et al.*, 2012). However, the interplay between seismicity, anomalous heat flow and stress field, which together influence the active faulting is poorly understood; leading to debate as to the cause of observed intraplate deformation (Jayawardena, 2013). Quaternary faulting within the Mount Lofty and Flinders Ranges has been interpreted as dip-slip reverse faulting (Clark & McCue 2003, Hillis *et al.* 2008) with up to several hundred metres of vertical displacement (Tokarev *et al.*, 1999, Sandiford, 2003, 2008; Quigley *et al.*, 2006b).

Much of this neotectonic intraplate deformation has been accommodated by the Paralana Fault Zone, which is a collection of sub-parallel faults that separates the north-eastern tip of the northern Flinders Ranges from the Mesozoic to Cenozoic sedimentary rocks of the Frome Embayment (Coats and Blissett, 1971; Preiss *et al.*, 1995; Davey, 2009; Thomas *et al.*, 2012). This long-lived set of faults were active in the Proterozoic when they acted as a rift-bounding normal faults during Adelaidean Rift Complex sedimentation (Paul *et al.*, 1999). Since then the fault zone has been reactivated as both reverse and strike-slip offsets (Paul *et al.*, 1999). The hangingwall of the Paralana Fault Zone, in the area of this study, is the Mesoproterozoic granitic and metasedimentary rocks of Mount Painter Inlier and the Neoproterozoic metasedimentary rocks of the Adelaidean Rift Complex (Preiss *et al.*, 1995). These have been thrust over Cenozoic to Recent sandstones and conglomerates of the Frome Embayment (Preiss *et al.*, 1995). Evidence of neotectonic faulting has been previously identified along the range front and estimated Quaternary displacements exceed ~150 m (C  lerier, 2005; Sandiford, 2008). Based on the onlapping, range bounding alluvial fan sequences, Sandiford (2003) and Quigley *et al.* (2006b) suggest between 800 and 1000 m of uplift has occurred since the end of the Miocene Meso-scale faults are observable within the Mesoproterozoic Mount Painter Inlier, Neoproterozoic Adelaidean Rift metasedimentary rocks, and the Cenozoic-Mesozoic sedimentary sequences of the Lake Frome Basin.

In this chapter we will explore the orientations and attitudes of meso-scale reverse faults along the eastern margin of the northern Flinders Ranges, proximal to the Mount Painter Inlier. Neotectonic thrust faulting in this area has been previously described (See C  lerier, 2005; Quigley *et al.*, 2006b; Sandiford, 2008, Hill and Hore, 2011; Jayawardena, 2013), though no

previous studies have catalogued the individual fault segments of the range front escarpment. Through this study we will be describing and analysing an understudied zone of Australia. The detailed analysis of the meso-scale faults that bound the Flinders Ranges conducted in this study will improve our understanding of the neotectonic evolution of this dynamic intraplate deformation zone.

2.1. Methods

2.1.1. Field Observations and Remote Sensing

Between April 2016 and November 2017, I conducted a total of 33 days field mapping. During this time, 55 faults were identified over an area approximately 150km² along the range front (Table 1; Figure 2.1). The research area extended from the Arkaroola Creek in the south to the Hidden Valley entrance in the north along the range front (Figure 2.1). Each observed fault was georeferenced, measured, described, photographed, and where possible, a fault rock sample was taken. Due to the sensitive ecology of the area and its protected status as a wilderness sanctuary, all fault rock sampling was completed with grab samples only; no oriented samples were taken.

Locality	Eastings	Northing	Strike	Dip	Dip Dir.	Max Age	Locality	Eastings	Northing	Strike	Dip	Dip Dir.	Max Age
1	348350	6651010	211	40	121	Pleistocene	29	349436	6655216	144	20	54	Mesoproterozoic
2	353356	6663862	26	31	116	Cretaceous	30	349314	6655202	285	22	195	Mesoproterozoic
3	354014	6664798	90	40	0	Pleistocene	31	344447	6646612	139	40	49	Neoproterozoic
4	373583	6680312	72	17	342	Cretaceous	32	352596	6662888	230	82	140	Mesoproterozoic
5	373583	6680312	6	48	276	Cretaceous	33	351902	6661919	331	41	241	Mesoproterozoic
6	346252	6646524	150	48	60	Neoproterozoic	34	351792	6661948	154	21	64	Mesoproterozoic
7	353798	6664880	0	48	270	Cretaceous	35	351743	6661972	319	43	229	Mesoproterozoic
8	353758	6665011	58	40	302	Neoproterozoic	36	351714	6661933	96	19	6	Mesoproterozoic
9	353758	6665011	104	12	14	Neoproterozoic	37	351138	6661000	303	26	213	Mesoproterozoic
10	353719	6665007	207	25	117	Neoproterozoic	38	351117	6660985	343	52	253	Mesoproterozoic
11	353657	6665131	40	62	310	Mesoproterozoic	39	351014	6660959	65	21	335	Mesoproterozoic
12	349440	6659645	326	38	236	Mesoproterozoic	40	350975	6660964	310	45	220	Mesoproterozoic
13	349287	6659476	14	22	284	Cretaceous	41	351001	6660855	228	35	138	Mesoproterozoic
14	349312	6659363	43	41	313	Cretaceous	42	354674	6665438	33	44	303	Mesoproterozoic
15	349222	6659097	52	45	322	Cretaceous	43	354586	6665421	35	68	305	Mesoproterozoic
16	349251	6659088	191	85	101	Cretaceous	44	354557	6665503	240	40	150	Mesoproterozoic
17	349251	6659088	62	87	332	Cretaceous	45	354557	6665503	216	56	126	Mesoproterozoic
18	349321	6659068	195	73	105	Cretaceous	46	354610	6665687	121	29	31	Mesoproterozoic
19	349718	6659014	256	72	166	Cretaceous	47	353376	6665592	203	29	113	Pleistocene
20	349924	6659660	268	48	178	Mesoproterozoic	48	349931	6660790	359	40	269	Mesoproterozoic
21	348970	6649200	290	45	200	Neoproterozoic	49	349931	6660790	39	18	309	Mesoproterozoic
22	348904	6648890	28	30	298	Neoproterozoic	50	356604	6667034	261	80	171	Mesoproterozoic
23	350305	6644613	171	41	81	Neoproterozoic	51	350176	6657586	346	20	256	Mesoproterozoic
24	348187	6653698	32	42	302	Mesoproterozoic	52	350041	6657656	198	13	108	Mesoproterozoic
25	348925	6654720	178	52	88	Mesoproterozoic	53	349924	6657777	148	22	58	Mesoproterozoic
26	348930	6654718	202	64	112	Mesoproterozoic	54	349776	6657767	258	34	168	Mesoproterozoic
27	349042	6654697	220	70	130	Mesoproterozoic	55	348993	6660249	325	25	235	Mesoproterozoic
28	349042	6654697	250	31	160	Mesoproterozoic							

Table 2.1: Table of fault observations

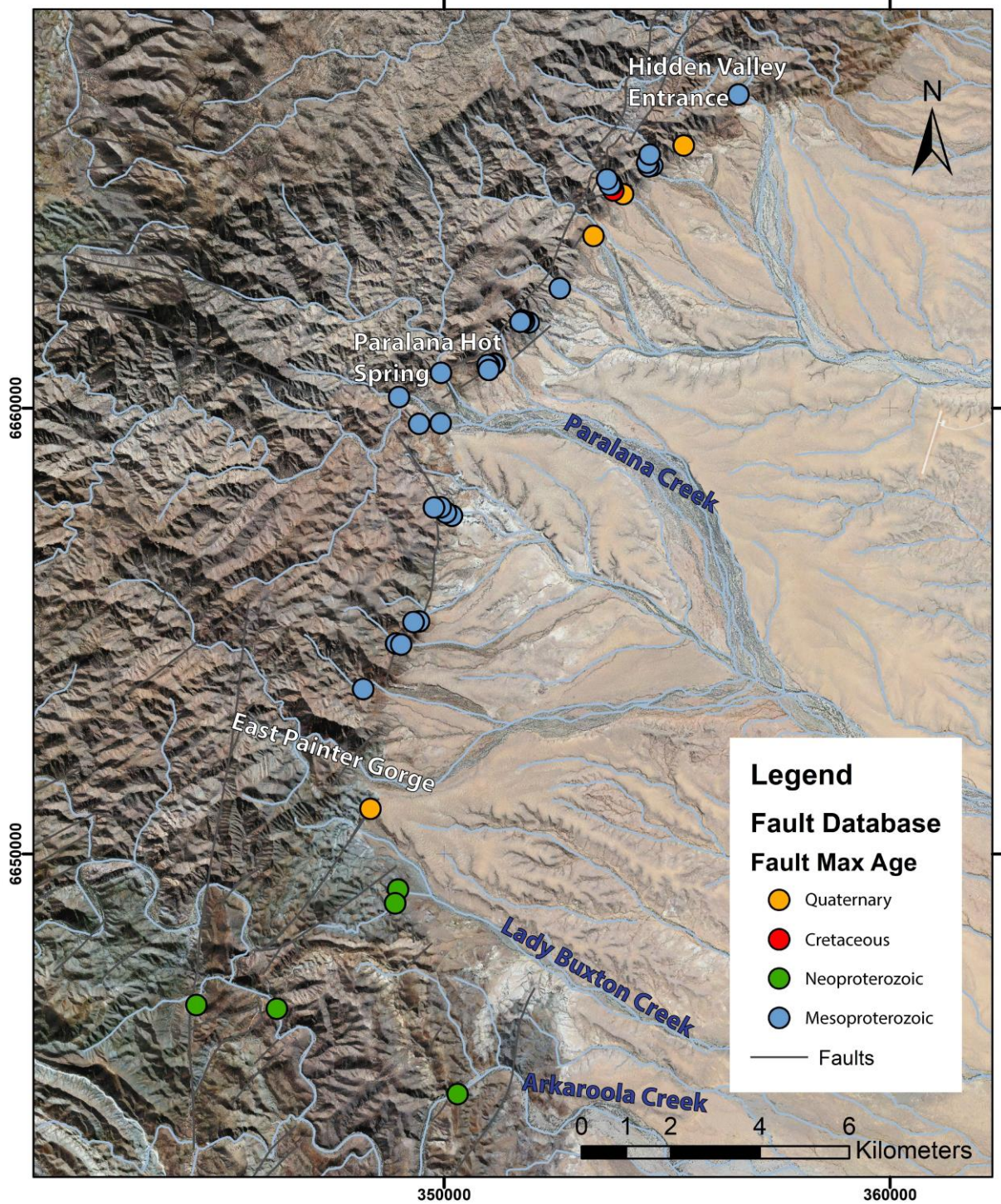


Fig 2.1: Map of the research area with observation locations coloured relative to the minimum age of the lithologies juxtaposed by the faulting.

Spatial mapping was conducted using the ArcMap suite of software. Maps and figures were facilitated by high-resolution Quickbird satellite imagery for the Mount Painter Inlier and surrounding area. The resulting imagery has a pixel size of 60 cm x 60 cm and was rectified relative to numerous control points leading to an overall positional accuracy of >50 cm horizontal and >1 m vertical accuracy. The imagery was kindly provided by the Government of South Australia Department of State Development. The image was heavily used for

orienting, spatial data interpretation and identification of ground features. Landsat 7 hyperspectral imagery was also used to identify lithological variations and structural zones across the research area. Several different band combinations were attempted to deduce which would be most useful for delineating rock packages in this area. A composite image with red, green, and blue colours corresponding to bands 7, 5, and 1, respectively, was chosen as it showed the greatest contrast between units (Figure 2.3). Landsat 7 band number 7 corresponds to the Shortwave Infrared (SWIR) 2 with a wavelength of 2.09 to 2.35 μm . Band 5 is the Shortwave Infrared (SWIR) 1, with wavelength ranging between 1.55 to 1.75 μm . Band 1 represents the colour blue within the visible light spectra and has a wavelength between 0.45 and 0.52 μm (Weng, 2007; Gul et al., 2012).

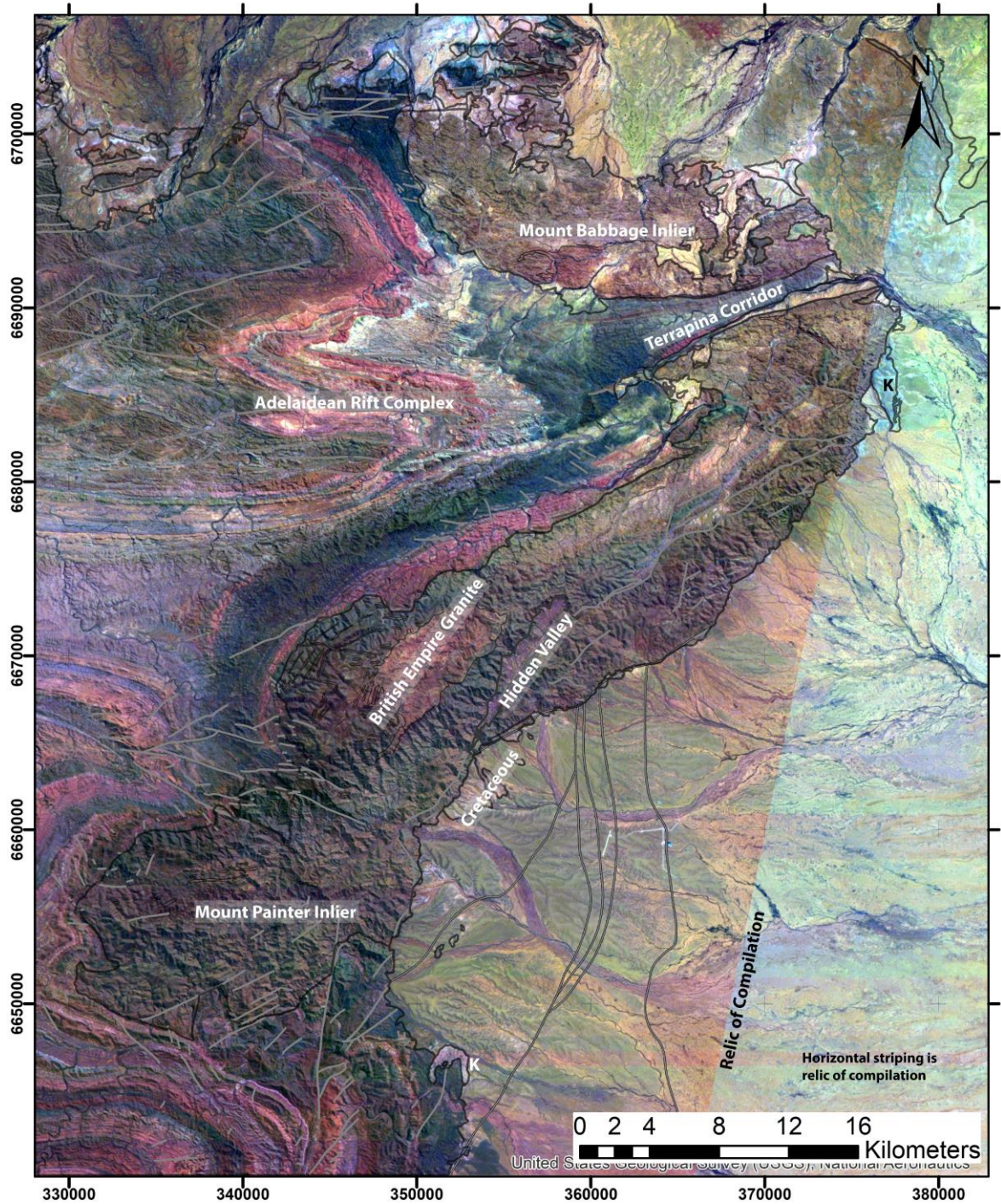


Fig 2.2: Landsat 7 hyperspectral image (Bands 7,5,1 corresponding to the R,G,B colours respectively). Grey lines represent faults identified by historical maps, AEM interpretation and field mapping. (Note: the horizontal striping and the line of anomalous colour on the left are relics of the compilation process)

2.2. Observations

2.2.1. Lady Buxton Fault Locality

The Lady Buxton Fault locality, (Fig. 2.4) is one of the most impressive and accessible examples of Neotectonic activity along the Paralana Escarpment. Neoproterozoic Wywyana Formation hanging wall is directly juxtaposed against the Pliocene Arrowie Formation footwall by a $\sim 30^\circ$ W-dipping thrust fault (Sandiford, 2003; C  lerier, 2005; Quigley et al., 2007). The northeastern-most tip of the fault's exposure offsets Pleistocene Arrowie formation, however, along much of the fault length the footwall consists of Wooltana Volcanics (790 Ma). The overall outcrop is approximately 10 m wide and 4 m high.

The Arrowie Formation footwall sediments, which are a submember of the reach a maximum of approximately 150 m thickness (Callen and Tedford, 1976), indicating at least 150 m of dip-slip displacement since the early Pliocene. The Arrowie formation consists of polymictic angular to subrounded outwash gravels with clasts reaching an observed maximum of 12 cm and set in a red-brown sandy matrix of quartz and haematite. Unique to this locality are abundant euhedral to anhedral maghemite crystals weathering out from the matrix and washing down the southern slope. (See subsection 2.4.2).

The Wywyana Formation hangingwall is a marble deposited early in the Adelaidean rift Complex sedimentation, approximately 780 Ma. A prominent ridge of thrustured Wywyana marble strikes 211° toward the range front. This marble is typically a buff-tan colour in outcrop with abundant recrystallized fractures and gashes and occasional ptymatically folded quartz veins

The fault plane has exceptional exposure at the historic Lady Buxton Mine, an artisanal copper mine exploited in the 1890s. The deposit hosted high-grade copper ($>15\%$ Cu) however mineralization did not continue at depth and the mine was abandoned. Abundant calcite precipitation has infiltrated fault-plane-parallel fractures within the 5 to 10-cm thick fault gouge, and there is minor gypsum.

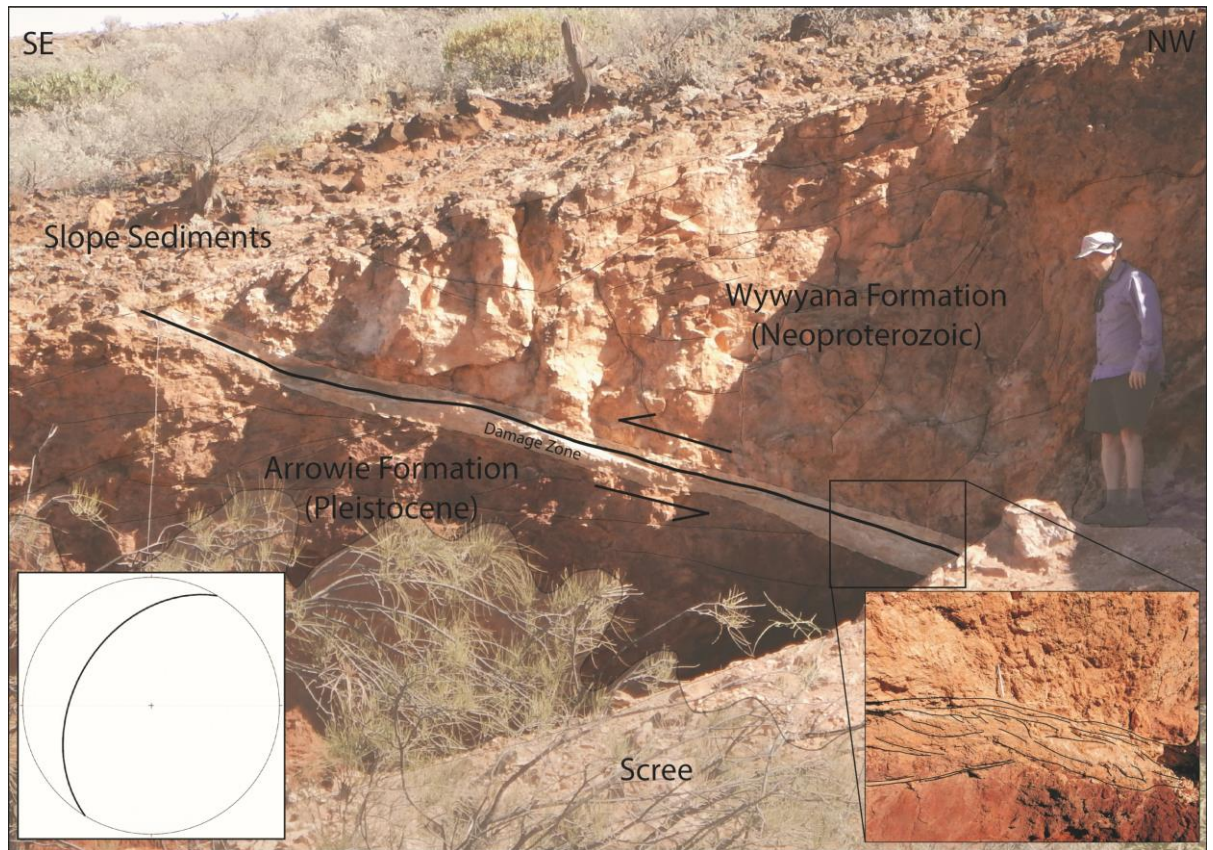


Fig 2.3: Lady Buxton Fault locality; Fault attitude:211/40NW

2.2.2. Teasdale Fault Locality

The Teasdale Fault locality (Fig. 2.5), named after Jon Teasdale who discovered the fault exposure in 1993 (Teasdale, 1993; Sandiford 2008) is located approximately 8 km north of the Paralana Hot Springs. The locality shows a set of SW-striking parallel imbricate thrust faults which dip $\sim 30^\circ$ NW (Fig. 2.4) within a 5m wide zone. The upper fault juxtaposes Mesoproterozoic Radium Creek metasedimentary rocks over the Eocene Eyre Formation. The approximately 2.5m thick Eyre Formation is subsequently thrust above Pleistocene Willawortina Formation by a lower fault plane.

The uppermost lithology in this imbricate set, the Radium Creek metasediments, consists of a bright red-orange mottled quartzite with welded quartz clasts ranging from 0.1 to 1 mm. The rock is heavily-fractured with no apparent preferential fracture orientation. The central block in the imbricate system consists of Eyre Formation, a fine- to medium-grained, compositionally mature sandstone. The footwall unit contains very angular, poorly sorted conglomerates presumed to be of the Willawortina Formation which is overlain by a wedge of faulted scree which contains angular polymictic clasts up to 20cm in diameter. The whole system is overlain by a thin veneer of Recent scree which obscures the trace of the fault northeast along the hill. The lower fault of the zone hosts faint slickenlines (trending 296 and dipping 29), preserving evidence of exclusively dip-slip movement.

Callen and Tedford (1974) measured the Willawortina Formation thickness at 150m. Thus, at least 150 m of offset must have occurred to expose the observed lithological relationships. The continuous veneer of Recent scree across the system implies that the most recent displacement must have predated the latest episode of scree formation. Sandiford (2008) provides an optically stimulated luminescence (OSL) age for the hill-scree wedge in the footwall to be no younger than 36 Ka (See section 2.3.1.). There is minor calcite and gypsum cementation within the fault gouge, indicating that this structure acts as a conduit for meteoric fluids and surficial weathering. The surface of the Willawortina formation in the system's footwall is also covered in a thin crust gypsum mineralization.

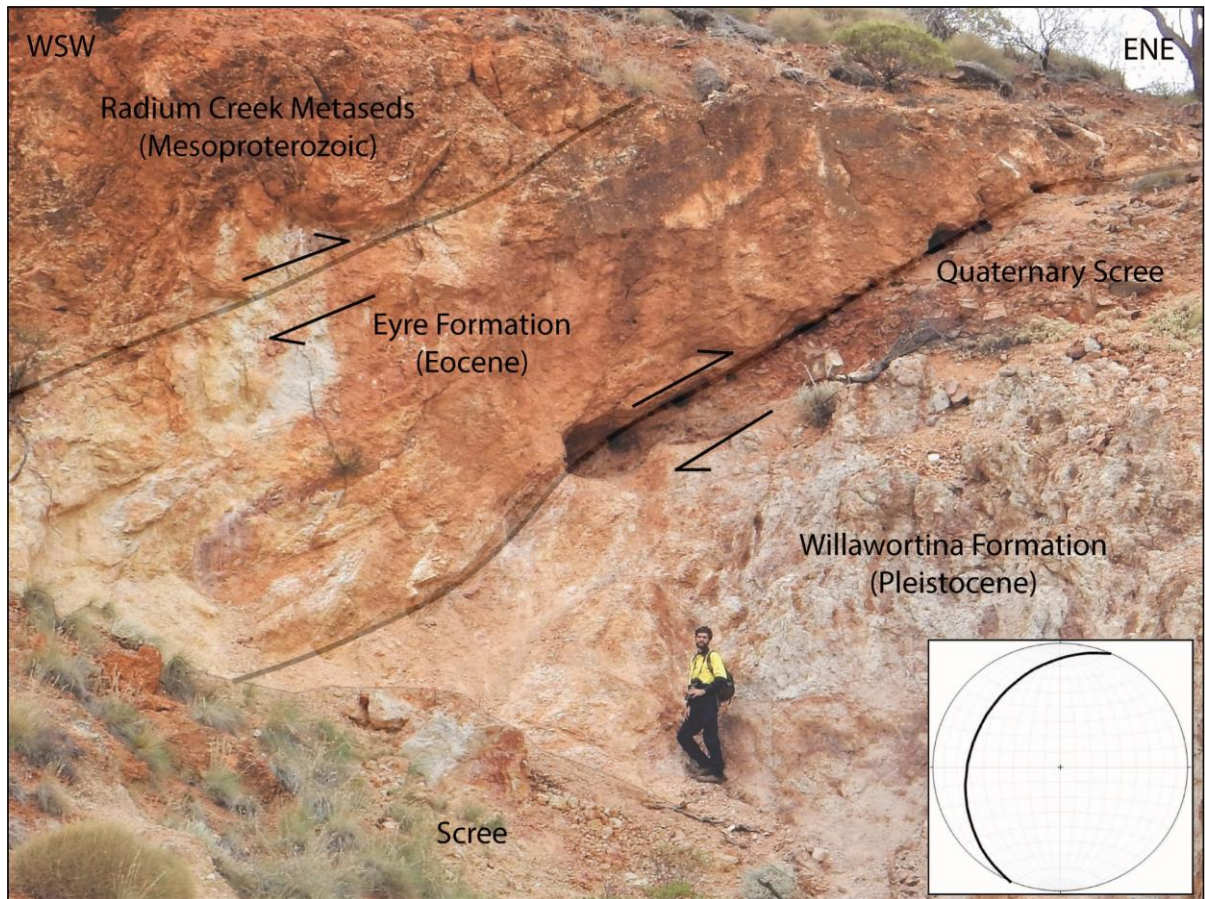


Fig 2.4: Teasdale Fault Locality; Fault attitude:203/29NW

2.2.3. Cadna-Owie Fault Locality

Approximately 5 km north of the Paralana Hot Springs is an example of faulting in which the Cretaceous Cadna-Owie Formation, a polymictic diamictite, is internally offset by a NE-SW striking, 30°SE dipping fault plane defined by a thin layer of calcite mineralization with minor gypsum. The Cadna-Owie Formation here has clasts ranging in size from a <10 mm to >1 m in diameter (Figure 2.6). Clasts are typically rounded to subrounded, though the occasional subangular clast can be seen in the river cut-bank. The clasts are matrix supported with a sandy-silty matrix that has been moderately to poorly cemented by carbonate. The fault has cross-cut and is offsetting a 45cm diameter granitic boulder by approximately 1m.

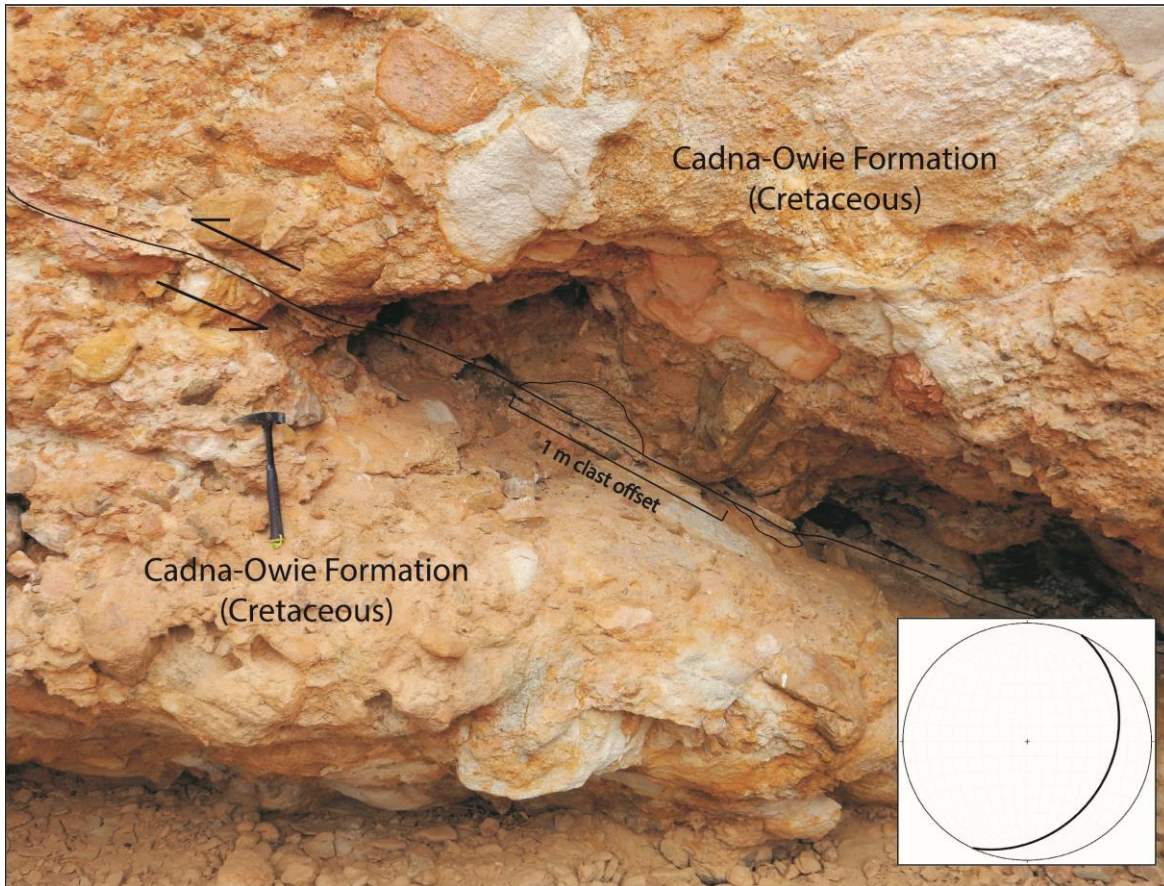


Fig. 2.5: Cadna-Owie Fault. *Fault attitude: 026/31 SE*

2.2.4. Faults within the Mount Painter Inlier

Most of the faults documented in this study do not record demonstrably neotectonic deformation, i.e. do not that directly involve Miocene to Recent rocks. Instead, most observed faults are hosted by Mesoproterozoic, Neoproterozoic or Cretaceous-aged rocks where an estimation of fault timings by stratigraphic relationships is ambiguous. Fault 26, for example, juxtaposes Mount Neil Granite (hangingwall), dated to a minimum age of 1569 ± 14 Ma (Hore, 2015), against Freeling Heights Quartzite, dated to a maximum age of ~ 1590 -1580 Ma via detrital zircons (Hore, 2015; Figure 2.6). Both the hangingwall and footwall lithologies host a set of fractures which roughly parallel the fault plane. The fault core is 10 cm wide, and the fault gouge is very friable. Other faults within the Mount Painter Inlier, including fault 27, (Fig. 2.7) host more secondary silica within the fault rocks. For an analysis of observed fault rock characteristics, please refer to Chapter 3. Table 2.1 outlines the remainder of the faults not directly described in text.

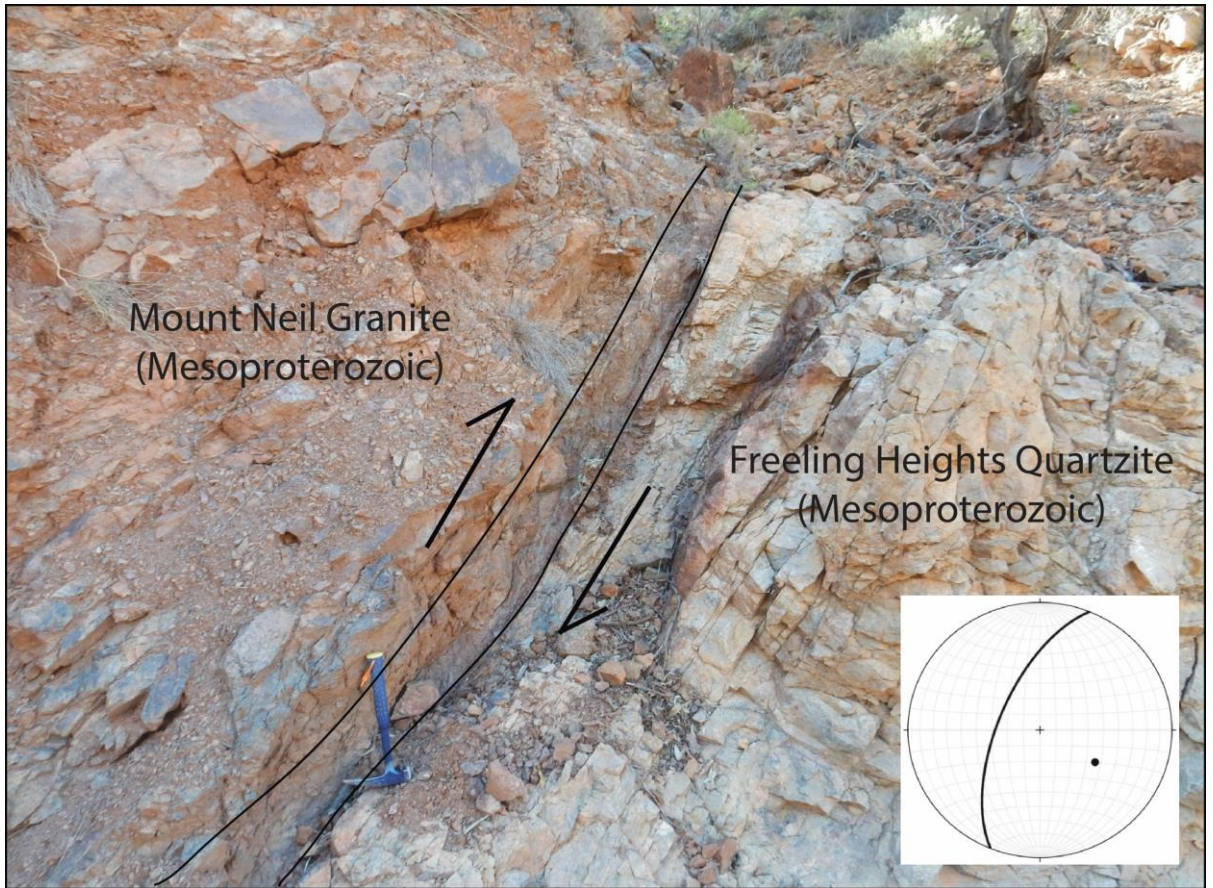


Fig. 2.6. Fault locality 26; Fault attitude: 202/64 NW

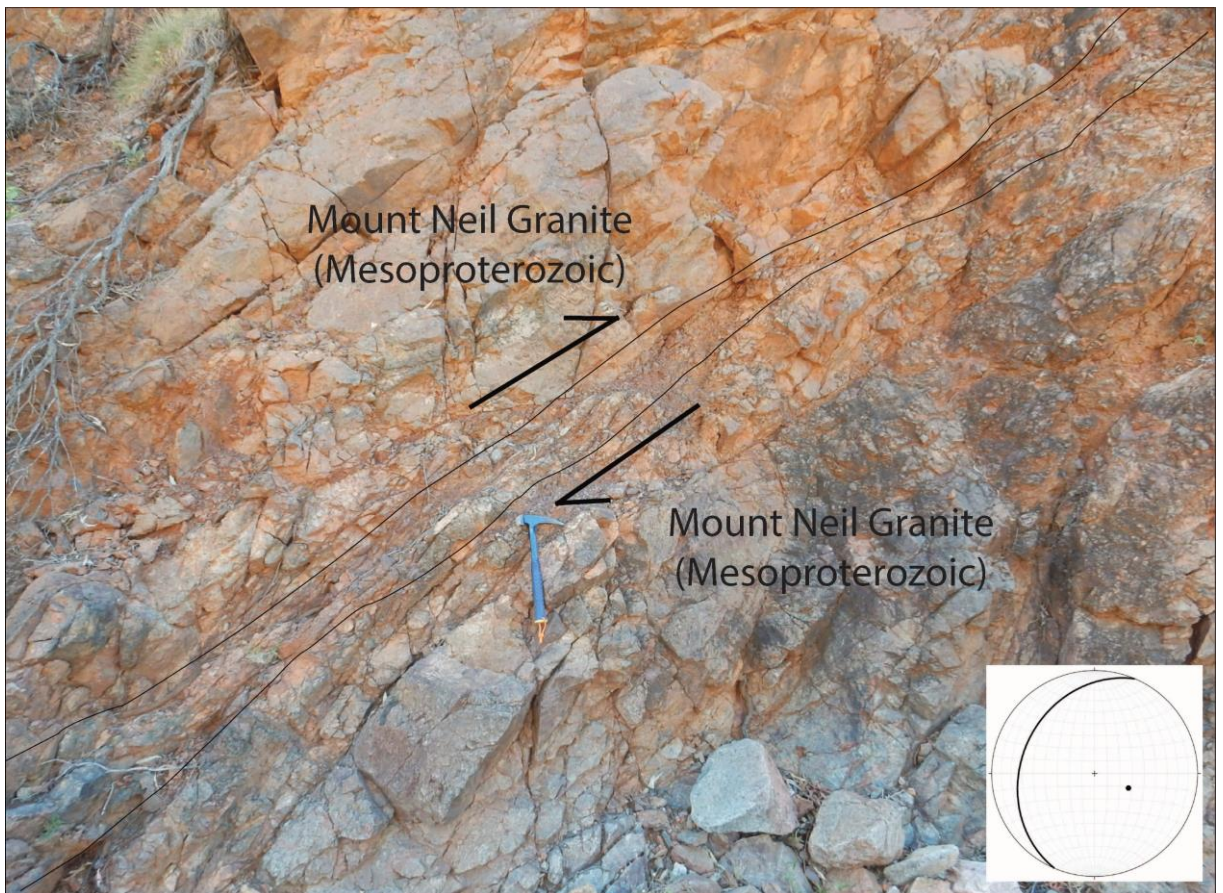


Fig. 2.7: Fault Locality 8; Fault attitude: 203/29NW

2.2.5. Conjugate sets of faults

Inputting measured faults for stereographic analysis revealed three individual conjugate sets within the data set. Conjugate sets of faults form predictably within a rock when subjected to stress, thus, the individual conjugate sets are considered related both structurally and temporally (Peacock et al., 2016; Peacock et al., 2017).

Conjugate Set 1 (Figure 2.3b) includes 18 individual reverse faults from along the Paralana Escarpment. The fault core width ranges from 5 cm to 30 cm and the fault rocks within show variable mineralogy and secondary cementation with calcite or silica. Four of the faults have preserved slickenlines, and all have internal fault rock fabrics representative of reverse movement. The overall orientations of these faults average NE-SW strike and dip variably to the NW and SE forming a conjugate set. Those that dip to the NW have an average strike of 035.8° (SD = 13.5°) and an average dip of 36.8° (SD = 7.7°). Those that dip to the SE have an average strike of 226.6° (SD = 19.4°) and an average dip of 36.3° (SD = 8.9°). Stereonet analysis of the fault set indicates that the principal stress direction (σ_1) was approximately NE-SW (311°) at the time of formation.

Conjugate Set 2 (Figure 2.3c) contains 12 faults, all of which are reverse faults measured either within the Mesoproterozoic Mount Painter Inlier or the Adelaidean sedimentary rocks south of the Mount Painter Inlier and spread along the range front. Fault cores for these faults range from 5 cm to 20 cm and show variable degrees of silica cementation; calcite cementation is absent. Fault rock mineralogy reflects the mineralogy of the host lithologies. The orientations of these faults have an overall E-W strike and variable N-S dip forming a conjugate set. The faults that dip N have an average strike of 280° (SD = 16.0°) and dip of 35° (SD = 10.2°). Those that dip S have an average strike of 74.8° (SD = 22.8°) and a dip of 17.4° (SD =). Stereonet analysis indicates that σ_1 was approximately N-S (004°) at the time of formation.

Conjugate Set 3 (Figure 2.3d) is a suite of 13 reverse faults observed exclusively within Mesoproterozoic-aged host rocks and spread along the range front. The cores of these faults range from 5 cm to 20 cm in width, and the fault rocks are variably silicified. Like Conjugate set 2, there is no evidence of calcite cementation. Faults of this set strike NW-SE with dips toward both NE and SW. Faults that dip to the NE have an average strike of 319° (SD = 9.7°) and a dip of 36.3° (SD = 8.0°). Those that dip to the SE have an average strike of 141° (SD = 11.6°) and a dip of 26.4° (SD = 7.5°). Conjugate set 3 has σ_1 of NE-SW (047°).

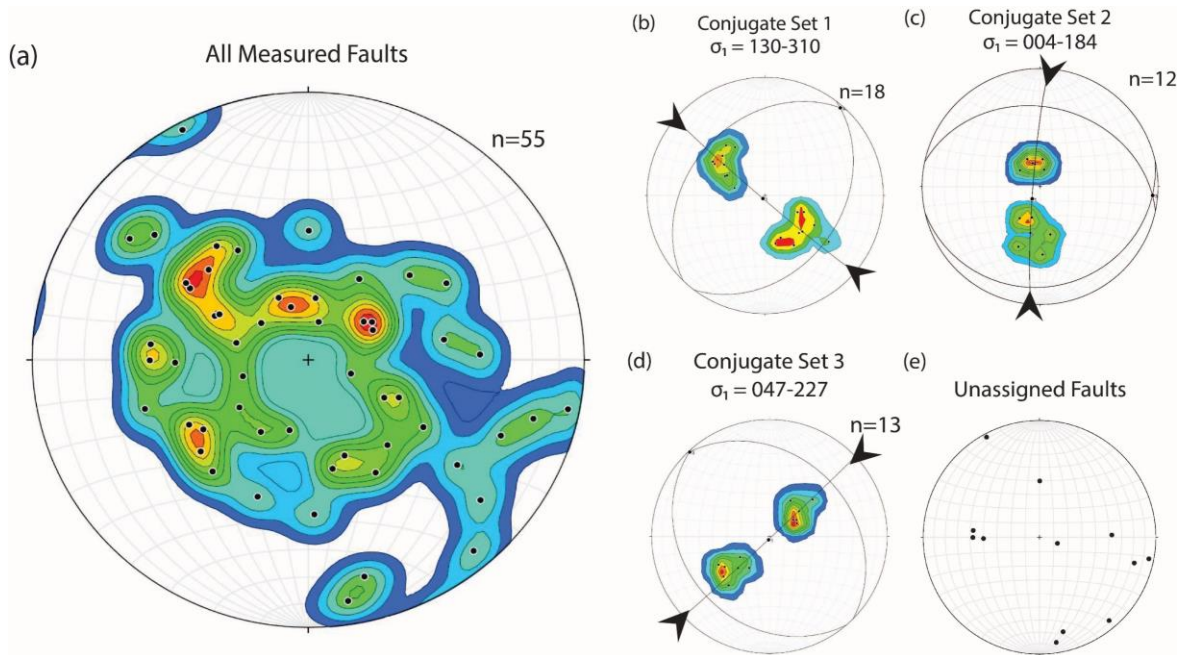


Fig. 2.8: Contoured equal area lower hemisphere stereonet plots: a) All 55 observed reverse faults, b) Conjugate Set 1 – Striking NE-SW, c) Conjugate Set 2 – Striking E-W, d) Conjugate Set 3 – Striking NW-SE, e) Unassigned Faults

The 12 faults that do not conform to one of these sets are outliers to the overall data trends (Figure 2.3e – Unassigned faults plot). These zones of weakness and other rheological abnormalities along the Parana escarpment could be responsible for anomalous accommodation strain. Unfortunately, there does not appear to be any clear spatial controls on the fault orientations observed.

2.3. Discussion

2.3.1. Relative Dating of Faults

Relative ages of planar features can be provided by cross-cutting relationships. Unfortunately, the veneer of Holocene to Recent sediments along the eastern range front of the Flinders Ranges have obscured much of the fault exposure, and no cross-cutting relationships could be deduced. Ages of the host rocks can be used to determine the relative age of faulting and is particularly useful where faults displace very young sediments, such as the Lady Buxton Fault and Teasdale Fault. However, for faults occurring in older sediments it is of limited use. In addition, conjugate sets, defined above, with their calculated maximum principal stress directions were compared to the paleostress models for Australia to aid determination of age (Figure 2.9) (Reynolds et al., 2002; Müller et al., 2012).

Conjugate set 1 contains all the observed examples of neotectonic faulting, as deduced by their stratigraphic relationships. The Calculated NW-SE (311°) maximum principal stress orientation corresponds to the current NW-SE compressive stress field (Reynolds et al., 2002; Müller et al., 2012). Thus, it can be assumed that these faults formed within the neotectonic stress regime within the last 6 Ma (Figure 2.9).

Conjugate set 2 incorporates faults with host ages ranging from Mesoproterozoic to Neoproterozoic; making the relative ages of the faults unreliable. However, this set, with its N-S (004°) compressive calculated principal stress field corresponds with the modelled paleostress of the Australian continent during the Cretaceous (Müller et al., 2012). This orientation of N-S compression was also prominent during the regional deformation of the Alice Springs Orogeny (450-300 Ma) in Central Australia (de Gromard et al., 2012). This regional deformational event was typified by abundant shearing in Central Australia (Fournier et al., 2016). Fournier et al., (2016) used Rb/Sr biotite ages to estimate cooling to 300°C (Sr closure temp for biotite) to have occurred between 335-290 Ma in the central Australian Alice Springs Orogeny, which is contemporaneous with an approximately 400°C cooling event and denudation in the northern Flinders Ranges (McLaren et al. 2002). Therefore, it is reasonable to conclude that these E-W striking structures have been reactivated during the Cretaceous (~ 100 Ma) after a possible initial phase during the Paleozoic (~ 450 -300 Ma). Additional research into the influence of the Alice Springs Orogeny on the Mount Painter Inlier is needed to deduce if these fault structures are reactivations or primary structures formed in the Cretaceous.

The calculated maximum principal stress orientation for conjugate set 3 is oriented NE-SW (047°). This orientation corresponds with Late Miocene (11 to 6 Ma) compression (Fig. 2.9B), as modelled by Müller et al., (2012). During the Late Miocene there was continued deposition of the Middle to Upper Namba Formation, followed by the onset of uplift of the northern Flinders Ranges. Interestingly, all examples of this conjugate set of faults are hosted by rocks of Mesoproterozoic age.

In some studies of the Flinders Ranges and Mount Lofty Ranges, the application of additional dating techniques have been used successfully to further refine the age of the latest deformational event (See Quigley et al., 2006a, b; Quigley et al., 2007b; Sandiford, 2008). For example, Optically-Stimulated Luminescence (OSL) dating has been applied in the central Flinders Ranges to date fault movement (eg., Quigley et al. 2006, 2007b,c; Jayawardena, 2012), the high levels of natural radioactivity in the Mount Painter Region mean that OSL is of little use (Sandiford, 2008). Elevated levels of radioactivity saturate the quartz grains used in the OSL dating within approximately 10,000 years (Sandiford, 2008). Thus, unfortunately, the

method is unable to elucidate ages earlier than the Holocene. Estimates of fault activity and fault slip rates can only be based on indirect measures such as the erosion rates inferred from cosmogenic studies.

The outlier faults which don't correspond to any of the previously-defined conjugate sets are interpreted to be the result of reactivation of faulting along a pre-existing plane of weakness within the Mount Painter Inlier. For example, there are six individual planar fabrics present with the Mount Painter Inlier (Teale, 1993), The most prominent of these is a steeply-dipping ENE-trending penetrative foliation defined by biotite and muscovite. These planes of weakness are interpreted to have been reactivated as slip planes facilitating the accommodation of oblique stresses. Thus, they do not correspond with previously-defined tectonic stress regimes.

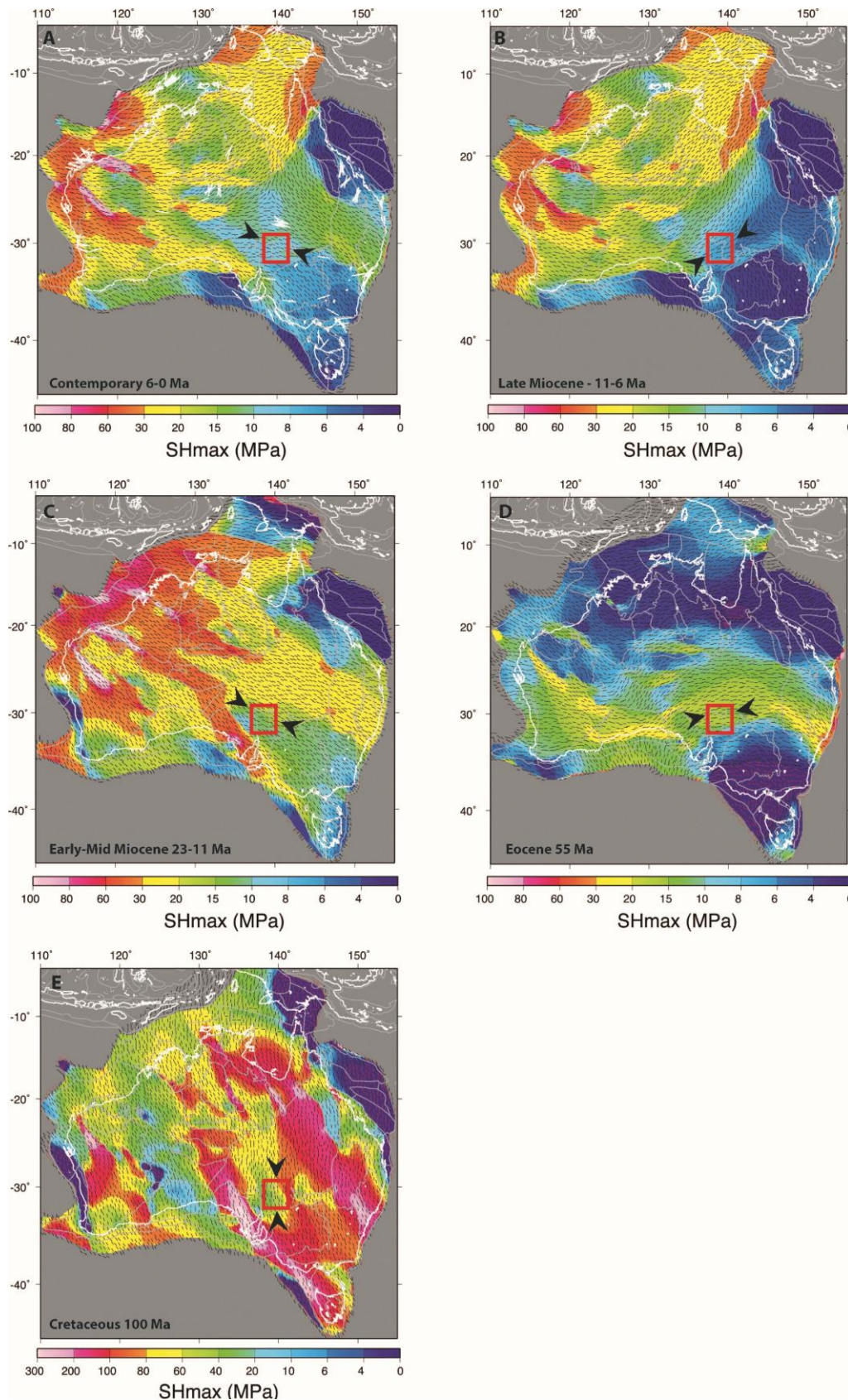


Fig. 2.9: Compilation of paleostress models through time from Muller et al., (2012). A) Modelled contemporary (6–0 Ma) maximum horizontal stress. B) Modelled maximum horizontal stress for the Late Miocene (11–6 Ma). C) Modelled maximum horizontal stress for the Early to Middle Miocene (23–11 Ma). D) Modelled maximum horizontal stress for the Eocene (ca 55 Ma). E) Modelled maximum horizontal stress for the Cretaceous (ca 100 Ma).

2.3.2. Neotectonic Landscape Evolution

The Paralana High Plains (Figure 2.10) are a region of alluvial fans deposition at the foot of the Northern Flinders Ranges. Their western margin abuts the Paralana Escarpment, while the eastern margin is marked by lineaments corresponding to approximately 10 metres of vertical offset. These lineaments also mark the transition from incised channel forms to the west to distributary channel forms to the east (Figure 2.10) The dissection of the plains was identified as being influenced by active faulting by Sandiford (2008) and corroborated with AEM surveying, as described by Roach et al, (2014). The southern linear feature (Wooltana Range Front Fault), aligns with the continuation of the Eastern Range Front in the vicinity of the Wooltana homestead. There have been no detailed studies of the Wooltana Range Front Fault escarpment and hence there has been no direct stratigraphic evidence of the tectonic activity of this fault. However, the morphological similarities between the Woolatana scarp and the Paralana scarp indicate that the Wooltana Range Front Fault is likely active.

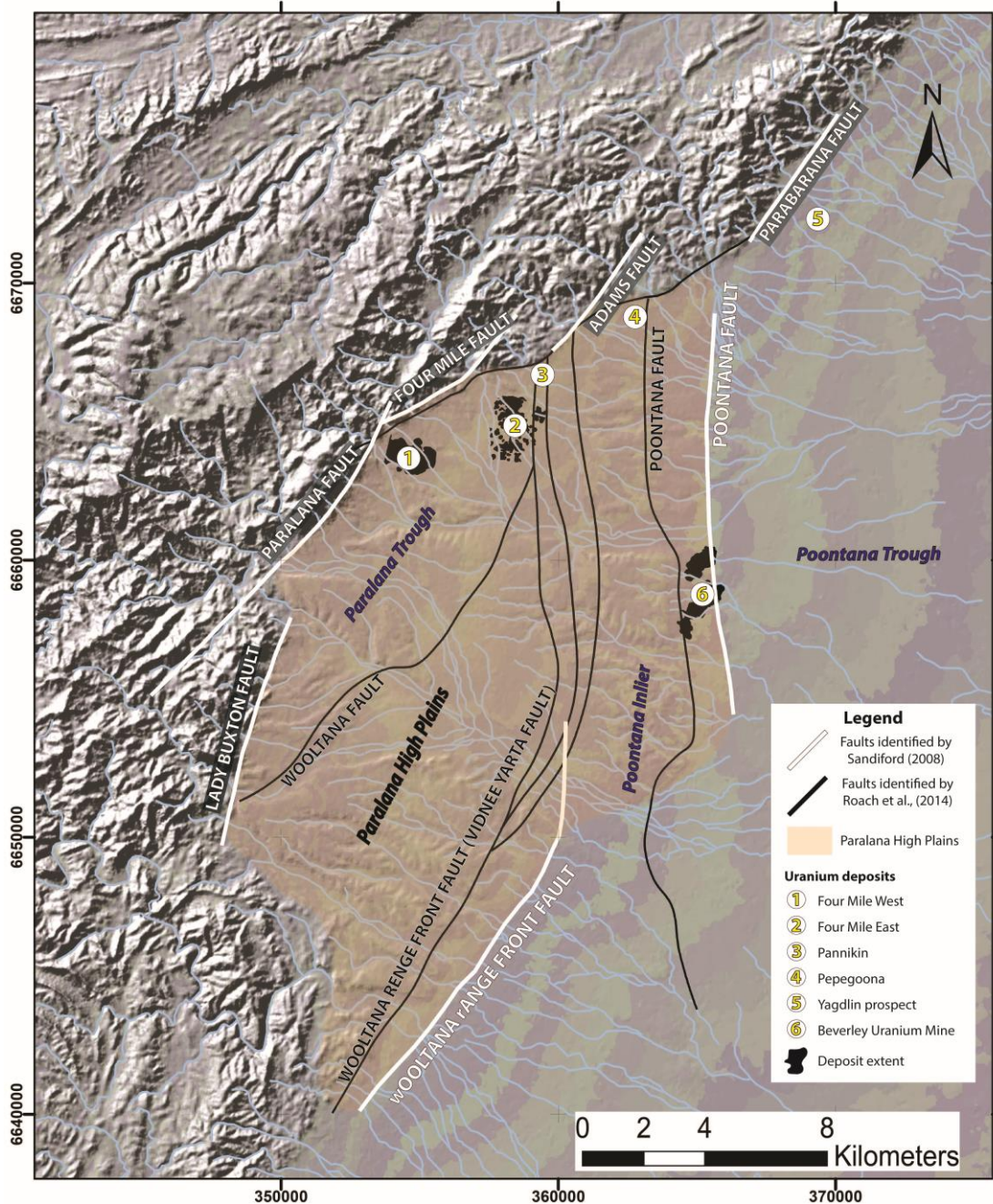


Figure 2.10: Shaded Relief Map of Eastern Range Front with overlain extent of the Parolana High Plains (Orange), Sandiford (2008) interpreted faults (White), AEM-interpreted faults (Black) (Roach et al., 2014), Locations of the Parolana and Poontana troughs), and locations of uranium deposits.

The Poontana and Wooltana faults, which delineate the eastern and western extents of the Poontana Inlier respectively, each displaces the Willawortina Gravels of the Parolana High Plains (Figure 2.11). As shown in the drainage patterns of the Arkaroola Creek, Lady Buxton Creek, and Four Mile Creek, both the Poontana and Wooltana faults displace the Parolana High Plains' Willawortina Formation by approximately 10 m (C  lerier et a., 2005; Sandiford, 2008). The Yadnamutana Gorge has a calculated incision rate of between 30-160 m/myrs (Quigley et

al., 2007b). Considering that Paralana High Plains have been incised approximately 30 m, the Willawortina Formation's youngest sediment ages are estimated at 200 Ka to 1 Ma (Sandiford, 2008). Thus, the most recent activity of the Poontana and Wooltana faults has a maximum age of 1 Ma.

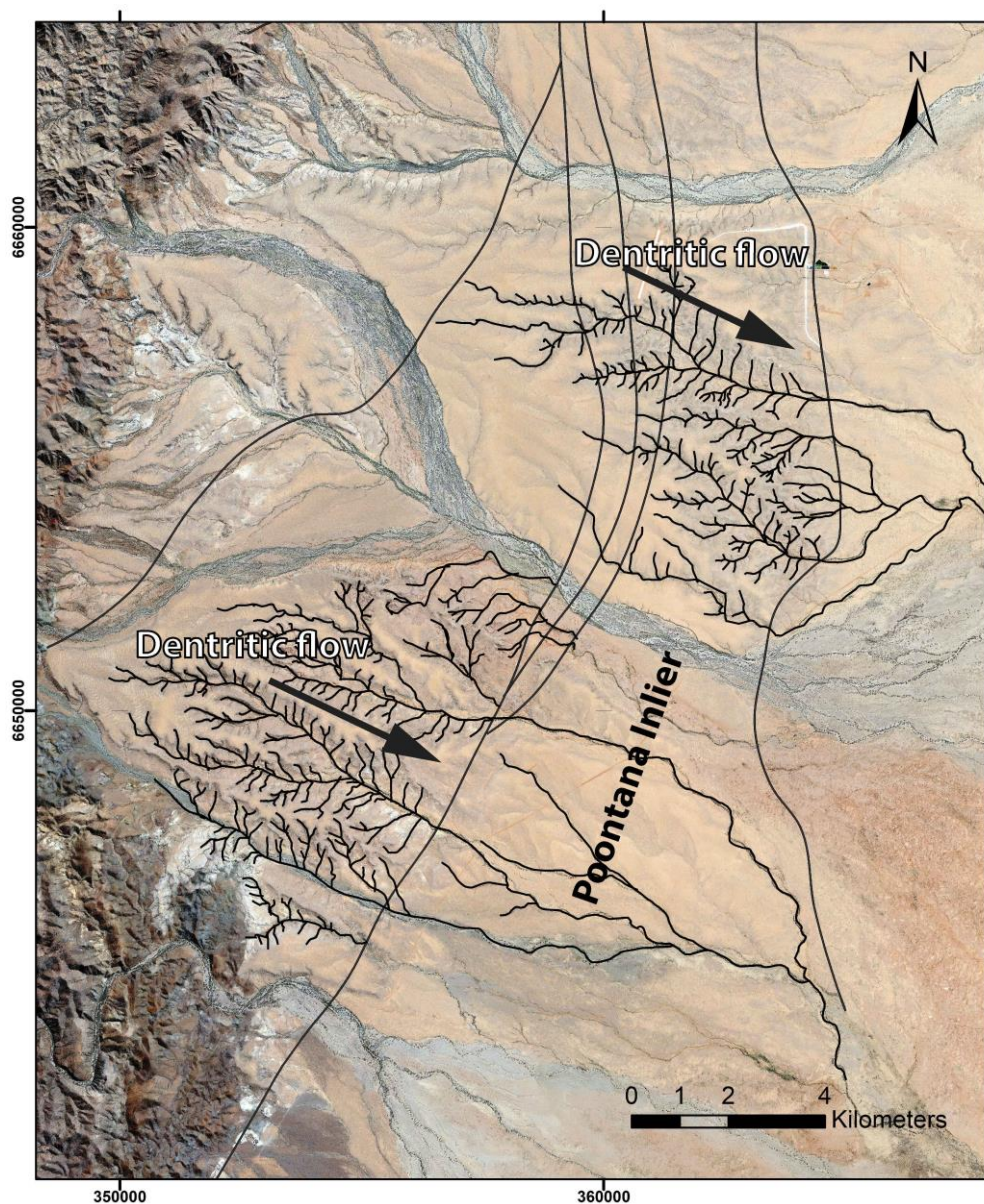


Figure 2.11: Map showing the coalescing drainage pattern representative of the Wooltana Fault and Poontana Fault, which define the eastern and western edges of the Poontana Inlier, respectively. Faults shown were identified by AEM in Roach et al., (2014).

In addition to the reverse faults of the Parana High Plains, there has also been a set of NE-SW normal faults identified which extend from the range front outward through the Parana High Plains (Hill and Hore, 2011). These normal-fault structures, which displace the Willawortina Formation by approximately 15 m, are involved in uplift and tilting of fault blocks at the foot of the range front. The uplift and exposure of the of oxidized sections of Cenozoic and Mesozoic strata near the Four Mile West deposit preserve an expression of paleo-roll front uranium mineralization, analogous to that exploited in the Four Mile deposit (Hore and Hill, 2010; Lubiniecki et al., *in. prep.*). No evidence of these normal faults was observed directly along the range front or within the Mount Painter Inlier.

2.3.3. Fault displacement estimation

The preservation of fault scarps is hindered by the unconsolidated nature of faulted sediments, and high rates of degradation due to locally enhanced erosion (Sandiford 2003a, Quigley *et al.* 2007a). This is exacerbated if the fault expression is such that it does not produce sufficient vertical offset to form long-lasting fault scarps and thick alluvial fans (Sandiford 2003a, 2003b). These factors, in combination with the recent overburden may have been masking the topographic evidence of faulting. If the fault scarps are generated with low slip rates they are more likely to be obscured by erosion, sedimentation and colluvial flow (Sylvester, 1988; Ihmle and Jordan, 1994; Peng and Gomberg, 2010; Vidale and Houston, 2012).

A veneer of Holocene-Recent piedmont sedimentation has obscured much of the continuous surface expression of individual fault rupture segments. While the lengths of individual faults segments may be difficult to observe, the use of the fault escarpment's geomorphology to infer fault segment length has been successful, as shown by Sandiford (2008). Using the fault lengths depicted by Sandiford (2008) in addition estimated fault lengths observed in the field and comparing those values relative to other reverse fault systems (Torabi and Berg, 2011) has produced a crude estimation of offset for the range-bounding faults (Figure. 2.12).

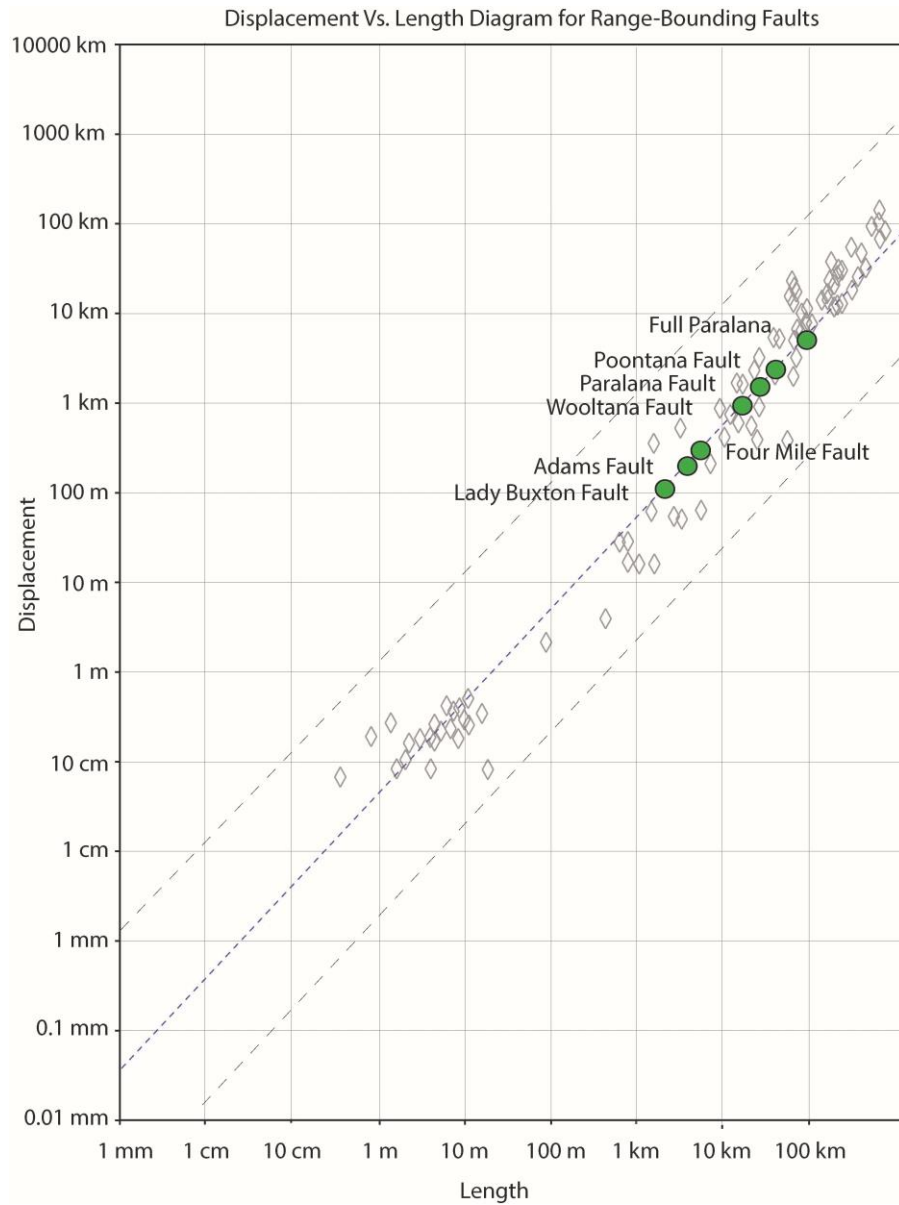


Figure 2.12: Displacement vs. length diagram for select faults using the fault-scaling properties described by Torabi and Berg (2011)

The estimated offsets generated by this fault-scaling method include excessively large ranges, due to the natural variations of fault zones globally. Table 2.2 contains the calculated maximum, mean, and minimum net slip for Sandiford's (2008) estimated fault lengths. The relationship between length (L) and Displacement (D_{max}) is commonly written as a power-law: $D_{max} = kL^n$ where k and n are constants (Davis et al., 2005). Unfortunately, this method of estimating fault displacement is of minimal use in this setting due to the excessive variability in the estimated fault slip. Calculated values for the Lady Buxton Fault, for example, range from a lower limit of 16 m to an upper limit of 11,000 m. This vast range, even with a relatively conservative mean slip value of 420m. This vast range in net slip of reverse faults speaks to the variability of reverse fault environments globally.

Fault	Length (m)	Max Slip (m)	Mean Slip (m)	Min Slip (m)
Lady Buxton Fault	4,202.00	11,000	420	16
Adams Fault	5,343.00	10,100	550	18
Four Mile Fault	6,462.20	10,550	790	23
Wooltana Fault	11,541.50	50,200	2,300	90
Paralana Fault	13,824.80	100,000	3,000	150
Poontana Fault	14,553.70	100,200	5,200	200
Paralana Full Extent	112,804.00	216,000	10,000	450

Table 2.2: Calculated Offset using Length vs. Displacement calculation

The height of a fault scarp generally indicates the minimum vertical displacement of the fault (Jayawardena, 2013). The scarp heights vary along the strike of a fault, depending on the distribution of vertical slip components (Peltzer and Tapponnier, 1988; Sylvester 1988). Figure 2.13 is a graphical representation of the range front elevation normalized relative to the pediplain elevation. In the absence of a clearly-defined fault scarp with which to measure overall offset, this graph can be used as a crude proxy for a displacement profile which can provide insight into fault interaction and growth history.

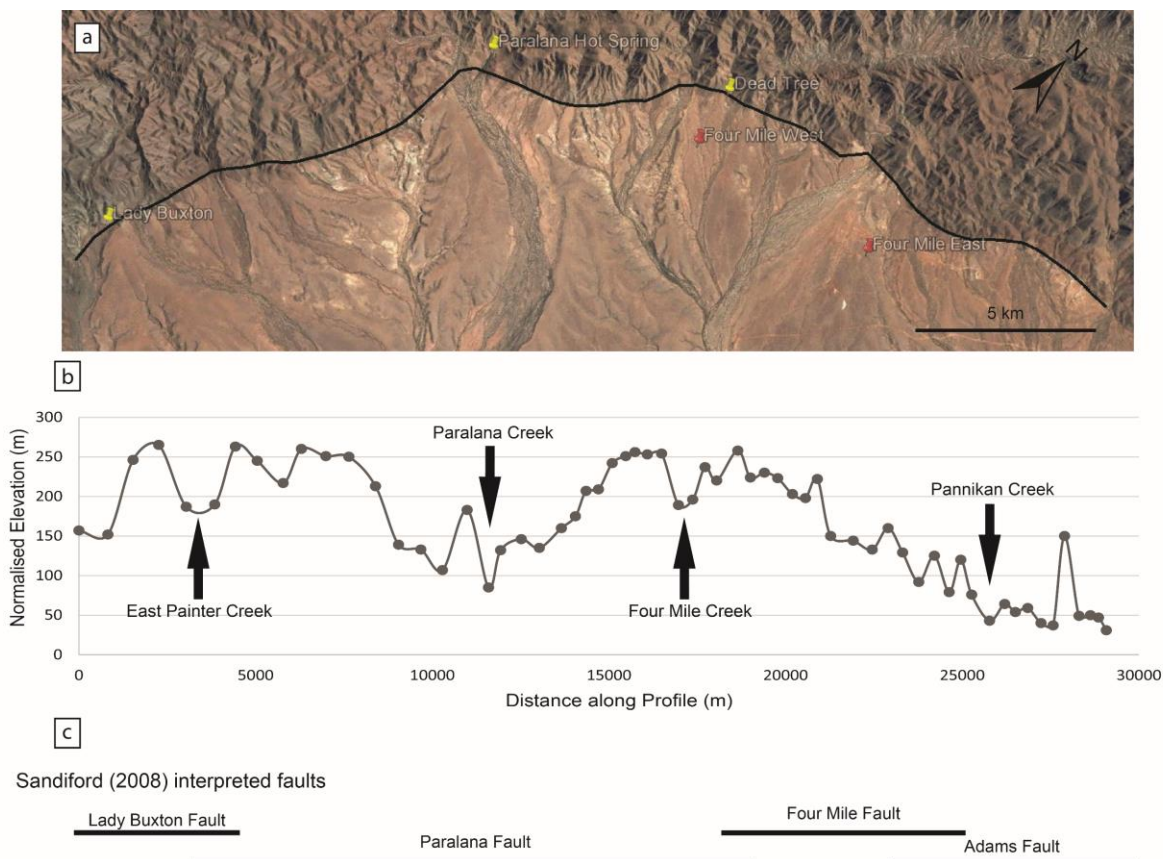


Figure 2.13: Range Front Elevation vs. Length profile as a proxy for displacement-length; imagery from Google Earth, 2018

The range-bounding faults, i.e. the Lady Buxton Fault, Paralana Fault, Four Mile Fault, Adams Fault, and Parabarana Fault have all had significantly greater total slip than the faults of the Eromanga Basin, as shown by the sharp elevation change at the range front. Slip rates for other demonstrably neotectonic faults in the Flinders Ranges are on the order of 20-50 m/myrs (Quigley et al., 2006b). Considering the current height of the range escarpment at ~250m, the upper limit of the slip rate, the present range front cumulative slip could have occurred within the last 5 Ma. This result is consistent with the conclusions of Callen & Tedford (1976), that the region was characterized by much lower relief in the Miocene during deposition of the Namba Formation (see also, Sandiford 2003).

2.3.4. Influence of Neotectonic Faulting on the Uranium systems

Sedimentary uranium deposits generally develop through dissolution of uranium from source rocks by percolating fluids, and transport along permeable pathways to the depositional environment (Skirrow, 2009). The degree to which neotectonic, near-surface faults interact with uranium-bearing fluids is poorly understood. Many attractively-simplistic depictions of the mineralization system responsible for the sediment-hosted uranium deposits of the Eromanga Basin demonstrate that mineralizing fluids have taken advantage of faults and fractures within the Mount Painter Inlier (ex. 2.14). These structures act as conduits for oxidized meteoric fluids to percolate through the uranium-rich granitoids of the Mount Painter Inlier before being pushed upward through other faults toward the overlying sedimentary pile (Figure 2.13) (Jaireth and Bastarok, n.d.; Hou et al., 2007; Skirrow, 2009, Sandiford et al., 2008). Neotectonic faulting could interact with uranium-rich fluid flow directly and/or indirectly. If the faults interact with the fluid flow directly, they will either act as baffles or as conduits to the fluid flow. Indirect interaction would entail the neotectonic faults acting exclusively to uplift the Flinders Ranges, providing the hydrostatic head necessary to facilitate uranium flow from the ranges to the mineralized sediments downstream.

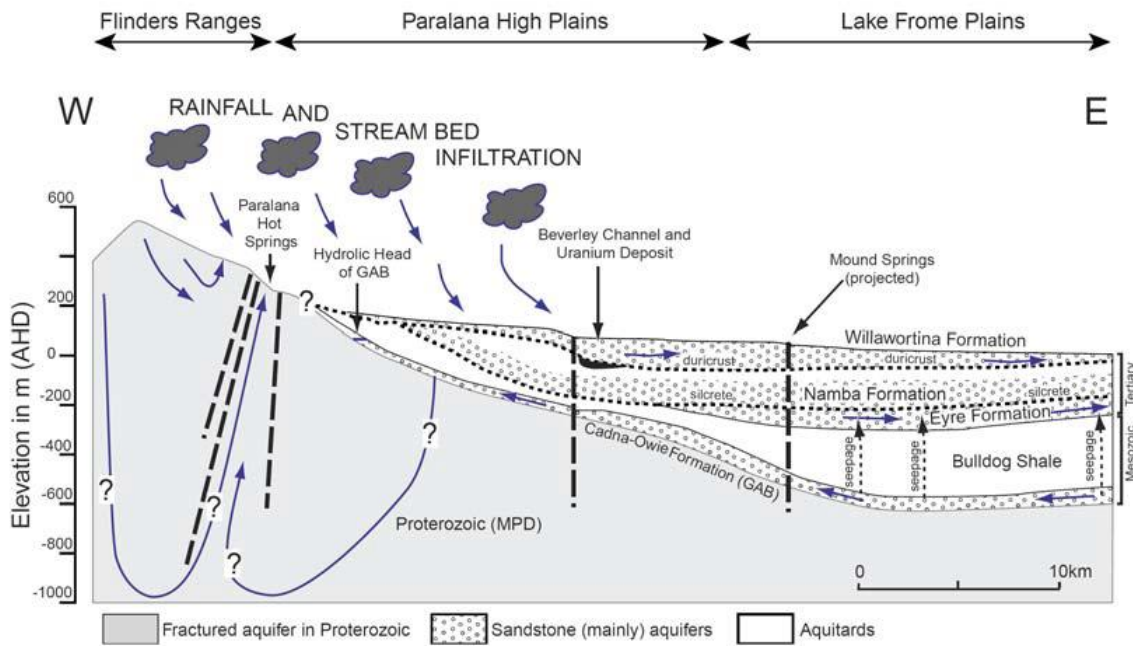


Figure 2.14: Conceptual hydrogeological model for the Four Mile region. From Brugger et al., (2005)

The timing of uplift is critical in the evolution of uranium mineral systems, as topography provides the potential energy necessary to drive fluids down into basins. Skirrow (2009) proposed three hypothetical timings of uplift and denudation that could potentially have triggered the formation of the uranium mineral system (Figure 1.3): a) Late Mesozoic-early Cenozoic (~90 Ma) whereby post-Eromanga Basin uplift of deeply-weathered basement could have potentially triggered gravitationally-driven flow of uranium-rich groundwaters into aquifers of the Eromanga Basin. b) Eocene-Oligocene (~35-28 Ma), uplift and exhumation in the Mt Painter Inlier, may have triggered fluid flow from basement areas into the Eyre Formation via south-to-north oriented paleochannels. c) Pliocene-Pleistocene uplift and exhumation of basement rocks in the Lake Frome region occurred since ~6 Ma, producing much of the present-day relief in the northern Flinders Ranges and Mount Painter Inlier (Quigley et al., 2006b). This uplift would have exposed deeply weathered basement allowing for the leaching of uranium and transport into permeable units of the Namba Formation, Eyre Formation or Eromanga Basin.

In the context of the fault structures observed and their inferred ages, we can see that conjugate set 3, which strikes NW-SE and has an inferred age of 11 to 6 Ma, may be temporally related with Skirrow's (2009) third possible mineralization event. There are no observed examples of this fault set directly interacting with the Cenozoic sedimentary rocks of the Eromanga Basin and are limited to the Mesoproterozoic rocks of the Mount Painter Inlier.

Conjugate set 2 has been interpreted to have formed in the Cretaceous (~100Ma) based on paleostresses calculated by Muller et al., (2012). This age is roughly contemporaneous with Skirrow's (2009) possible mineralization event. The N-S strike of this fault set would make them unlikely conduits to fluid flowing from the uplifted ranges to the lowlands. There were no observed interactions between conjugate set 2 and Eromanga Basin.

Of the structural trends identified, only conjugate set 1 has been observed to directly interact with the onlapping sediments of the Lake Eyre Basin. These faults are the most obvious example of neotectonic faulting and have been interpreted to have formed by the onset of Late-Miocene uplift of the ranges ~6 Ma (Müller et al., 2012). This age corresponds not only with Skirrow's possible mineralization (a) but also with the mineralization age of the Beverley Uranium Deposit (Wülser, 2009). This fault set strikes NE-SW roughly parallel the range front. While the orientation of these faults does not directly preclude their role as conduits to oxidized fluid flow from the ranges to the plains, their orientation is unlikely to readily shuttle fluids into the Eromanga Basin.

The uplift of the Northern Flinders Ranges circa 6 Ma was facilitated by reactivation of faults along the Paralana Fault Zone (Celerier et al., 2005). These neotectonic faults were responsible for accommodating the roughly 800-1000 m of overall uplift experienced since the Miocene (Sandiford, 2008; Quigley et al., 2007b). As the bedrock of the Mount Painter Inlier was uplifted, it weathered, allowing uranium to be leached. The continued uplift provided the hydrostatic head necessary for uranium-rich oxidized fluids to flow from the ranges into the onlapping sediments of the Eromanga Basin. Thus, while the neotectonic faults of the Paralana escarpment could have directly interacted with fluids as conduits, there is little evidence of this interaction based on the orientations of the observed faults. Chapter 3 will discuss the fault rocks and attempt to deduce further whether there has been an interaction between mineralizing fluids and the fault rocks collected.

Chapter 3 – Microstructures and Fluid Flow events

Faults can act as either baffles or conduits to fluid flow, depending on the characteristics of the fault rocks, the geometry of the fault relative to the rheology of surrounding rocks and the relative stress field of the area (Barton et al., 1995). The texture of the fault rocks has a profound effect upon the permeability of a fault, and thus directly influence the fluid flow characteristics, as per Darcy's Law of fluid flow (Bense et al., 2013). Brecciation is the most prominent fault rock process in crystalline rocks and can result in drastic increases in permeability of over four to five orders of magnitude (Walker et al., 2013). However, cementation of the fault rocks created by brecciation or continued milling will lead to a reduction in permeability (Bense et al., 2013).

The interaction of faults with groundwater flow is of crucial importance to understanding the uranium mineral system in place in the Northern Flinders Ranges. Current models for the flow of uranium-bearing fluids between from the Mount Painter Inlier into the onlapping Eromanga Basin imply that faults act as major conduits to fluid flow.

Sampling the fault rocks and analyzing their textures and mineralogy will allow the application of these principles to determining the interaction of uranium-enriched, reduced fluids with neotectonic faults. The complex fluid-rock interactions of the area have been studied using textural descriptions of fault rocks and mineralized fractures, petrology, and SEM analysis. Evidence of fluid flow was observed most clearly in mineralized fractures which preserve clearly defined microtextures and useful mineral assemblages for deducing the composition of fluids that passed through or along them.

3.1. Fault rock classification

Due to the sensitive ecology and cultural significance of the Arkaroola Wilderness Sanctuary, only small, discreet sampling was possible. Grab samples were taken from observed fault cores. A subset was selected from the collected grab samples to provide a representation of the textures and mineralogy of the fault rocks. Due to the friable nature of the fault rocks, each sample was encased in resin before being cut to preserve the fault textures. Polished thin sections were prepared from each sample to study the mineralogy and textures of the fault rocks with standard optical and Scanning Electron microscopes (SEM). Using the fault rock classification scheme proposed by Woodcock and Mort (2008; Figure 3.1), four distinct fault rock textures were identified; crackle breccia (75-100% large clasts >2 mm) (Fig. 3.1), mosaic breccia (60-75% large clasts >2 mm) (Fig. 3.2), chaotic breccia (30-60% large clasts >2

mm) (Fig. 3.3), and fault gouge (<30% large clasts >2 mm). The fault rock classification scheme used in this study considers all coarse-grained faulted rocks to be termed fault rocks, regardless of cohesion. Cohesiveness was determined by the ability to break the sample with fingers. The mineralogy of the individual fault rock samples broadly reflects the mineralogy of their parent rock. Samples from within the Mount Painter Inlier were more likely to contain polycrystalline quartz clasts, indicating entrainment of wall rock fragments within the fault gouge.

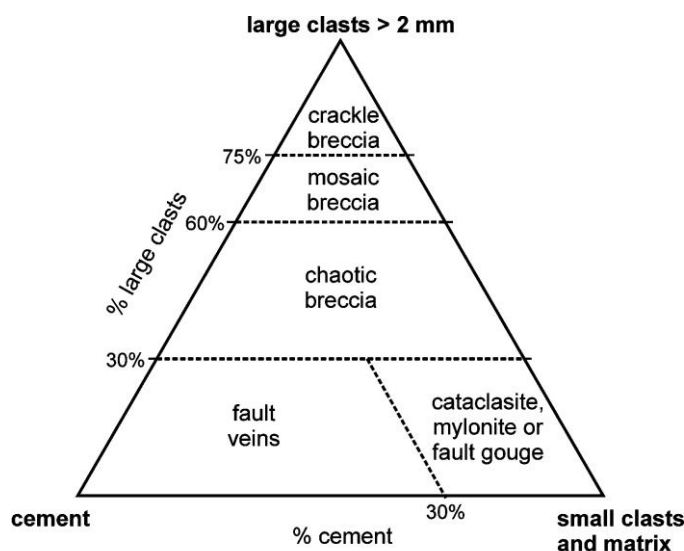


Figure 3.1: Fault rock classification scheme proposed by Woodcock and Mort (2008) and adopted for the classification of samples for this study.

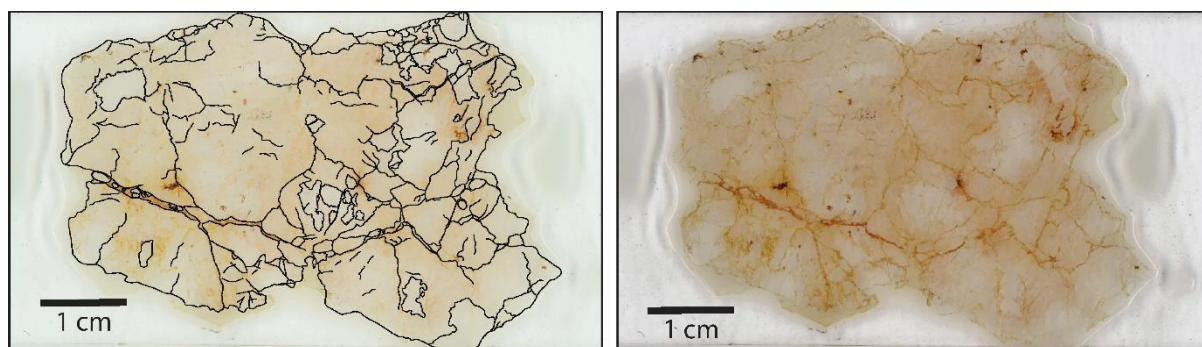


Fig. 3.2: Crackle Breccia. Left: fractures and grain boundaries highlighted to facilitate textural analysis. Right: unaltered optical scan of the sample. (sample JB16-015)

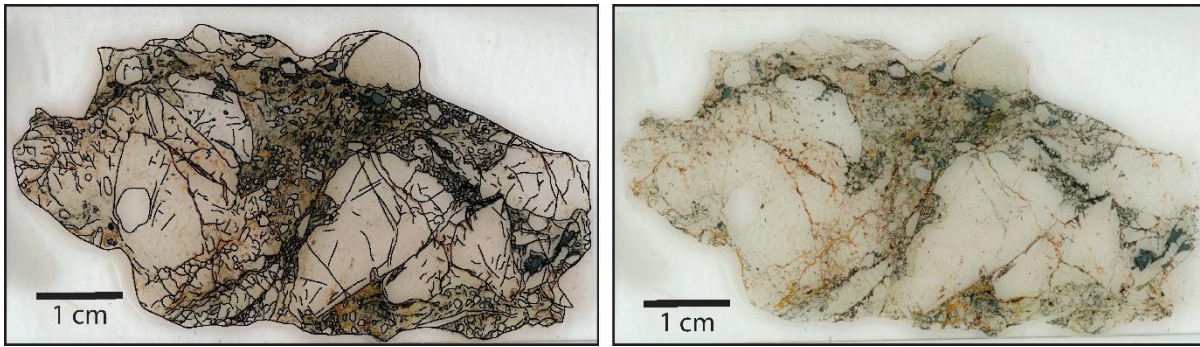


Fig. 3.3: Mosaic Breccia. Left: fractures and grain boundaries highlighted to facilitate textural analysis. Right: unaltered optical scan of the sample. (sample JB16-007)

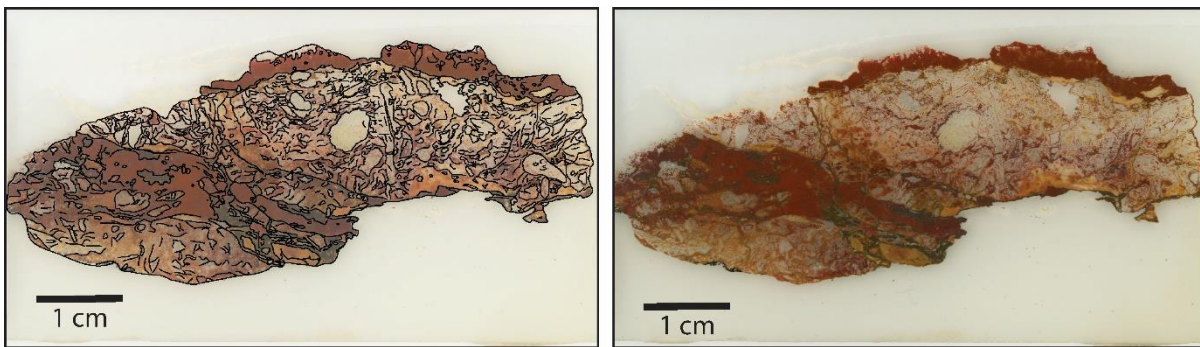


Fig. 3.4: Chaotic Breccia. Left: fractures and grain boundaries highlighted to facilitate textural analysis. Right: unaltered optical scan of the sample. (sample JB16-022)

3.2. Cementation

Three different types of cementation were observed within the fault rock samples. Hematite was by far the most common cement, found within seven of the faults (ex. Figures 3.2, 3.3, and 3.4). Sample JB16-008 showed quartz cementation which effectively rendered the sample impermeable due to the complete cementation of fractures in the sample. Only the Lady Buxton Fault locality (JB16-LB1) has calcite cement. The calcitic source for the Lady Buxton fault calcite cement is likely marbles of the Neoproterozoic Wywyanna Formation in the hangingwall. A summary of the fault rock sample locations, textures, cohesiveness, and cementation is provided in Table 3.1.

Sample #	Fault #	Easting	Northing	Maximum age (footwall lithology)	Fault Rock Texture	Cohesiveness	Secondary cementation
JB16-005	24	348187	6653698	Mesoproterozoic	Fault gouge	Incohesive	Minor haematite
JB16-006	25	348925	6654720	Mesoproterozoic	Crackle breccia	Incohesive	Minor haematite
JB16-007	26	348930	6654718	Mesoproterozoic	Mosaic breccia	Incohesive	-
JB16-008	27	349042	6654697	Mesoproterozoic	Crackle breccia	Incohesive	Minor silica
JB16-009	29	349436	6655216	Mesoproterozoic	Chaotic breccia	Incohesive	Haematite
JB16-010	30	349314	6655202	Mesoproterozoic	Crackle breccia	Incohesive	-
JB16-012	2	353356	6663862	Cretaceous	Fault gouge	Incohesive	-
JB16-015	34	351792	6661948	Mesoproterozoic	Crackle breccia	Cohesive	Haematite
JB16-016	35	351743	6661972	Mesoproterozoic	Fault gouge	Incohesive	-
JB16-017	39	351014	6660959	Mesoproterozoic	Fault gouge	Cohesive	Haematite
JB16-021	47	355376	6665892	Pleistocene	Fault gouge	Incohesive	-
JB16-022	48	349931	6660790	Mesoproterozoic	Chaotic breccia	Cohesive	Major haematite
JB16-026	5	373583	6680312	Cretaceous	Mosaic breccia	Cohesive	Haematite
JB16-027	51	350176	6657586	Mesoproterozoic	Crackle breccia	Incohesive	-
JB16-LB1	1	348350	6651010	Pleistocene	Fault gouge	Incohesive	Minor calcite

Table 3.1: Fault rock samples and the classification of their textures using the proposed methods of Woodcock and Mort (2008).

3.3. Mineralized Fracture

Sample JB16-024A is a hematite-mineralized vein located within the Freeling Heights Quartzite (1556 ± 10 Ma). The sample is unique to the study area and was collected due to its proximity to the Four Mile East deposit and owing to its unique texture. In hand sample and thin section, there appears to be a weathering front extending outward from the vein, altering the host rocks (Figure 3.5 A). In reflected light, the vein infill shows composite syntaxial growth and crack-filling textures leading to a pseudo wood-grain style texture (Figure 3.5 B). Under the SEM, this feature is even more striking (Figure 3.6 A-D).

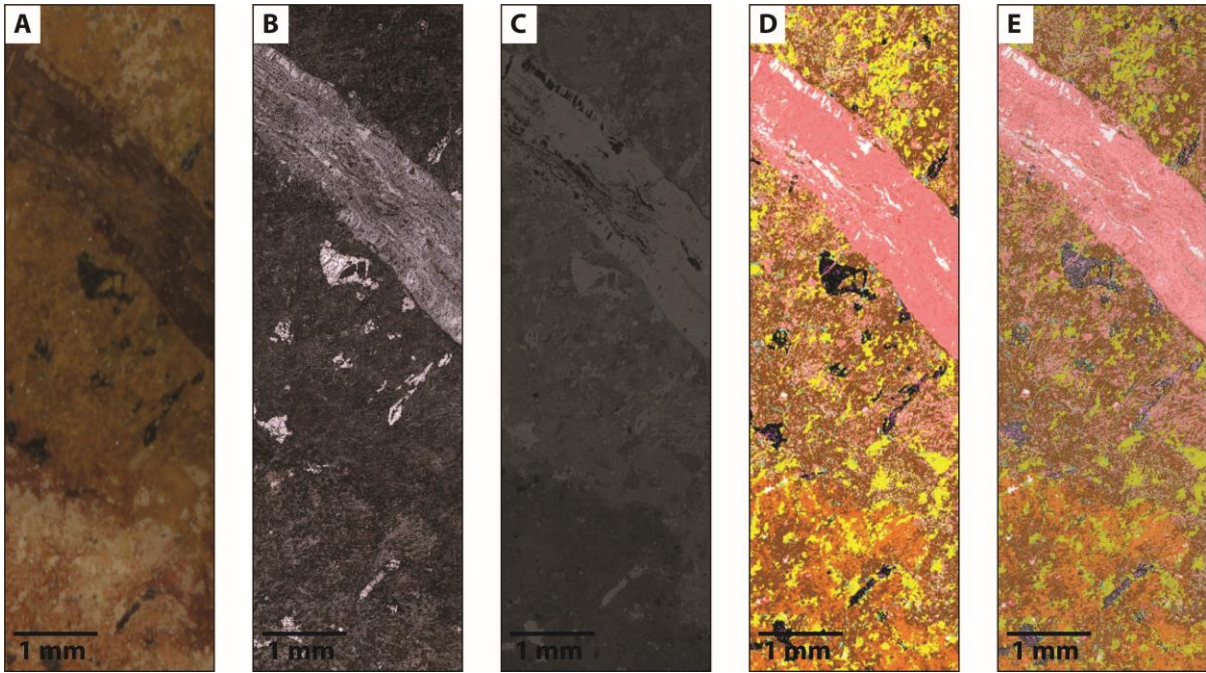


Figure 3.5: Sample JB16-024A. (A) imaged in plane-polarized light, (B) Reflected Light, (C) SEM, (D) Mineral Liberation Analysis (MLA), (E) MLA over reflected light to visualize textures.

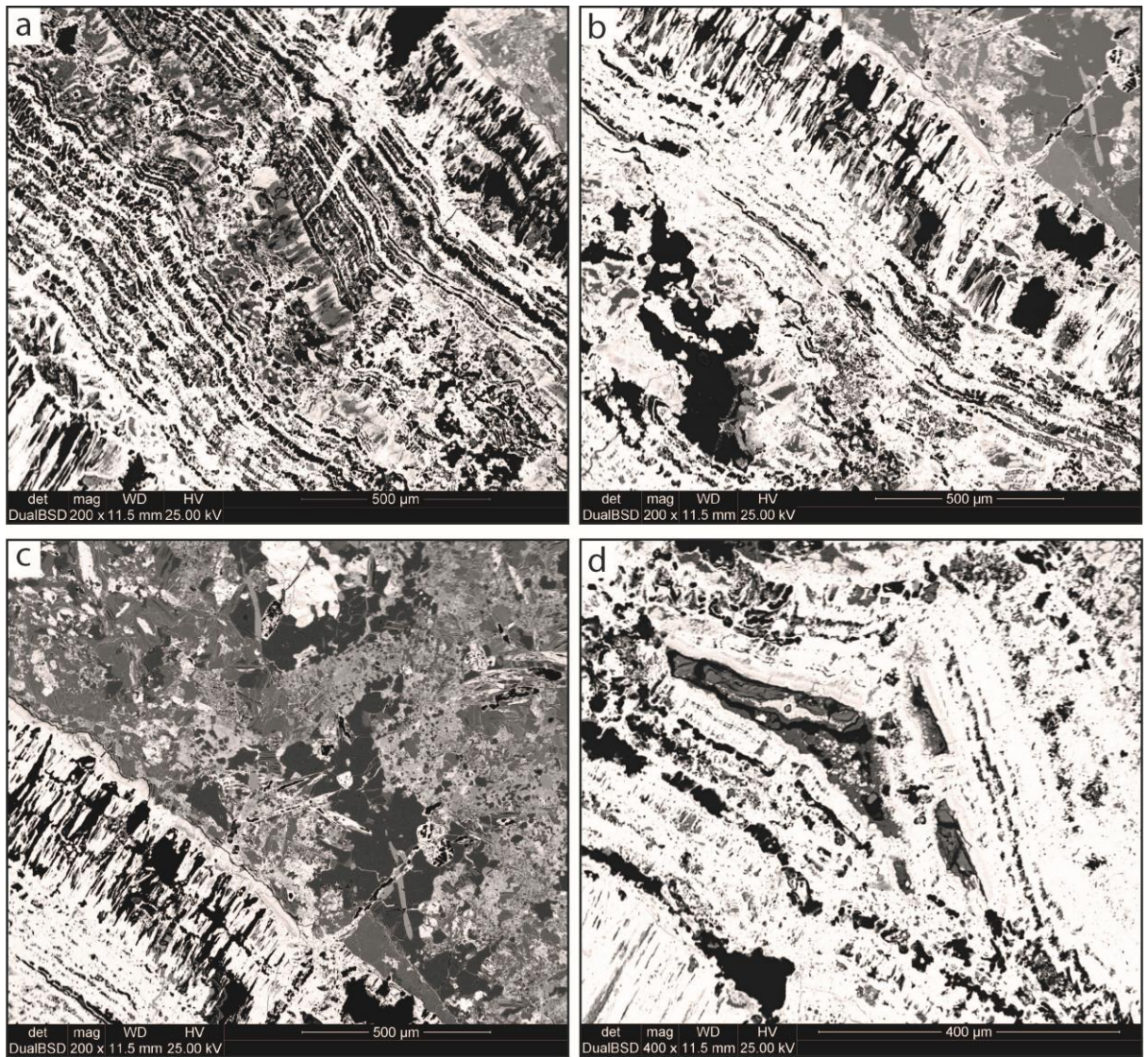
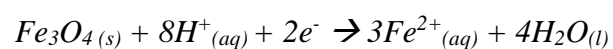


Figure 3.6: SEM images of Hematite filled fracture showing composite syntaxial and crack seal infill textures leading to a pseudo wood-grain texture (Sample JB16-024A)

The rock surrounding the vein has been subjected to chemical weathering, as shown by the weathering front observable along the middle-bottom of Figures 3.5 A, C, and D. Both inside and outside this weathering front are abundant subhedral to anhedral maghemite grains which exhibit spectacular boxwork weathering (Figure 3.7 A-D). This weathering is interpreted to represent the preferential weathering of more Fe^{2+} -rich (magnetitic – Fe^3O_4) zones of the maghemite mineral, leaving behind a skeleton of Fe^{3+} -rich (hematitic – Fe^2O_3) material. The dissolution of magnetite is expressed by the following formula (White et al., 1994):



This reaction requires acidic conditions to provide the necessary protons. The Paralana Hot Springs, which are the remnants of a long-lived hydrothermal system in the Mount Painter Inlier (Brugger et al., 2005), were measured as part of Chapter 4 to be acidic at $\text{pH} = 4.0$. If this

hydrothermal system has been larger in the past, as has been interpreted by Brugger et al. (2005), then similar fluids to those observed in the Paralana Hot Spring could have been responsible for the weathering features observed. Boxwork maghemites can be observed throughout the sampled area, despite the alteration front observed. Therefore the weathering of maghemite grains predates the hematite vein infill.

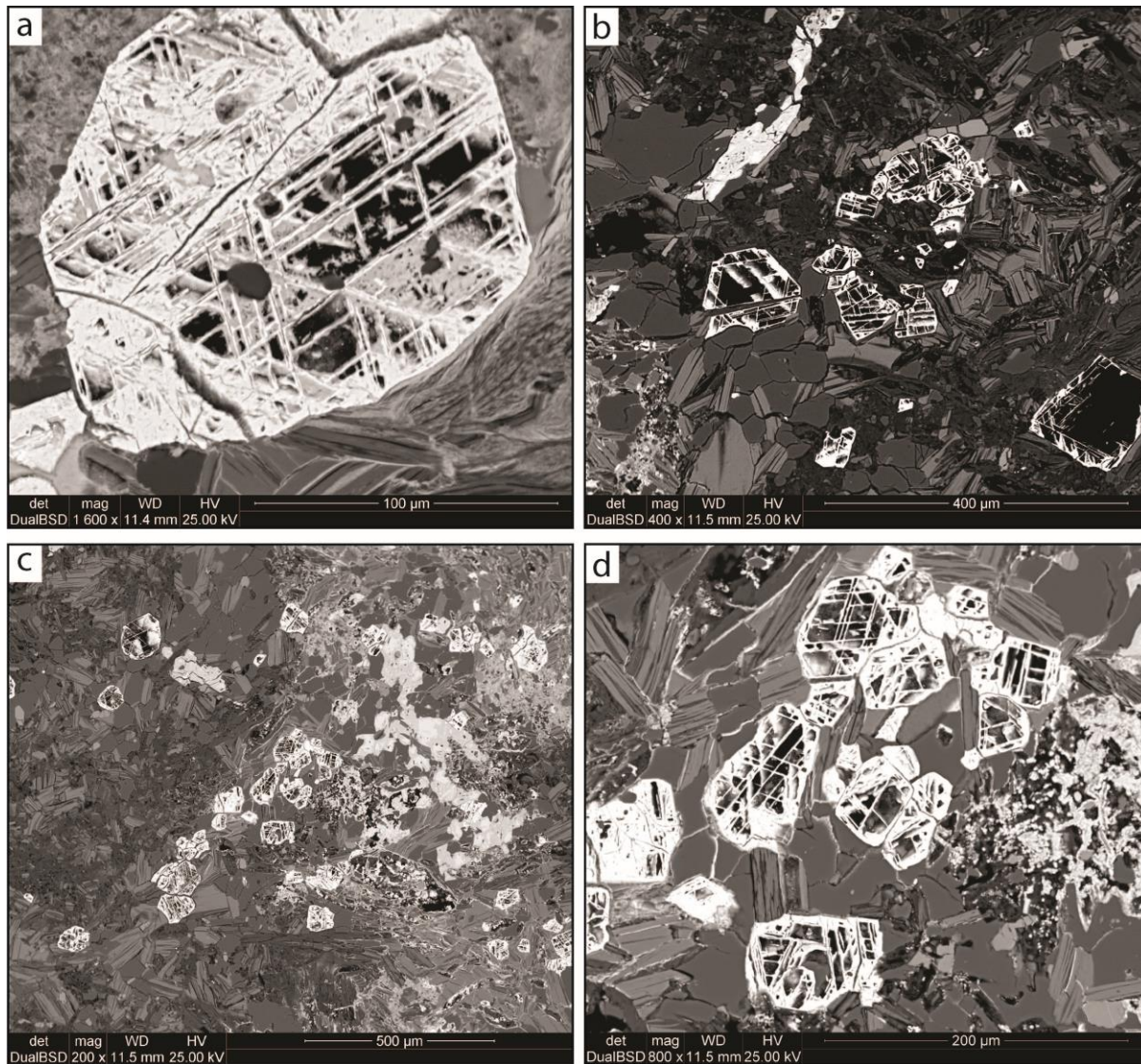


Figure 3.7: SEM images of Maghemite crystals exhibiting boxwork weathering (Sample JB16-024A)

Mineral Liberation Analysis (MLA) on a Quanta 600 SEM was conducted on the vein to determine the textural relationship between different mineral species within the sample. The resulting colourized image (Figure 3.8) represents spot SEM analyses every 4 microns across a 2 mm x 8 mm area. The image shows a clear differentiation of the weathered zone (closer to the vein) from the less weathered zone (bottom). The MLA image shows that iron oxides (pink) are more abundant proximal to the vein. The less weathered zone (bottom) exhibits abundant Al-Si ± Fe clay mineralization (Orange).

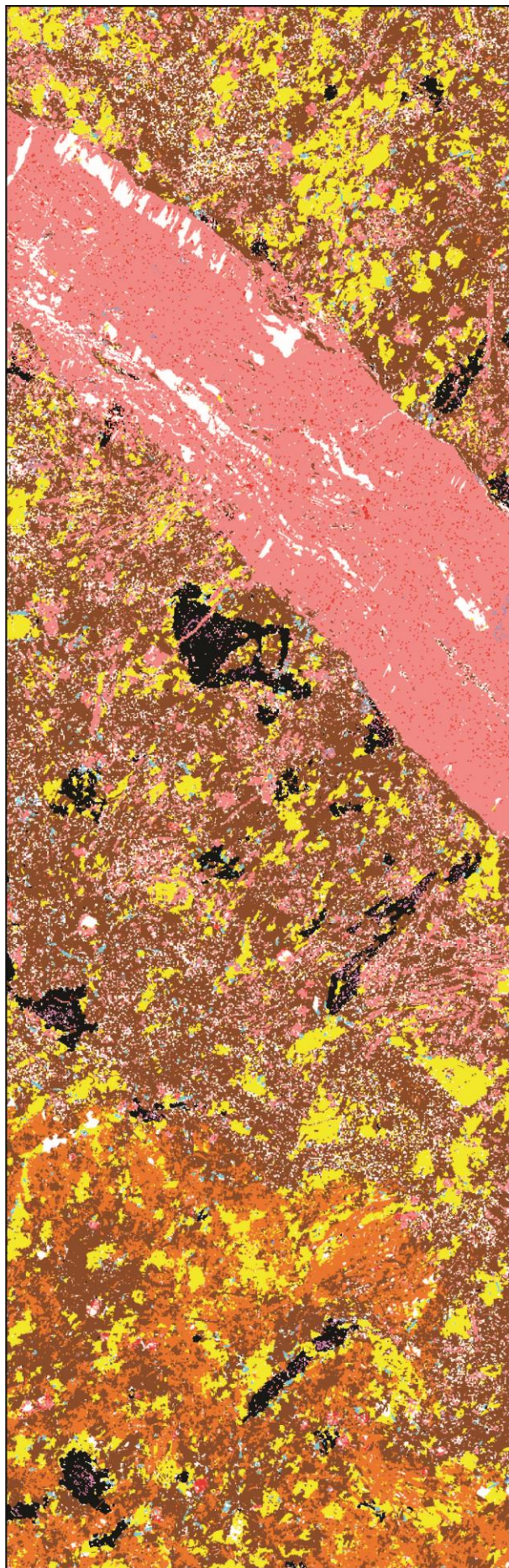



Figure 3.8: Mineral Liberation Analysis of sample JB16-024A. Note the hematite vein on the left side of the image and stark change in mineralogy in the centre-right with abundant aluminum-silicate ± Iron clay (Orange).

Mineral List

	Biotite
	Quartz
	Ilmenite
	Ti-Ilmenite (ilmenohepatite)
	Zircon
	Xenotime
	Apatite
	Ilmenorutile
	Goethite/Magnetite/Hematite
	Fe-P-Ca-REE
	Al-Si +/- Fe
	Unknown/No X-Ray

Most of the fault rock samples collected are incohesive, with little cementation indicating either that the faults have experienced active movement relatively recently, before cementing fluids have had a chance to infiltrate the permeable structures, or that the surficial faults have not acted as conduits to mineralizing fluids. There is evidence of oxidizing fluid flow through the Mount Painter Inlier, as observed with the hematite-veined sample described here. Furthermore, there is a locality described by Hore and Hill (2010) and Lubiniecki et al., (in prep) called the Dead Tree Section which preserves evidence of a paleoredox front within the Eyre Formation. The Dead Tree Section is located approximately 5.5 km northeast of the Paralana Hot Springs along the range front and is 800 m northwest of the of the Four Mile West deposit. The Eyre Formation at this locality preserves the redox roll-front front commonly associated with sediment-hosted uranium deposits but is rarely visible in outcrop. This feature provides evidence that there is indeed fluid flow coming from the ranges into the Eromanga Basin. The preserved roll-fronts are situated approximately 200 m from the Paralana Escarpment. In between the roll fronts and the escarpment there were three observed meso-scale faults, none of which show evidence of recent fluid flow. Therefore, the meso-scale faults of the Paralana Escarpment are interpreted not to act as conduits to mineralizing fluid flow.

- The fault rocks collected from range-bounding faults show little evidence of cementation which implies recent movement of the faults.
- Lack of active fluid flow in the form of cement implies that surface-rupturing faults are not acting as fluid flow conduits.
- Mineralization observed at the Dead Tree locality is not related to fault-shuttled fluids.

Chapter 4 – Hydrogeology of the Northern Flinders Range's Natural Springs

The Great Artesian Basin (GAB), which underlies ~22% of the Australian continent (Habernehl, 1980), is the water source for most of the natural springs in north-eastern South Australia. Mound springs associated with the GAB are common around the basin fringes, and form zones with several springs proximally to one another (Ponder, 1986). The Northern Flinders Ranges host several natural springs which expel fluids along the Paralana Escarpment, which separates the Mesoproterozoic Mount Painter Inlier from the Cenozoic to Recent sedimentary rocks of the Lake Eyre Basin and Callabonna Sub-Basin. Several studies have been conducted on these range-proximal springs to determine their most likely sources (ex. Brugger et al., 2005), their usefulness for pastoral or infrastructural purposes (Mawson, 1927; Grant, 1938), and their relationship to the uranium mineralizing systems of the Paralana and Poontana Troughs (Heathgate, 1998; Brugger et al., 2005). The use of groundwater sampling in uranium exploration has been employed extensively in the Lake Frome Basin (Fabris and Sheard, 2008; Michaelsen et al., 2016), since groundwaters directly interact with mineralogy at depth. However, groundwater concentrations of a target element as an exploration tool can be misleading due to hydrological factors and interactions including pH, fluid mixing, precipitation-dissolution of minerals, and reduction-oxidation conditions of the fluids (Fabris and Sheard, 2008). These processes often represent a long, complex evolution, further obscuring a direct relationship between groundwater and economic mineralization.

This study endeavours to further expand on these previous works by providing a new series of geochemical analyses and field observations. Temperatures of the discharged waters range from 23.1°C to 57.0°C, indicating variable source depth. The spring waters are observed to be depleted in uranium, which is consistent with regional and historical trends. This depletion, despite the uranium-rich setting of the Mount Painter Inlier and the Frome Embayment, indicates that the springs are not being sourced from uranium-enriched zones. Considering the proximity of these springs to previously-identified faults, it is inferred that the faults are not acting directly as uranium-shuttling structures.

The interaction of fluids in the subsurface of the Mount Painter Inlier and the onlapping Frome Embayment is a field of ongoing study. The sediment-hosted uranium deposits are actively being remobilized by these fluids (Skirrow et al., 2009; Michaelsen et al., 2016). By providing observations from previously understudied springs, the aim is to provide general context to the uranium mineral system.

4.1 Geologic Setting

4.1.1. *Hydrostratigraphy of the Paralana Trough*

Within the Four Mile Region there are five main hydrogeological units, each one containing an important aquifer (Figure 4.1). The Willawortina Formation, containing the Willawortina Aquifer, consists of two distinct facies: fine upper facies and coarse lower facies (Callen et al., 1995). The fine facies consists of a fining-upward sequence of sandy mudstone and silty dolomite with grey-green interbeds of calcareous paleosols (Callen et al., 1995). The coarse facies is a series of braided fans of framework-supported gravels and matrix-supported debris flows (Callen et al., 1995). The Beverley Aquifer is contained within the Namba formation which consists of three distinct members (Alley and Benbow, 1995). The uppermost member comprises the Beverley Clays, which act as an aquitard between the Beverley Sands below and the Willawortina Formation above (Curtis et al., 1990). The Beverley Sands, which host the Beverley uranium deposit, are grey silts with fine to medium-grained sandstone lenses (Curtis et al., 1990). The lowest member of the Namba Formation is the Alpha mudstone which contains occasional lignite lenses (Skirrow et al., 2009). The Alpha mudstone effectively blocks the transmission of fluids between the Beverley aquifer and the underlying Four Mile Aquifer (Skirrow et al., 2009). The Eyre Formation, which hosts the Four Mile Aquifer, is composed of pyritic, carbonaceous mature sandstones of variable size up to gravel, interpreted to represent braided stream deposits (Callen and Benbow, 1995). In the Callabonna Sub-Basin, the Eyre Formation also incorporates the Murnpeowie Formation which hosts lignite layers (Skirrow et al., 2009). The Cadna-Owie Formation hosts part of the Great Artesian Basin aquifer system, which is separated from the overlying units by the organic-rich Bulldog Shale (Skirrow et al., 2009). Mound springs which tap the Great Artesian Basin can be found around the Lake Frome Area. The final aquifer of importance for this study is the Mount Painter Inlier. Meteoric waters which percolate through the fractured rock are debouched back to the surface at the Paralana Hot Spring (Brugger et al., 2005).

Epoch	Basin		Stratigraphy	Description	Aquifer
Pleistocene	Callabonna Sub-Basin	Namba Formation	Willawortina Fm.	<i>Gravel, Sandy Mud</i>	<i>Willawortina Aquifer</i>
Pliocene					
Miocene			Beverley Clay	<i>Clay</i>	
			Beverley Sands	<i>Sand with organic material and pyrite</i>	<i>Beverley Aquifer</i>
			Alpha Mudstone	<i>Mudstone with organic material</i>	
Eocene		Eyre Fm.	<i>Sand, gravel and silt with mud interbeds</i>	<i>Four Mile Aquifer</i>	
Cretaceous	Eromanga Basin		Bulldog Shale	<i>shaly mudstone, micaceous silt, fine sand</i>	
			Cadna-Owie Fm.	<i>Sandstone, minor siltstone, carbonaceous siltstone</i>	<i>Great Artesian Basin</i>
Proterozoic			Mount Painter Inlier	<i>Fractured crystalline basement</i>	<i>Mount Painter Aquifer</i>

Figure 4.1: Simplified Stratigraphic column of the Callabonna Sub-Basin area with stratigraphic positioning of major aquifers

4.2 Site Descriptions

Five sample sites were chosen along the range front to provide a regional survey of natural spring waters along the ranges. Sampled locations are shown in Figure 4.2.

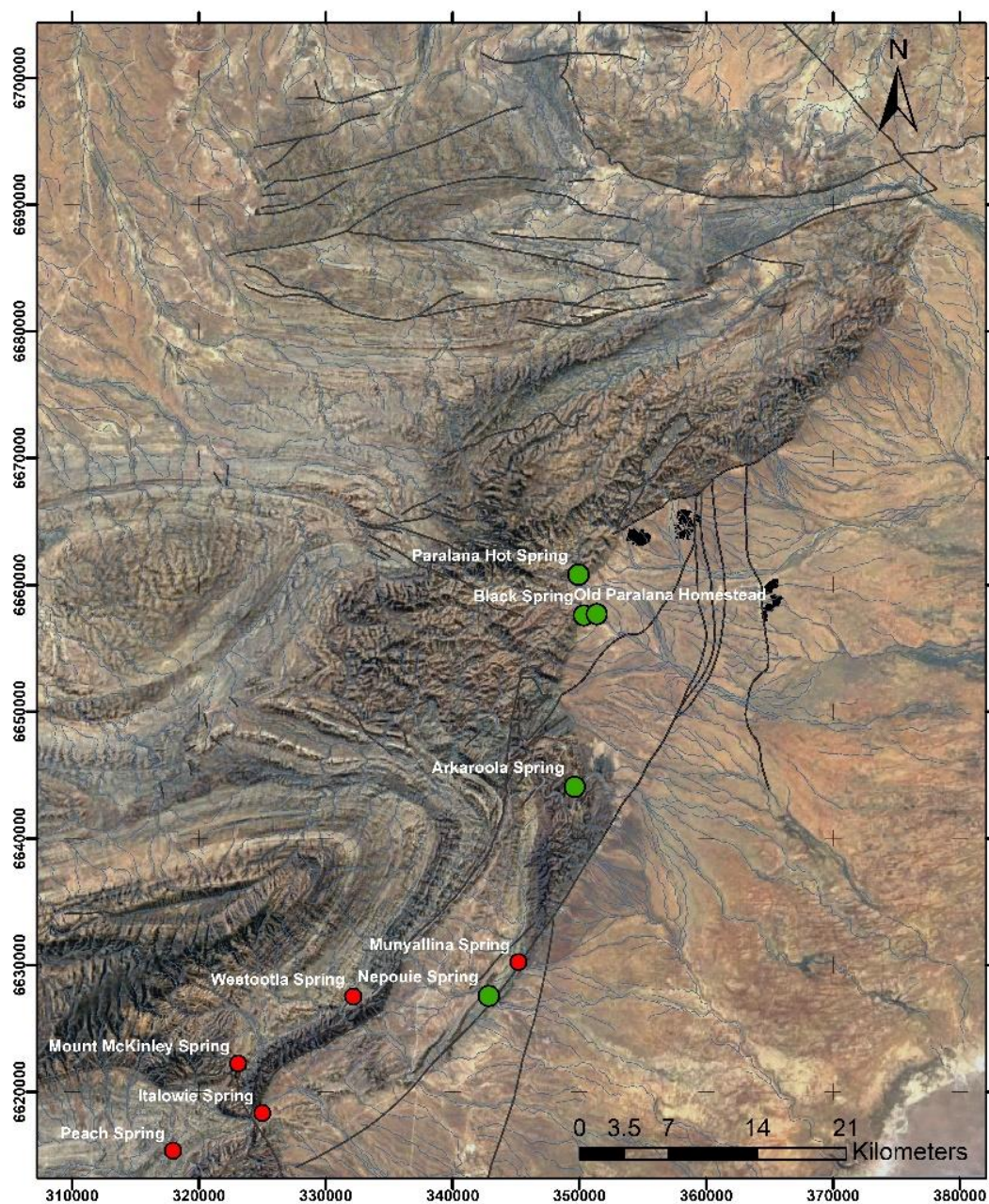


Figure 4.2: Spring locations of the Northern Flinders Ranges. Sampled springs are in green. Base map from Google Earth, 2018

4.2.1. Paralana Hot Spring

The Paralana Hot Springs are the sole example of a hot spring in the Northern Flinders Ranges (Mawson, 1927; Brugger et al., 2005). The amagmatic nature of the spring heat source is not only unique within the Flinders Ranges, but is exceedingly rare globally (Brugger et al., 2005). The heat source for the ongoing hydrothermal system has been interpreted to be the

uranium and thorium enriched granitoid rocks of the Mount Painter Inlier (Mawson, 1927; Coats and Blissett, 1971; Brugger et al., 2005). This radioactive heating was once thought to imbue the waters with restorative powers and in 1926-28 there was a small resort built on site at the Paralana Hot Springs (Mawson, 1927; Purvis, 1927). Grant (1938) measured the radioactivity of both the water and escaping gases and deduced that the natural radioactivity is due to elevated concentrations of radon and trace (560 ppm) radiogenic helium. More recently, Brugger et al. (2005) measured the radon concentration from the springs at 10,952 Bq/m³.

There have been significant changes to the expression and outflow of the Paralana Hot Springs over the past 91 years. In 1927 there were two separate pools, the largest being ~80 m² and 1 to 1.5 m deep (Mawson, 1927; Purvis, 1927; Figure 4.3). Large pools of spring water were still in place, though no longer used for bathing, in 2005, as described by Brugger et al. (2005). Estimates on spring flow rate have risen from >4,500 L/h (Mawson 1927) to ~57,600 L/h (~16 ± 2 L/s; Brugger et al., 2005). On the 9th -10th April 2010, a major rain event (34.7 mm over two days) resulted in an influx of stream sediment which greatly altered the geometry of the hot springs (McNeil et al., 2011). The post-flood pools are much smaller at approximately 3 m³ and the Paralana Creek draining the pools ranges from 0.5 m to 2 m wide and approximately 0.2 m deep (Figure 4.4). While the area is arid and drought-prone, the average rainfall has been relatively steady around 250 mm per year over the past 80 years between 1938 and 2018 (Bureau of Meteorology, n.d.). There was an extremely wet year in 1974 with a record 1,270 mm of rainfall (Sprigg, 1984).

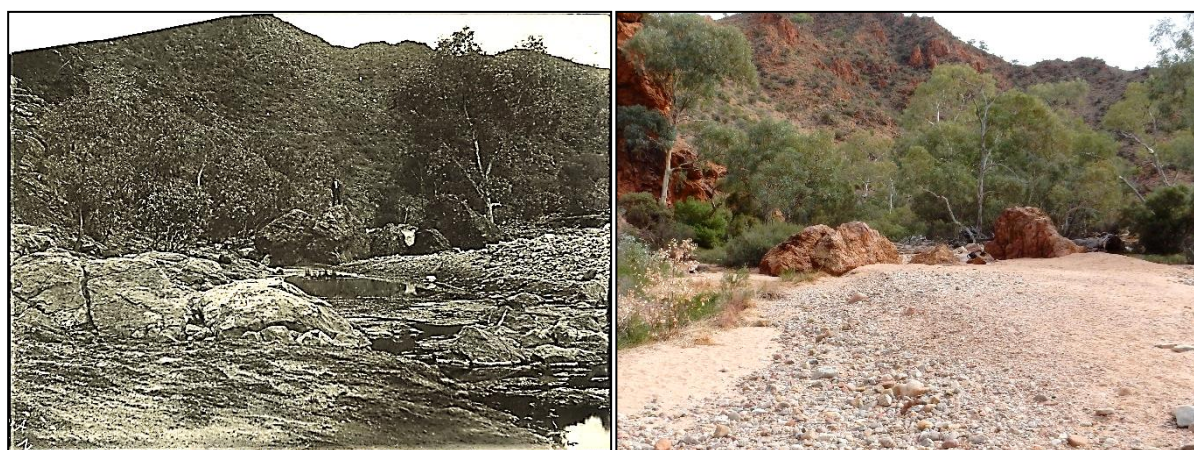


Figure 4.3: Paralana Hot Springs through time
Left: 1897 (approximately) by Robert Mitchell (Mitchell, 1897)
Right: 2016 – As part of this study



Figure 4.4: Paralana Hot Spring (54J 349934E 6660782N) looking upstream (NE) towards the Flinders Ranges

4.2.2. Black Spring

Black Spring, also known as Woolja Spring, is 3 km south of the Paralana Hot Springs, approximately 800 m east of the range front (Figure 4.5). Black Spring has a very small surface expression and is typified by a thick wall of tall grasses and woody stalks which make accessing the spring difficult. A small palm tree is also growing along the edge of the spring (Figure 4.6). There is no surficial creek draining the spring; all the expelled water is absorbed by vegetative surroundings. The creek valley which hosts Black Spring consists of deeply-incised Miocene-Pliocene Willawortina Formation with a bed of Pleistocene Pooraka Formation. Proximal silcrete exposures northeast (80 m) of the springs within quartzose Cenozoic sediments indicate that the Black Spring has been actively shuttling siliceous fluids to the surface since the Paleocene (Hore and Hill, 2015).



Figure 4.5: Aerial photo of the Black Spring Locality. (Google Earth, 2018)

The proximity of the Paralana Hot Spring and Black Spring to the Paralana fault system suggests that the underlying faults provide a conduit for groundwater (Brugger et al., 2005). However, Black Spring waters are expelled at roughly ambient air temperatures, 23.1°C, as opposed to the 55°C of the Paralana Hot Springs, indicating a very different depth of fluid sources.



Figure 4.6: Black Spring obscured by a thick wall of vegetation (54J 350366E 6657590N)

4.2.3. Old Paralana Homestead Spring

Paralana Homestead Spring is approximately 1 km East of Black Spring (Figure 4.7). It is easily located due to the tall rushes and an anomalous large palm trees which was planted on the banks of the very small ~ 50 cm² spring-fed pool (Figure 4.8). The hills surrounding Paralana Homestead Spring consist of Miocene-Pliocene Willawortina Formation and the valley floor is composed of Pleistocene to Recent sediments.



Figure 4.7: Aerial photo of the Paralana Homestead Spring and Black Spring Localities. (Google Earth, 2018)

While still proximal to Paralana Hot Springs and Black Spring localities, Paralana Homestead Spring is more distal from the range front. Waters from this spring are expelled at 25.8°C, indicating a similar aquifer depth to that of Black Spring.



Figure 4.8: Old Paralana homestead's very small spring-fed pond (54J 351369E 6657693N)

4.2.4. Arkaroola Spring

Arkaroola Spring is a perennial spring-fed waterhole situated 16.7 km south of Paralana Hot Spring and approximately 3 km from the range front within the Neoproterozoic Adelaidean Rift sedimentary rocks (Figure 4.9). Waters within the ~50 m² Arkaroola Spring pool are stagnant, with no surficial flow from the pool (Figure 4.10). Pool waters were measured in November 2017 at 26.1 °C and by Brugger et al. (2005) at 28.3 °C. Whether this temperature is representative of the spring temperature or the equilibrium temperature of the pool is unclear. The perennial nature of the spring is evident as small crustaceans were observed within the pool in 2017.

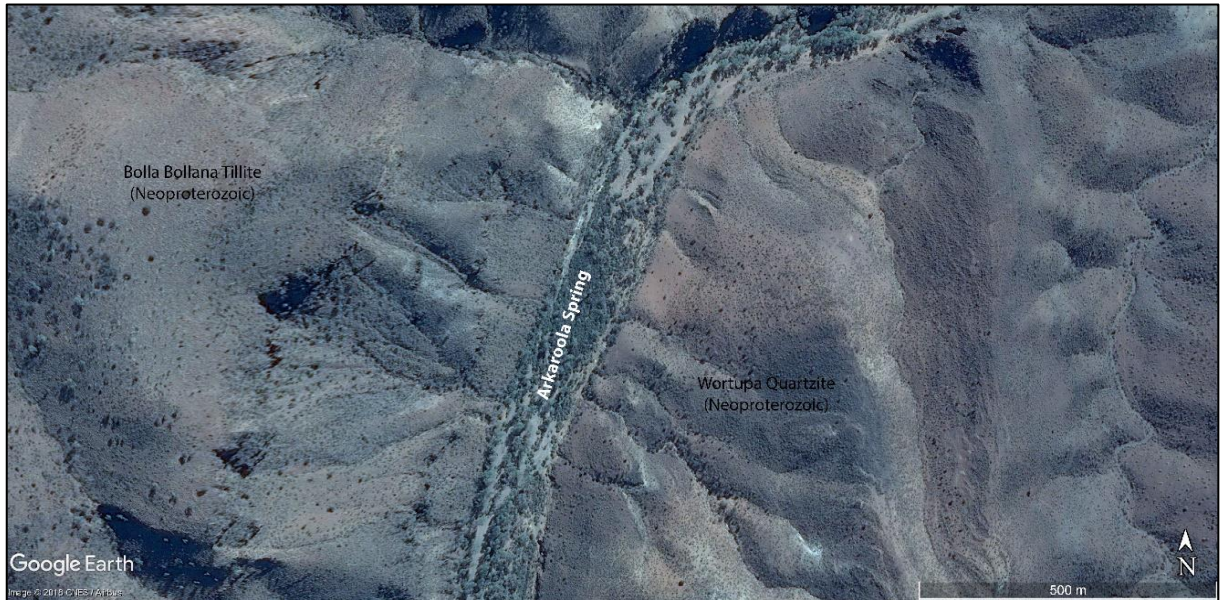


Figure 4.9: Aerial photo of the Arkaroola Spring Locality. (Google Earth, 2018)



Fig. 4.10: Arkaroola Spring (54J 349831E 6644483N)

4.2.4. Nepouie Spring

Nepouie Spring is located on the Wooltana Station, approximately 9 km southeast of the Wooltana Homestead along the eastern range front of the Flinders Ranges. This spring has been previously described by McNeil et al. (2011) during a regional ecological survey as the Nepouie Spring is home to a rare endemic species of fish, *Mongurnda clivicola*, which are only found in two localities in the Flinders Ranges. The spring has sufficient flow to produce a stream ~2

km long with numerous small pools (Figures 4.11; 4.12). Waters at the flow head were measured at 30.4 °C in November 2017 and 27 °C in May of 2010.

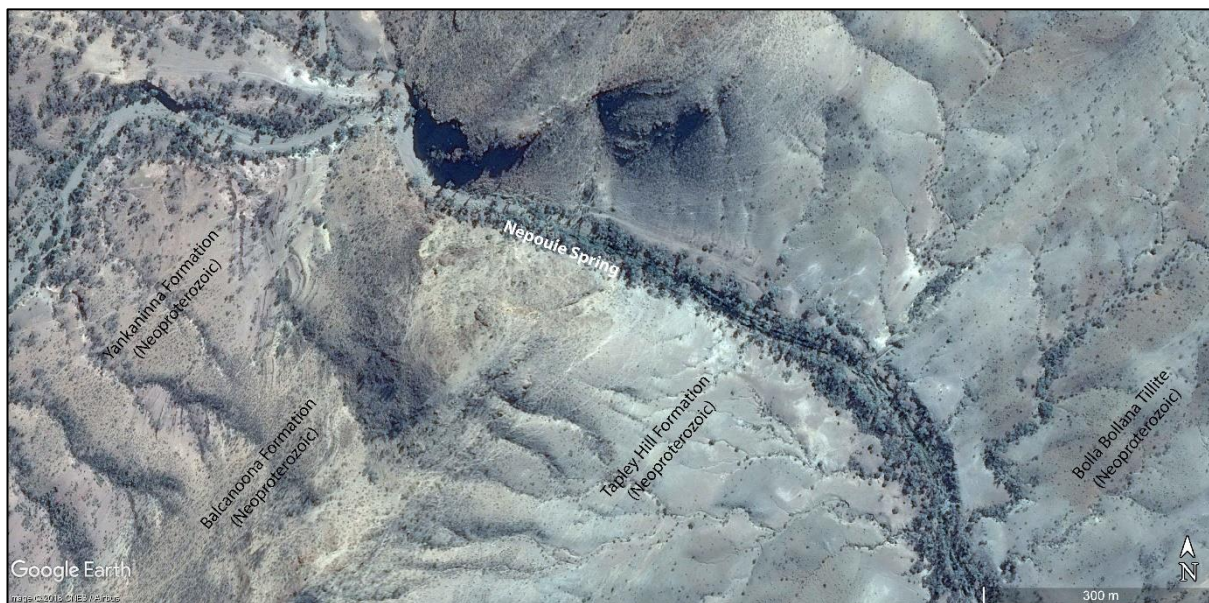


Figure 4.11: Aerial photo of the Nepouie Spring Locality. (Google Earth, 2018)



Figure 4.12: Nepouie Spring (54J 342433E 6627939N)

4.3 Methods and Results

4.3.1. *Water Sampling methodology*

Field observations and water samples were collected from Paralana Hot Springs, Black Spring, Paralana Homestead, Arkaroola Spring and Nepouie Spring during field excursions conducted between May 2016 and November 2017. Water from each spring was manually compression-filtered through 0.45 μm cellulose-nitrate filters into new, acid-washed HDPE bottles to avoid contamination. These samples were then analyzed by the CSIRO water chemistry laboratory in Adelaide for element geochemistry. Major and minor element analyses were conducted using inductively coupled plasma optical emission spectrometry (ICP-OES) and inductively coupled plasma mass spectrometry (ICP-MS). The summary of these results and comparison to historical sampling conducted is shown in tables 4.1 and 4.2.

4.3.2. *Temperature of the range-proximal springs*

The Paralana Hot Spring was measured in this study to be between 53.0 °C (May 2016) and 55.0 °C (November 2017). Comparing these results to historical readings (Table 2) shows a gradual cooling from 62.0 °C in 1927 and 1938 (Mawson, 1927; Grant, 1938) through 56.8 °C (Brugger et al., 2005) to 55.0 °C as observed in November of 2017. Nepouie spring is the only other spring observed with a temperature that deviates from atmospheric temperatures. Previous observations of Nepouie Spring by McNeil et al. (2011) indicated a water discharge temperature of 27 °C in May 2010, whereas discharge there was measured at 30.4 °C in November 2017. Arkaroola Spring discharge temperature has ranged between 28.3 °C (Brugger et al., 2005) to 26.1 °C (this study). Black Spring has ranged between 24.4 °C (Brugger et al., 2005) and 23.1 °C (this study). Paralana Homestead Spring was measured in this study to be 25.8 °C.

4.3.3 Elemental Geochemistry

The concentration of dissolved major cations within Paralana Hot Springs samples did not vary between May 2016 and November 2017 (Table 4.1). Paralana Hot Springs and Nepouie Spring are relatively depleted in Na^+ by comparison with Black Spring, Arkaroola Spring and Paralana Homestead Spring. Nepouie Spring is enriched in Ca^{2+} and depleted in K^+ when compared with samples acquired at the other springs. Arkaroola spring is heavily enriched in Mg^{2+} at 123 ppm, especially in comparison to Paralana Homestead Spring, which measures just 9-10 ppm Mg^{2+} .

Trace element concentration (Table 4.2) show relatively stable values for most tested elements within the Paralana Hot Spring between April 2016 and November 2017. There are some significant deviations from this trend, especially in Fe and Mn concentrations, which are enriched in the November 2017 samples. The cause of this enrichment is unclear. The waters from Paralana Homestead Spring and Black Spring show markedly different concentrations of As, Fe, Mn, Mo, and V. The differences in trace element composition indicate that these springs are tapping different aquifers, despite their geographic proximity.

		Paralana Hot Springs						Black Spring			Arkaroola Spring		Nepouie Spring	Paralana Homestead	
		This Study 11/11/17	This Study 21/05/16	Brugger et al., (2005)	Mawson (1927)	Grant (1938)	Heathgate (1998)	This Study	Brugger et al., (2005)	Mawson (1927)	This Study	Brugger et al., (2005)	This Study	This Study 11/11/17	This Study 24/04/17
Temp	°C	55.0	57.0	56.8	62	62	60	23.1	24.4	-	26.1	28.3	30.4	25.8	-
pH		-	4.0	6.4	-	8.2	-	-	7.86	-	-	8.43	-	-	-
<i>Major Cations</i>															
Na ⁺	ppm	277	278	272	368	333	300	361	428	435	355	160	235	351	361
K ⁺	ppm	26	25	23	96	37	24	34	29	45	30	18	11	26	30
Ca ²⁺	ppm	45	45	42	56	59	46	66	75	60	48	51	80	46	54
Mg ²⁺	ppm	17	17	15	3	27	16	17	19	15	123	48	84	9	10

Table 4.1: Temperature, pH and Major Cation analyses from natural spring along the range front.

	Paralana Hot Springs					Black Spring		Arkaroola Spring		Nepouie Spring	Paralana Homestead	
	This Study 11/11/17	This Study 24/04/17	Brugger et al., (2005)	Heathgate (1998)	Grant (1938)	This Study	Brugger et al., (2005)	This Study	Brugger et al., (2005)	This Study	This Study 11/11/17	This Study 11/04/17
Ag ppb	<0.05	<0.05	0.029	-	12	<0.05	0.033	<0.05	0.017	<0.05	<0.05	<0.05
Al ppb	-	-	5.41	<50	100	-	5.71	-	1.61	-	-	-
As ppb	10.4	10.6	37.4	<100	-	1.3	45.8	26.0	22	1.4	17.8	13.5
Au ppb	-	-	0.361	-	-	-	0.408	-	0.309	-	-	-
B ppm	0.16	0.16	0.19	0.21	0.8	0.32	0.39	0.28	0.17	0.19	0.30	0.32
Ba ppb	-	-	93.8	<100	200	-	22.8	-	104	-	-	-
Cd ppb	<0.1	<0.1	0.138	<10	-	<0.1	0.039	<0.1	0.05	<0.1	<0.1	<0.1
Co ppb	<0.05	<0.05	0.247	<20	<3	0.1	1.231	0.4	0.751	<0.05	<0.05	<0.05
Cr ppb	<0.5	<0.5	2.75	<30	2	<0.5	4.65	<0.5	2.84	<0.5	<0.5	<0.5
Cs ppb	-	-	16.2	-	400	-	0.456	-	<0.003	-	-	-
Cu ppb	<0.5	0.60	10.9	<20	12	<0.5	13.6	1.90	4.95	<0.5	<0.5	<0.5
Fe ppm	125.0	<1	0.06	0.69	0.02	32.0	0.41	1.0	<0.01	6.0	21.0	5.0
Ga ppb	<0.5	<0.5	2.94	-	-	<0.5	6.6	<0.5	2.99	<0.5	<0.5	<0.5
Ge ppb	-	-	3.1	-	2	-	0.713	-	0.357	-	-	-
Li ppm	-	-	0.049	-	0.6	-	0.125	-	0.004	-	-	-
Mn ppb	69.00	31.00	97.3	<20	1	12.40	392	<0.5	33	53.20	77.50	36.80
Mo ppb	25.6	28.9	32.8	<50	60	2.7	2.8	2.1	2.07	1.2	22.0	17.4
Nb ppb	-	-	0.045	-	-	-	0.303	-	<0.001	-	-	-
Ni ppb	<0.5	<0.5	6.68	50	<3	<0.5	12	<0.5	8.35	<0.5	<0.5	<0.5
Os ppb	-	-	0.351	-	-	-	0.8	-	0.188	-	-	-
Pb ppb	<0.05	<0.05	0.495	-	5	<0.05	0.422	<0.05	0.307	<0.05	<0.05	<0.05
Pd ppb	-	-	0.357	-	-	-	1.166	-	0.88	-	-	-
Pt ppb	-	-	0.00054	-	-	-	0.006	-	0.005	-	-	-
Rb ppb	-	-	195	-	-	-	151	-	5.94	-	-	-
Re ppb	-	-	0.0041	-	-	-	0.012	-	0.007	-	-	-
Rh ppb	-	-	0.0348	-	-	-	0.087	-	0.066	-	-	-
S ppm	-	-	47	-	-	-	28	-	21	-	-	-
Sb ppb	<0.2	0.4	0.608	-	-	<0.2	0.123	0.3	0.139	<0.2	<0.2	<0.2
Sc ppb	-	-	17.1	-	-	-	23.5	-	4.85	-	-	-
Se ppm	<0.05	<0.05	0.01	<0.01	-	<0.05	0.02	<0.05	0.02	<0.05	<0.05	<0.05
Si ppm	26	26	34.3	-	-	27	32.5	5.2	6.1	6.9	18	20
Sn ppb	<0.5	<0.5	0.058	-	10	<0.5	0.164	<0.5	0.062	<0.5	<0.5	<0.5
Sr ppb	0.34	0.34	339	-	500	0.51	600	0.68	496	1.2	0.37	0.42
Tl ppb	0.28	0.54	0.574	-	-	<0.05	0.0351	<0.05	0.007	<0.05	0.16	0.11
U ppb	0.22	0.23	0.0704	250	-	0.99	2.9	6.72	1.58	3.31	1.37	0.69
V ppb	0.1	0.2	17.8	<50	3	1.6	36.6	3.1	11.9	0.8	<0.1	0.4
W ppb	-	-	11	-	3	-	1.08	-	<0.01	-	-	-
Y ppb	<0.05	<0.05	0.395	-	-	0.3	0.954	<0.05	0.047	<0.05	<0.05	<0.05
Zn ppb	<0.5	0.5	11.4	<20	<30	<0.5	15.9	0.5	7.81	<0.5	<0.5	7.1
La ppb	<0.05	<0.05	0.0149	-	-	0.2	0.864	<0.05	0.0051	<0.05	<0.05	<0.05
Ce ppb	<0.05	<0.05	0.041	-	-	0.4	1.43	<0.05	0.0091	<0.05	<0.05	<0.05
Pr ppb	<0.05	<0.05	<0.001	-	-	0.05	0.172	<0.05	<0.001	<0.05	<0.05	<0.05
Nd ppb	<0.05	<0.05	0.0039	-	-	0.2	0.73	<0.05	0.0016	<0.05	<0.05	<0.05
Sm ppb	<0.05	<0.05	0.001	-	-	<0.05	0.158	<0.05	0.0012	<0.05	<0.05	<0.05
Gd ppb	<0.05	<0.05	<0.001	-	-	0.1	0.246	<0.05	<0.001	<0.05	<0.05	<0.05
Tb ppb	<0.05	<0.05	<0.001	-	-	<0.05	0.0283	<0.05	<0.001	<0.05	<0.05	<0.05
Dy ppb	<0.05	<0.05	<0.001	-	-	<0.05	0.161	<0.05	<0.001	<0.05	<0.05	<0.05
Ho ppb	-	-	<0.001	-	-	-	0.0261	-	<0.001	-	-	-
Er ppb	<0.05	<0.05	<0.001	-	-	<0.05	0.0777	<0.05	<0.001	<0.05	<0.05	<0.05
Tm ppb	<0.05	<0.05	<0.001	-	-	<0.05	0.0078	<0.05	<0.001	<0.05	<0.05	<0.05
Yb ppb	<0.05	<0.05	<0.001	-	-	<0.05	0.0482	<0.05	<0.001	<0.05	<0.05	<0.05

Table 4.2: Major element and stable isotope analyses from natural springs along the range front. Elements quoted in ppm were measured by ICP-AES and those in ppb by ICP-MS. All concentrations from Grant (1938) and Heathgate Resources (1998) were quoted in ppm and are converted to ppb by Brugger et al., (2005).

4.4. Discussion

4.4.1. Faults as fluid conduits and sources

Fluids of the Paralana Hot Springs differ from the other natural springs in the area most notably because they are around 30 °C warmer. This stark difference denotes a different source for the fluids expelled here than elsewhere along the range front. Paralana Hot Springs are coincident with the intersection of the Paralana Fault and a rightward kink in the ranges. Based on the ~57 °C temperature of the expelled fluids and the placement of the spring relative to major geological and geomorphic features, Paralana Hot Springs are interpreted to be tapping the Paralana Fault. The oxygen and hydrogen stable isotope ratios measured by Brugger et al. (2005) indicate that the fluids from Paralana Hot Springs are of meteoric origin. Further, Brugger et al. (2005) suggest that the relatively low levels of dissolved elements, gypsum and silica mineralization proximal to the springs indicates that the fluids expelled from Paralana Hot Springs have not reached high temperatures. They confirm this through geothermometric calculations which show that the temperature of the most recent water-rock interaction is in equilibrium at 95.5 °C. The 76 °C/ km measured geothermal gradient from a geothermal energy pilot project east of the ranges (Petratherm, n.d.) suggests circulation depths of approximately 1.4 km to reach the equilibrium water-rock interaction temperature suggested by Brugger et al. (2005). Estimates for the residence time of fluids expelled were proposed to be between a minimum of 9 years up to a maximum of 226,500 years, depending upon the hydraulic conductivity of the Mount Painter Inlier at depth (Brugger et al., 2005). Based on the proximity of Black Spring and the Paralana Homestead Spring to the Paralana Host Spring, it has been suggested that all these springs are similarly tapping meteoric fluids circulating within the Mount Painter Inlier (Brugger et al., 2005).

An identified problem with assuming that the Mount Painter Inlier is the source for fluids released from Paralana Hot Springs is that calculated infiltration rates for meteoric fluids based upon the annual rainfall and catchment area are insufficient to produce the discharge rate observed today (Brugger et al., 2005). However, the calculations of Brugger et al. (2005) used an incorrect value for the annual rainfall in the Mount Painter Inlier. Brugger et al. (2005) used a value of 20.3 mm/year over a catchment area of 147 km², which yielded a total rain water flow rate of 1.21 L/s. However, the long-term average rainfall, as measured at Arkaroola Village, is 260.7 mm/year between 1938 and 2018 (Bureau of Meteorology, n.d.). Thus, the calculation is as follows:

$$V_r = A_c \times H_r$$

$$V_r = 147 \text{ km}^2 \times 260.7 \text{ mm/year}$$

$$V_r \approx 3.832 \times 10^7 \text{ m}^3/\text{year}$$

$$V_r \approx 1215 \text{ L/s}$$

Where V_r is the volume of rainwater fallen within the catchment area (A_c) at an annual rainfall height of (H_r).

Present precipitation is therefore sufficient to maintain the discharge rate of 16 L/s calculated by Brugger et al., (2005). The above calculation relies on the unrealistic assumption that all precipitation infiltrates the Mount Painter Inlier, and none is lost to evapo-transpiration or surface runoff. Despite the errors in calculation, Brugger et al., (2005) still concluded that the Mount Painter Inlier is indeed the water source based upon the isotopic composition and the relatively short calculated residence time.

4.4.2. Dissolved uranium within the spring waters

The low concentration of uranium dissolved within the spring waters sampled (Figure 4.13) is of interest considering their proximity to uranium-enriched crystalline rocks of the Mount Painter Inlier and uranium deposits hosted by Eromanga Basin sediments. In the case of Paralana Hot Springs, Skirrow et al. (2011) suggested that the low uranium concentrations are due to the meteoric origin of the source fluids and their saturation in oxygen and carbon dioxide. The oxidized waters readily dissolve uranium at 25 °C, but are reduced gradually by interactions with fresh granites as the fluid temperature approaches 100 °C. Thus, the fluids escaping from Paralana Hot Springs, which have been calculated to have equilibrated at 95.5 °C by Brugger et al., (2005) are in a reduced state and unable to transport uranium to the surface (Skirrow et al., 2011). This model provides concise geochemical evidence against neotectonic faults of the area acting as pathways for uranium-rich fluids on their way into the Eromanga Basin.

The uranium concentrations of springs and wells proximal to the range front are heavily depleted in uranium and there is a relatively steady increase in groundwater uranium concentrations away from the ranges up to a maximum of 710 ppb approximately 30 km east of the ranges. Michaelsen et al. (2016) has interpreted this depletion of groundwater uranium in the vicinity to the Paralana Trough to be the result of an active hydrocarbon system in the area. The high geothermal gradient of the underlying Mount Painter Inlier is providing the heat necessary to produce hydrocarbons from the organic-rich Bulldog Shale, which underlies the

mineralized Eyre and Namba formations. Migrating hydrocarbons act as the reducing agents necessary to precipitate uranium out of solution. Thus, the zone of anomalously low groundwater uranium concentrations proximal to the ranges is due to the uranium having been dropped out of solution and existing in mineral form. Further away from the ranges, where the Mount Painter Inlier is more deeply buried, the organic-rich Bulldog Shale is not sufficiently mature to produce hydrocarbons and uranium is able to exist in solution within the groundwater (Michalesen et al., 2016).

The above hypotheses are robust explanations for the low uranium concentrations of the groundwater from Paralana Hot Springs and the Paralana Trough. Why then are the waters sampled from other springs in the area similarly depleted uranium? Arkaroola Spring contains 6.72 ppb U, Nepouie Spring contains 3.31 ppb U and both springs are hosted by Adelaidean Rift metasedimentary rocks as opposed to crystalline rocks of the Mount Painter Inlier. Based upon the low uranium concentrations of groundwaters being naturally expelled from springs distal to the active hydrothermal system of Paralana Hot Springs, it is concluded that upwelling fluids of the Northern Flinders Ranges are not the source of uranium.

Airborne radiometrics of the Mount Painter Inlier and Frome Embayment (Figure 4.13) shows a striking pattern of uranium-rich sediments being shed from the Mount Painter Inlier. While the drainage pattern observed today is not representative of the paleodrainage patterns measured within the Eyre Formation (Hill and Hore, 2011), the erosion of uranium-rich sediments from the Mount Painter Inlier into the surrounding basins has been an ongoing process since at least the Late Cretaceous while the Mount Painter Inlier has been exposed (Skirrow et al., 2009). As such, the interpreted source of uranium is not the aquifers of the Frome Embayment, but the uranium-rich detritus shed from the Mount Painter Inlier. Future research should include: the redox potential of meteoric fluids, the infiltration rate of meteoric fluids into the Eromanga Basin sediments, and the chemical composition of ground waters from specific aquifer depths.

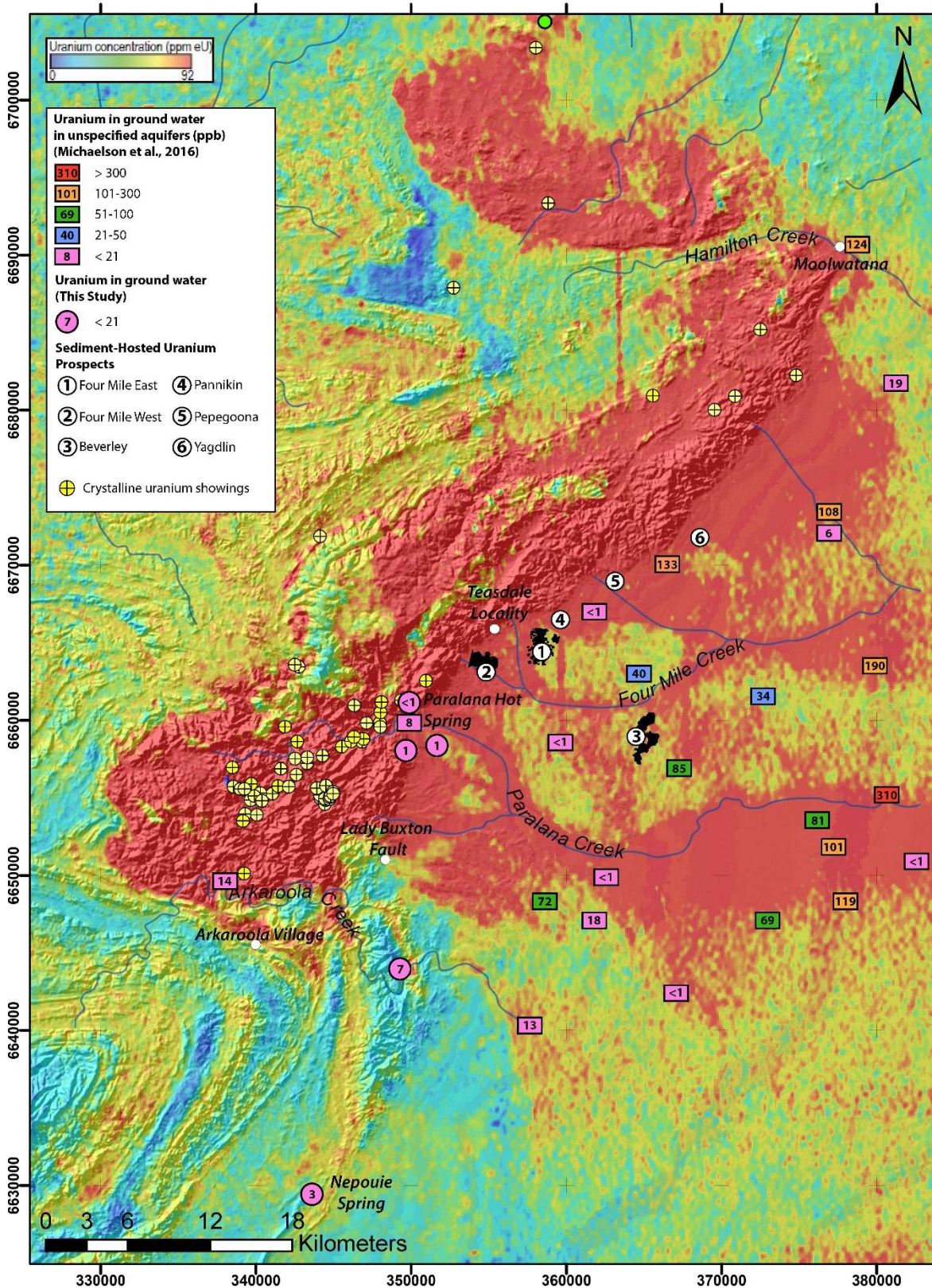


Figure 4.13: Uranium radiometric map of the Mount Painter Inlier with superimposed historical ground water concentrations of uranium (modified from Michaelson et al., 2016)

Conclusions

The main aims of this study were to identify the meso-scale faults of the Paralana Escarpment in order to examine the interactions of these faults with uranium-bearing fluids. Through the use of field mapping along the Paralana Escarpment, graphical analysis of observed faults, SEM and Optical microscopy of fault rocks, and hydrogeochemical analysis of natural spring waters, the following conclusions have been reached:

- i) The structures identified show three main orientations, only one of which actively interacts with the sediments of the mineralized Eromanga Basin
- ii) None of the fault rocks sampled show direct evidence of oxidized fluid flow. The only observed example of oxidation due to fluid flow was collected from a cemented fracture, not a fault surface.
- iii) Groundwater from springs along the range front show depleted U concentrations relative to more distal samples

As such, I conclude that the neotectonic faults along the Paralana Escarpment do not directly influence uranium fluid flow. These Miocene to Recent faults are responsible for accommodating the uplift of the Flinders Ranges of the region, and hence are indirectly responsible for the hydrostatic head which forces the flow of fluids.

Recommendations for future work

The Arkaroola area has been well studied from a multitude of different research direction. Despite this ongoing interest in the area, the area is still relatively poorly understood. With regard to where future research should focus in order to build upon this study, the following recommendations are provided:

- Oriented Samples of fault rocks for further microstructural analysis of fault kinematics to determine if all catalogued faults are indeed representative of exclusively dip-slip movement.
- Whole-rock geochemical comparison of fault rocks with wall rocks to determine whether there is a bulk chemical change which could be attributed to oxidized fluid flow.
- Deeper research into the hydrogeochemical conditions of the Paralana Trough to positively correlate escaping spring waters to individual aquifers.

References

- Alley, N. F. and Benbow, M. C., (1995). Interior non-marine basins. In: Drexel, J. F. and Preiss, W. V. (eds). *The Geology of South Australia*. Adelaide. South Australia Geological Survey. Bulletin 54, Vol. 2, 187-200.
- Allmendinger, R. (2016). Stereonet (Version 9.8.6). Retrieved from <http://www.geo.cornell.edu/geology/faculty/RWA/programs/stereonet.html>
- Barton, C. A., Zoback, M. D., & Moos, D. (1995). Fluid flow along potentially active faults in crystalline rock. *Geology*, 23(8), 683-686.
- Bastrakov, E. N., Jaireth, S., & Mernagh, T. P. (2010). Solubility of uranium in hydrothermal fluids at 25 to 300 C. *Geoscience Australia Record*, 2010/29.
- Belperio, A. P. (1995). Quaternary. In: Drexel, J. F. and Preiss, W. V. (eds). *The Geology of South Australia*. Adelaide. South Australia Geological Survey. Bulletin 54, Vol. 2, 219-280.
- Bense, V. F., Gleeson, T., Loveless, S. E., Bour, O., & Scibek, J. (2013). Fault zone hydrogeology. *Earth-Science Reviews*, 127, 171-192.
- Brugger, J., Long, N., McPhail, D. C. & Plimer, I. (2005). An active amagmatic hydrothermal system: The Paralana hot springs, Northern Flinders Ranges, South Australia. *Chemical Geology* 222, 35-64.
- Bureau of Meteorology (n.d.). *Summary Statistics Arkaroola*. Retrieved February 06, 2018, from http://www.bom.gov.au/climate/averages/tables/cw_017099.shtml
- Callen, R. A. & Tedford, R. H. (1976). New late Cainozoic rock units and depositional environments, Lake Frome area, South Australia. *Royal Society of South Australia Transactions* 100, 125-167.
- Callen, R. A., Alley, N. F. & Greenwood, D. R. (1995). Tertiary: interior non-marine basins - Lake Eyre basin. In: Drexel, J. F. and Preiss, W. V. (eds). *The Geology of South Australia*. Adelaide. South Australia Geological Survey. Bulletin 54, Vol. 2, 188-194.
- Callen, R. A., Sheard, M. J., Benbow, M. C. & Belperio, A. P. (1995). Quaternary: Alluvial fans and piedmont slope deposits. In: Drexel, J. F. and Preiss, W. V. (eds). *The Geology of South Australia*. Adelaide. South Australia Geological Survey. Bulletin 54, Vol. 2, 241-243.
- C  lerier, J., (2002). Neotectonics and intraplate deformation in the Northern Flinders Ranges, South Australia. Unpublished B.Sc. Honours Thesis, The University of Adelaide, School of Earth and Environmental Sciences, Department of Geology and Geophysics. Adelaide.
- Celerier, J., Sandiford, M., Hansen, D. L. and Quigley, M. C. (2005). Modes of active intraplate deformation, Flinders Ranges, Australia. *Tectonics*. 24, 1-17.
- Coats, R. P. & Blissett, A. H. (1971). Regional and Economic Geology of the Mount Painter Province. Adelaide: A. B. James, Government Printer. Bulletin 43, pp.
- Curtis, J. L., Brunt, D. A. & Binks, P. J. (1990). Tertiary Paleochannel Uranium Deposits of South Australia. In: Hughes, F. E. (ed.) *Geology of the Mineral Deposits of Australia and Papua New Guinea*. Melbourne. Australian Institute of Mining and Metallurgy, 1631-1636.
- Davey, J. E. (2009). Tectonostratigraphic evolution of an intracontinental terrain: the geological evolution of the Frome Embayment, Eromanga Basin, Australia. Unpublished PhD thesis. University of Adelaide, School of Earth and Environmental Sciences and Australian School of Petroleum. Adelaide

- Davis, K., Burbank, D. W., Fisher, D., Wallace, S., & Nobes, D. (2005). Thrust-fault growth and segment linkage in the active Ostler fault zone, New Zealand. *Journal of Structural Geology*, 27(8), 1528-1546.
- de Gromard, R. Q. (2013). The significance of E–W structural trends for the Alice Springs Orogeny in the Charters Towers Province, North Queensland. *Tectonophysics*, 587, 168-187.
- Drexel, J. F. and Preiss, W. V. (Eds.) (1995). The Geology of South Australia. Vol. 1, The Precambrian, *South Australia Geological Survey, Bulletin*, 54.
- Drexel, J. F. and Preiss, W. V. (Eds.) (1995). The Geology of South Australia. Vol. 2, The Phanerozoic, *South Australian Geological Survey, Bulletin*, 54.
- Elburg M. A., Andersen T., Bons P. D., Weisheit A., Simonsen S. L., Smet I. (2012) Metasomatism and metallogeny of A-type granites of the Mt Painter–Mt Babbage Inliers, South Australia. *Lithos*, 151, 83–104
- Elburg, M. A., Bons, P. D., Dougherty-Page, J., Janka, C. E., Neumann, N. & Schaefer, B. (2001). Age and metasomatic alteration of the Mount Neill Granite at Nooldoonooldoona Waterhole, Mount Painter Inlier, South Australia. *Australian Journal of Earth Sciences* 48, 721-730.
- Elburg, M. A., Bons, P. D., Foden, J., & Brugger, J. (2003). A newly defined Late Ordovician magmatic–thermal event in the Mt Painter Province, northern Flinders Ranges, South Australia. *Australian Journal of Earth Sciences*, 50(4), 611-631.
- Fabris, A. J. and Sheard, M. J., (2008) Guides for mineral exploration through and within the regolith – central Gawler Craton and Curnamona Province. *Mesa Journal*, 51, 41-45.
- Fanning, C. M., Teale, G. S. & Robertson, R. S. (2003). Is there a Willyama Supergroup sequence in the Mount Painter Inlier? In: Peljo, M. (ed.) *Broken Hill Exploration Initiative*. Broken Hill, Australia: Geoscience Australia, 38-41.
- Flöttmann, T. and James, P. (1997). Influence of basin architecture on the style of inversion and fold-thrust belt tectonics - the southern Adelaide Fold-Thrust Belt, South Australia. *Journal of Structural Geology*. 19(8): 1093-1110.
- Flöttmann, T., James, P., Rogers, J. and Johnson, T. (1994). Early Palaeozoic foreland thrusting and basin reactivation at the Palaeo-Pacific margin of the southeastern Australian Precambrian Craton: a reappraisal of the structural evolution of the Southern Adelaide Fold-Thrust Belt. *Tectonophysics*. 234(1–2): 95-116.
- Foden, J., Elburg, M. A., Dougherty-Page, J. & Burt, A. (2006). The timing and duration of the Delamerian Orogeny: correlation with the Ross Orogen and implications for Gondwana assembly. *The Journal of Geology*. 114. 189–210.
- Glanville, D. H. (2010). Australian seismological report 2010, *Geoscience Australia*. record 2011/16: 77.
- Government of South Australia, Department for Environment and Conservation. (2011, July 22). *Arkaroola to be Protected Forever* [News Release]. Retrieved from https://www.arkaroola.com.au/documents/ArkaroolaProtected_media_release_20110722.pdf
- Government of South Australia, Minister for Sustainability, Environment and Conservation. (2012, February 29). *Historic Arkaroola Legislation Passes Upper House* [News Release]. Retrieved from https://www.premier.sa.gov.au/images/news_releases/12_02Feb/Arkaroola.pdf
- Grant, K. (1938). The radioactivity and composition of the water and gases of the Paralana Hot Spring. *Transactions of the Royal Society of South Australia*, 62, 357-364.
- Greenhalgh, S. A., Love, D., Malpas, K. and McDougall, R. (1994). South Australian earthquakes, 1980-92. *Australian Journal of Earth Sciences*. 41. 483-495.

- GSSA, 1983. NATMAP Umberatana Map Sheet. Primary Industries and Resources South Australia, South Australia.
- Gül, M., Gürbüz, K., & Kalelioğlu, Ö. (2012). Lithology discrimination in foreland basin with Landsat TM. *Journal of the Indian Society of Remote Sensing*, 40(2), 257-269.
- Hancock, P. L. (1988). Neotectonics. *Geology Today*. 4(2): 57-61.
- Hasterok, D. (2011, January 12). The International Heat Flow Commission. *The Global Heat Flow Database*. Retrieved February 12, 2018, from <http://www.heatflow.und.edu/index2.html>
- Heathgate Resources, 1998. Beverley Uranium Mine: Environmental Impact Statement. Heathgate Resources Pty Ltd, South Australia.
- Heathgate Resources, 2009. Beverley Four Mile project: public environment report and mining lease proposal. Adelaide, Heathgate Resources Pty Ltd.
- Hill, S. M., & Hore, S. B. (2011). Key insights into range-front mineral system expression and evolution from regolith and long-term landscape history, NE Flinders Ranges. *Mesa Journal*, 63, 20-31.
- Hillis, R. R., Sandiford, M., Reynolds, S. D. and Quigley, M. C. (2008). Present-day stresses, seismicity and Neogene-to-Recent tectonics of Australia's 'Passive' margins: intraplate deformation controlled by plate boundary forces. *Geological society, London, special publications*. 306: 71-89.
- Holford, S. P., Hillis, R. R., Hand, M., & Sandiford, M. (2011). Thermal weakening localizes intraplate deformation along the southern Australian continental margin. *Earth and Planetary Science Letters*, 305(1-2), 207-214.
- Hore, S. B., & Hill, S. M. (2009). Palaeoredox fronts: setting and associated alteration exposed within a key section for understanding uranium mineralisation at the Four Mile West deposit. *MESA Journal*, 55, 34-39.
- Hore, S. B. and Hill, S. M., (2015). Geological Field Excursion Guide: from Arkaroola to Paralana Hot Springs. Arkaroola Education and Research Foundation Pty. Ltd.
- Hore, S.B., 2015. Mount Painter Regional Geological Map, Geological Survey of South Australia, Adelaide
- Hou, B., Fabris, A. J., Keeling, J. L., & Fairclough, M. C. (2007). Cainozoic palaeochannel-hosted uranium and current exploration methods, South Australia. *Mesa Journal*, 46, 34-39.
- Ihmle, P. F. and Jordan, T. H. (1994). Teleseismic search for slow precursors to large earthquakes. *Science* 266: 1547-1551.
- Jaireth, S., Bastrakov, E. N. and Fisher, L., (2008). Two types of sandstone uranium systems in the Frome Embayment? Preliminary results of fluid flow and chemical modelling. *AusIMM International Uranium Conference 2008*, Adelaide, 18-19 June 2008.
- Jayawardena, C.L. (2013). Characteristics of neotectonic faulting in the Mount Lofty and Flinders Ranges, South Australia. Unpublished PhD Thesis. University of Wollongong, School of Earth and Environmental Sciences, Sydney.
- Jeuken, B., (2008). Groundwater flow modelling of migration of mining fluids from the proposed Four Mile East mining zone. Final report. Heathgate Beverley Mine report.
- Krieg, G. W., Alexander, E. M. & Rogers, P. A. (1995). Mesozoic: Jurassic-Cretaceous epicratonic basins: Eromanga basin. In: Drexel, J. F. and Preiss, W. V. (eds). *The Geology of South Australia*. Adelaide. South Australia Geological Survey. Bulletin 54, Vol. 2, 101-127.
- Leonard, M. (2006). One hundred years of earthquake recording in Australia. *Bulletin of the Seismological Society of America* 97.

- Love, D. N., Preiss, W. V. and Belperio, A. P. (1995). Seismicity, neotectonics and earthquake risk. In: Drexel, J. F. and Preiss, W. V. (eds). *The Geology of South Australia*. Adelaide. South Australia Geological Survey. Bulletin 54, Vol. 2, 268-270.
- Loveley, D. R., Phillips, E. J. P., Gorby, Y. A. and Landa, E. R., (1991). Microbial reduction of uranium. *Nature*, 350, 413-416.
- Lubiniecki, D. C., King, R. C., Holford, S. P., Bunch, M. C., Hore, S. B., Hill, S.M., (in prep) The effects of deformation band on uranium mineralization in sedimentary sequences
- Mawson, D. (1927). *The Paralana hot spring*. Royal Society of South Australia.
- McConachy, G., McInnes, D. & Paine, J. (2006). Airborne Electromagnetic signature of the Beverley Uranium deposit, South Australia. In: Geophysicists, S.o.E. (ed.) *SEG - 66th Annual Meeting*. New Orléans, 790-794.
- McLaren, S., Dunlap, W. J., Sandiford, M. & McDougall, I. (2002). Thermochronology of the high heat-producing crust at Mount Painter, South Australia: Implications for tectonic reactivation of continental interiors. *Tectonics* 21(4). 1-17.
- McLaren, S., Sandiford, M., Powell, R., Neumann, N., & Woodhead, J. (2006). Palaeozoic Intraplate Crustal Anatexis in the Mount Painter Province, South Australia: Timing, Thermal Budgets and the Role of Crustal Heat Production. *Journal of Petrology*, 47(12), 2281-2302.
- McNeil, D. G, White, M. and Schmarr, D. W. (2011). Assessment of endemic fish (*Mogurnda clivicola*) and native vegetation at springs in the northern Flinders Ranges. Report to the South Australian Arid Lands Natural Resources Management Board, Port Augusta. South Australian Research and Development Institute and South Australian Department for Water. *SARDI Research Report Series*. 518.
- Mitchell, R. (1897). *Hot Springs at Paralana* [Photograph found in Mitchell Collection and Paralana Springs Collection, State Library of South Australia, Adelaide]. Retrieved February 7, 2018, from https://collections.slsa.sa.gov.au/resource/PRG_1610/11/139 (Originally photographed 1897)
- Müller, R. D., Dyksterhuis, S., & Rey, P. (2012). Australian paleo-stress fields and tectonic reactivation over the past 100 Ma. *Australian Journal of Earth Sciences*, 59(1), 13-28.
- Neumann, N., Sandiford, M. & Foden, J. (2000). Regional geochemistry and continental heat flow; implications for the origin of the South Australian heat flow anomaly. *Earth and Planetary Science Letters* 183, 107-120.
- Otake, T., Wesolowski, D. J., Anovitz, L. M., Allard, L. F., & Ohmoto, H. (2007). Experimental evidence for non-redox transformations between magnetite and hematite under H₂-rich hydrothermal conditions. *Earth and Planetary Science Letters*, 257(1-2), 60-70.
- Paul, E., Flöttmann, T. & Sandiford, M. (1999). Structural geometry and controls on basement-involved deformation in the northern Flinders Ranges, Adelaide Fold Belt, South Australia. *Australian Journal of Earth Sciences*. 46, 343-354.
- Peacock, D. C., Nixon, C. W., Rotevatn, A., Sanderson, D. J., & Zuluaga, L. F. (2016). Glossary of fault and other fracture networks. *Journal of Structural Geology*, 92
- Peacock, D. C., Nixon, C. W., Rotevatn, A., Sanderson, D. J., & Zuluaga, L. F. (2017). Interacting Faults. *Journal of Structural Geology*, 97.
- Peltzer, G. and Tapponnier, P. (1988). Formation and evolution of strike-slip faults, rifts, and basins during India-asia collision: an experimental approach. *Journal of Geophysical Research*. 93: 15085-15172.
- Peng, Z. and Gomberg, J. (2010). An integrated perspective of the continuum between earthquakes and slow-slip phenomena. *Nature Geoscience*, 3(9). 599-607.

- Petratherm confirms 'exceptionally high' temp gradient. (2005, October 18). RWE Business News Information Service. Retrieved from <http://link.galegroup.com.proxy.library.adelaide.edu.au/apps/doc/A137692134/ITOF?u=adelaide&sid=ITOF&xid=5b8ec74e>
- Pointon, V.J. (2010). Structure and Thermochronology of an E-W profile through the Mount Painter Province, Northern Flinders Ranges, South Australia: is this a southern example of deformation and exhumation driven by the Alice Springs Orogeny?. Unpublished B.Sc. Honours Thesis, The University of Adelaide, School of Earth and Environmental Sciences, Department of Geology and Geophysics. Adelaide.
- Ponder, W. F. (1986). Mound springs of the great artesian basin. In *Limnology in Australia* (pp. 403-420). Springer, Dordrecht.
- Preiss, W. V. (1987). The Adelaide Geosyncline: Late Proterozoic stratigraphy, sedimentation, palaeontology and tectonics. Geological Survey of South Australia Bulletin, 53, 438 pp.
- Preiss, W. V. (1995). Delamerian Orogeny. In: Drexel, J.F. and Preiss, W. V. (eds). *The Geology of South Australia*. Adelaide. South Australia Geological Survey. Bulletin 54, Vol. 1, 101-127.
- Preiss, W. V. (2000). The Adelaide Geosyncline of South Australia and its significance in Neoproterozoic continental reconstruction. *Precambrian Research*. 100, 21-63.
- Preiss, W. V., Belperio, A. P., Cowley, W. M. & Rankin, L. R. (1995). Neoproterozoic. In: Drexel, J.F. and Preiss, W. V. (eds). *The Geology of South Australia*. Adelaide. South Australia Geological Survey. Bulletin 54, Vol. 1, 171-203.
- Purvis, W. J. (1927, November 25). PARALANA HOT SPRINGS. *Port Adelaide News (SA :1913 - 1933)*, p. 3. Retrieved February 8, 2018, from <http://nla.gov.au/nla.news-article212969581>
- Quigley, M. C., Cupper, M. L. and Sandiford, M. (2006b). Quaternary faults of South-Central Australia: palaeoseismicity, slip rates and origin. *Australian Journal of Earth Sciences*. 53, 285-310.
- Quigley, M. C., Sandiford, M. and Cupper, M. L. (2007a). Distinguishing tectonic from climatic controls on range-front sedimentation. *Basin Research*. 19, 491-505.
- Quigley, M. C., Sandiford, M., Fifield, L. K. and Alimanovic, A. (2006a). Bedrock erosion and relief production in the northern Flinders Ranges, Australia. *Earth Surface Processes and Landforms*. 32, 929-944.
- Quigley, M. C., Sandiford, M., Fifield, L. K. and Alimanovic, A. (2007b). Landscape responses to intraplate tectonism: Quantitative constraints from Be nuclide Abundances. *Earth and Planetary Science Letters*. 261, 120-133.
- Roach, I. C., Jaireth, S., & Costelloe, M. T. (2014). Applying regional airborne electromagnetic (AEM) surveying to understand the architecture of sandstone-hosted uranium mineral systems in the Callabonna Sub-basin, Lake Frome region, South Australia. *Australian Journal of Earth Sciences*, 61(5), 659-688.
- Sandiford, M. (2003a). Neotectonics of southeastern Australia: Linking the Quaternary faulting record with seismicity and In-situ stress. *Geological Society of Australia Special Publication*. 22, 101-113.
- Sandiford, M. (2003b). Geomorphic Constraints on the Late Neogene Tectonics of the Otway Range, Victoria. *Australian Journal of Earth Sciences*. 50, 69-80.
- Sandiford, M. (2008) Four Mile Creek Report for URS. In: Heathgate (2009). Beverley Four Mile project: public environment report and mining lease proposal. Adelaide, Heathgate Resources Pty Ltd.

- Sandiford, M., & Egholm, D. L. (2008). Enhanced intraplate seismicity along continental margins: some causes and consequences. *Tectonophysics*, 457(3-4), 197-208.
- Sandiford, M., Hand, M. & McLaren, S. (1998). High geothermal gradient metamorphism during thermal subsidence. *Earth and Planetary Science Letters*. 163, 149-165.
- SARIG. (n.d.). South Australian Resources Information Gateway. Government of South Australia. Retrieved Feb 17, 2018 from <https://map.sarig.sa.gov.au/>
- Senior, B. R. & Mabbutt, J. A. (1979). A proposed method of defining deeply weathered rock units based on regional geological mapping in south-west Queensland. *Journal of the Geological Society of Australia*. 28, 491-500.
- Skirrow, R. G., (Ed.) (2009). Uranium ore-forming systems of the Lake Frome region, South Australia: regional spatial controls and exploration criteria. *Geoscience Australia Record*, 2009/40.
- Skirrow, R. G., (Ed.) (2011). Uranium mineralisation events in Australia geochronology of the Nolans Bore, Oasis, Kintyre, Mt Gee-Armchair and Maureen uranium deposits. *Geoscience Australia Record*, 2011/12.
- SKM, (2008). Environmental studies for the Four Mile Project - Conceptual hydrogeological model of the Four Mile region. Sinclair Knight Merz. 44.
- Sprigg, R. C. (1945). Some aspects of the geomorphology of a portion of the Mount Lofty Ranges. *Transactions of the Royal Society of South Australia*. 69, 227-304.
- Sprigg, R. C. (1984). *Arkaroola-Mount Painter in the northern Flinders Ranges, SA: the last billion years*. Arkaroola.
- Sylvester, A. G. (1988). Strike-slip faults. *Geological Society of America Bulletin*. 100(11), 1666-1703.
- Teale, G. S. (1993). Paleoproterozoic: Mount Painter and Mount Babbage Inliers. In: Drexel, J. F. & Preiss, W. V. (eds.) *The Geology of South Australia*. Adelaide: South Australia Geological Survey, 93-100.
- Teasdale, J. (1993). Proterozoic tectonic models with application to the Mount Painter Inlier. Unpublished B.Sc. Honours Thesis, The University of Adelaide, School of Earth and Environmental Sciences, Department of Geology and Geophysics. Adelaide.
- Thomas, M., Clarke, J. D. A., Gostin, V. A., Williams, G. E., & Walter, M. R. (2012). The Flinders Ranges and surrounds, South Australia: A window on astrobiology and planetary geology. *Episodes*, 35(1), 226-235.
- Tokarev, V. (2005). Neotectonics of the Mount Lofty Ranges (South Australia). Unpublished PhD thesis. University of Adelaide, School of Earth and Environmental Sciences, Department of Geology and Geophysics. Adelaide
- Tokarev, V., Sandiford, M., & Gostin, V. (1999). Landscape evolution in the Mount Lofty Ranges: implications for regolith development. In *New approaches to an old continent, 3rd Australian Regolith Conference Proceedings, Regolith*. 98, 127-134.
- Torabi, A., & Berg, S. S. (2011). Scaling of fault attributes: A review. *Marine and Petroleum Geology*, 28(8), 1444-1460.
- Vidale, J. E. and Houston, H. (2012). Slow slip: A new kind of earthquake. *Physics Today* 65(1): 38-43.
- Walker, R. J., Holdsworth, R. E., Armitage, P. J., & Faulkner, D. R. (2013). Fault zone permeability structure evolution in basalts. *Geology*, 41(1), 59-62.
- Weisheit, A., Bons, P. D., Danišik, M., & Elburg, M. A. (2014). Crustal-scale folding: Palaeozoic deformation of the Mt Painter Inlier, South Australia. Geological Society, London, Special Publications, 394(1), 53-77.
- Weng, Q. (Ed.). (2007). *Remote sensing of impervious surfaces*. CRC Press.

- White, A. F., Peterson, M. L., & Hochella Jr, M. F. (1994). Electrochemistry and dissolution kinetics of magnetite and ilmenite. *Geochimica et Cosmochimica Acta*, 58(8), 1859-1875.
- Willey, J. D., Mullaugh, K. M., Kieber, R. J., Avery Jr, G. B., & Mead, R. N. (2012). Controls on the redox potential of rainwater. *Environmental science & technology*, 46(24), 13103-13111.
- Woodcock, N. H., & Mort, K. (2008). Classification of fault breccias and related fault rocks. *Geological Magazine*, 145(3), 435-440.
- Wülser, P. A., Brugger, J., Foden, J., & Pfeifer, H. R. (2011). The sandstone-hosted Beverley uranium deposit, Lake Frome Basin, South Australia: mineralogy, geochemistry, and a time-constrained model for its genesis. *Economic Geology*, 106(5), 835-867.
- Wülser, P.A., (2009). Uranium metallogeny in the North Flinders Ranges region of South Australia. Unpublished PhD thesis. University of Adelaide, School of Earth and Environmental Sciences, Department of Geology and Geophysics. Adelaide